MICROCOPY RESOLUTION TEST CHART

NATIONAL BUREAU OF STANDARDS-1963-A

AD A139441

CSDL-T-809

THERMAL EVALUATION OF SELECTED
ABLATIVE MATERIALS IN TRANSIENT
LOW HEAT FLUX ENVIRONMENTS

by

Joseph Peter Marques

May 1983

Master of Science, Ocean Engineer's Thesis
Massachusetts Institute of Technology

The Charles Stark Draper Laboratory, Inc.

Cambridge, Massachusetts 02139

DTIC
ELECTE
MAR 2 7 1984

A

84 01 09 012

CSDL-T-309

THERMAL EVALUATION OF SELECTED ABLATIVE MATERIALS
IN TRANSIENT, LOW HEAT FLUX ENVIRONMENTS

by

Joseph Peter Marques
Lieutenant, United States Navy

B.S. Naval Architecture
United States Naval Academy
(1977)

SUBMITTED TO THE DEPARTMENT OF OCEAN ENGINEERING
IN PARTIAL FULFILLMENT OF THE REQUIREMENTS FOR THE
DEGREES OF

OCEAN ENGINEER

and

MASTER OF SCIENCE IN MECHANICAL ENGINEERING

at the

MASSACHUSETTS INSTITUTE OF TECHNOLOGY

May 1983

© Joseph Peter Marques, 1983

MAR 2 7 1984

A

Signature of Author _____
Department of Ocean Engineering
May 6, 1983

Certified by _____
Warren M. Rohsenow
Thesis Supervisor

Approved by _____
A. Douglas Carmichael
Reader

Accepted by _____
A. Douglas Carmichael
Chairman, Ocean Engineering Department Committee

Accepted by _____
Warren M. Rohsenow
Chairman, Mechanical Engineering Department Committee

THERMAL EVALUATION OF SELECTED ABLATIVE MATERIALS
IN TRANSIENT, LOW HEAT FLUX ENVIRONMENTS

by

Joseph Peter Marques

Submitted to the Department of Ocean Engineering

on May 6, 1983 in partial fulfillment of the

requirements for the degrees of

Ocean Engineer and Master of Science

in Mechanical Engineering

ABSTRACT

This thesis attempts to evaluate the thermal performance of abla-
tive materials subjected to a common, transient, low-heat flux environ-
ment. Experiments were conducted to provide backface, substrate, and
surface temperature histories for each of the ten ablators under exami-
nation. The tests are useful in determining the relative merit of the
materials, and can be used as a screening tool by removing obviously
poor performers from further evaluation. Data obtained during testing
are correlated with results of a sophisticated computer ablation model.
The ultimate objective of these experimental evaluations is the relative
ranking of materials studied, and subsequent selection of the ablator
which provided the best thermal protection in the environment of concern,
based upon applicable thermal insulation performance indices.

Thesis Supervisor: Warren M. Rohsenow
Title   : Professor of Mechanical Engineering

ACKNOWLEDGEMENTS

Accession For

NTIS GRA&I

DTIC TAB

Unannounced

Justification

Distribution/

Availability Codes

Avail and/or

Dist | Special

A-1

3

TABLE OF CONTENTS

TABLE OF CONTENTS (Continued)

TABLE OF CONTENTS (Continued)

LIST OF FIGURES

LIST OF FIGURES (Continued)

8

9

LIST OF FIGURES (Continued)

LIST OF FIGURES (Continued)

LIST OF TABLES

12

LIST OF TABLES (Continued)

LIST OF SYMBOLS

Symbol	Definition	Units
A	exposed specimen surface area	(ft^2)
B	the transpiration number	–
c_p	specific heat at constant pressure	$(Btu/lbm{-}^\circ F)$
$c_{p_{gi}}$	initial specific heat of pyrolysis gas	$(Btu/lbm{-}^\circ F)$
f_v	the fraction of the material which undergoes phase change or reaction	–
G	correction factor for surface convective flux due to pyrolysis gas injection	–
h_{cw}	gas enthalpy at a cold wall	$(Btu/ft^2{-}s{-}^\circ F)$
h_e	gas enthalpy at the boundary layer edge	$(Btu/ft^2{-}s{-}^\circ F)$
h_{hw}	gas enthalpy at the ablative surface temperature	$(Btu/ft^2{-}s{-}^\circ F)$
h_s	effective heat of reaction	$(Btu/lbm{-}ft^2{-}s)$
H_{v_j}	heat of vaporization of ablation material per unit volume	$(Btu/lbm{-}ft^3)$
k,K	thermal conductivity	$(Btu/ft{-}s{-}^\circ F)$

14

Symbol	Definition	Units
K_{bs}	thermal conductivity of backup structure	(Btu/ft-s-°F)
L	specimen length	(ft)
l_f	final specimen length	(ft)
l_o	original specimen length	(ft)
Δl	change in specimen length	(ft)
m	mass of material	(lbm)
$\dot{m}$	total mass flux transfer	(lbm/ft^2-s)
m_f	final specimen mass	(g)
$\dot{m}_i$	initial mass flow rate	(lbm/s)
m_o	original specimen mass	(g)
Δm	change in specimen mass	(g)
Q_k	heat absorbed/liberated per unit length of material	(Btu/ft^3-s)
Q^*	heat of ablation	(Btu/lbm)
$\dot{q}$	incident heat flux	(Btu/ft^2-s)
$\dot{q}_c$	conduction heat transfer rate	(Btu/ft^2-s)
$\dot{q}_{cw}$	heat transfer rate to a cold wall	(Btu/ft^2-s)
Q^*_{cw}	cold-wall heat of ablation, as defined by Equation (6-2)	(Btu/lbm)

LIST OF SYMBOLS (Continued)

Symbol	Definition	Units
$\dot{q}_{hw}$	hot-wall heat flux	(Btu/ft^2-s)
q_I^*	cold-wall heat of insulation, as defined by Eq. (6-4)	(Btu/lbm)
$\dot{q}_{rr}$	reradiation heat flux	(Btu/ft^2-s)
$\dot{q}_s$	sublimation heat transfer rate	(Btu/ft^2-s)
$\dot{q}_t$	transpiration heat flux	(Btu/ft^2-s)
T	temperature	$(°F)$
t	time	(s)
T_{amb}	ambient temperature	$(°F)$
t_b	time of burn duration	(s)
$T_{BF_{max}}$	maximum backface temperature	$(°F)$
$t_{BF_{max}}$	time of maximum backface temperature	(s)
T_{BF_o}	original backface temperature	$(°F)$
T_s	surface temperature	$(°F)$
t_{ss}	time to reach steady state ablation	(s)
T_{ss_o}	original substrate temperature	$(°F)$

16

Symbol	Definition	Units
$t_{T_{max}}$	time to reach maximum temperature	(s)
$t_{\Delta T}$	time interval for temperature increase ΔT	(s)
ΔT	temperature change	(°F)
V_w	linear rate of ablation	(ft/s)
w_i	initial material weight	(lbm)
w_f	final material weight	(lbm)
x	distance	(ft)
α	thermal difusivity	(ft^2/s)
$\alpha_{\Delta T}$	thermal pseudodiffusivity, as defined by Eq. (6-3)	(ft^2/h)
ε	emissivity	—
ν	volume	(ft^3)
ρ	density	(lbm/ft^3)
σ	Stefan-Boltzmann constant, 4.806×10^{-13}	$(Btu/ft^2\text{-}s\text{-}°F^4)$
τ	time	(s)

PREFACE

This thesis is the result of an investigation conducted at The
Charles Stark Draper Laboratory, Inc. by my colleagues, LCDR James M.
Leary, Lt. Richard A. Schwarting, and myself. Primarily, our research
efforts concentrated on analytically and experimentally screening candi-
date ablative materials, with the ultimate objective of recommending
possible alternate ablative materials to be used for insulating electronic
components subjected to a transient, low heat flux, radiant environment.
Our work encompassed analytical selection of candidate ablative materials,
thermal testing of those materials in transient, low heat flux environ-
ments, and analytically modeling the ablative process using a modified
computer simulation program.

My work consisted of organizing and implementing a thermal evalu-
ation program designed to provide all pertinent data required to relatively
rank candidate materials, as well as supply input to the computer model
for data correlation of specimen backtrace, substrate, and surface tempera-
tures. In all, ten ablative materials were evaluated under each of four
different test conditions.

For a broader understanding of the entire investigation conducted,
I recommend the reading of my colleagues' theses[19,31] jointly with mine.

18

CHAPTER 1

INTRODUCTION

Advances in the theater of high temperature technology have cre-
ated new environments of extremely high temperatures. Composite ab-
lative materials, which are used for thermal protection of reentry space
vehicles, rocket motor nozzles, and as general purpose fire-retardant
coatings, therefore, have been the subject of study during recent years.
Knowledge of the thermal response of ablative materials is necessary to
select the type and amount of thermal protection material required for a
given application.

The object of this research was to evaluate the thermal perfor-
mance of ten candidate ablative materials by subjecting each to a common,
transient, low-heat flux radiative environment. Although other factors
such as applicability, bondability and toxicity were important, the in-
herent thermal protection offered by candidate materials was of primary
concern in this study.

The intent of this series of evaluation tests was threefold.
First, by monitoring backface temperature of standard thickness speci-
mens, a method of selectively screening the materials is realized. The
test is useful in determining the relative merit of ablators, partic-
ularly in weeding out obviously poor performers from further, more so-
phisticated testing.

Second, the testing provides a means of evaluating cold-wall
heat of ablation for each material. The heat of ablation, a property
which is a function of both the material and the environment to which

it is subjected, provides a measure of the ability of a material to serve as a heat protection element under severe thermal environments. Thus, in both respects, the testing serves as a materials screening evaluation and is useful in providing a means of performing material selection studies.

Third, experimental data obtained from the various evaluation tests are compared to predicted results generated from a sophisticated computer ablation model in an effort to better understand the complicated thermal process at hand.

In all, three types of evaluation tests were conducted on each of the ten candidate materials. Each test supplied specific data to be used both to aid in the relative ranking of materials, and to be correlated with computer simulation output data.

The first evaluation test provides a rapid, inexpensive means of relatively ranking the materials studied by considering the temperature rise of the backface of a two-inch square panel specimen which is exposed to a radiant heat flux provided by a vertical quartz lamp bank. A high degree of insulation effectiveness is indicated by a slow rise to a relatively low backface temperature. Each specimen type is of the same physical dimensions and subjected to the same heat flux so as to ensure good relative data correlation among the various candidate materials.

The second type of test provides substrate temperature data at various depths from the ablating surface for direct correlation with the computer simulation model. A one-inch-diameter, two-inch-long cylindrical specimen is instrumented with six thermocouples to monitor in-depth temperatures as a function of time. The specimen, exposed to a quartz lamp generated heat flux, experiences one-dimensional heat flow along its length.

The final evaluation test provides surface temperature data as a function of time for correlation with data obtained from the computer

model. Once again, the specimen surface is exposed to a normal incident heat flux provided by the quartz lamps, and surface temperature is monitored with a radiation pyrometer.

Experimental apparatus, procedures, and results for each test type, as well as physical dimensions and characteristics of each test specimen, will be described in detail in subsequent chapters.

CHAPTER 2

SIMPLIFIED ABLATION THEORY

2.1   Introduction

Ablation of plastic materials is essentially a heat and mass
transfer process in which a large amount of thermal energy is expended
by a sacrificial loss of ablator surface material, resulting in the re-
striction of high environmental temperatures to a very thin surface
region. Mechanisms of heat transfer in this phenomena include:

(1)   Heat conduction into the material substrate and storage
      by its effective heat capacity.

(2)   Material phase changes and endothermic chemical reactions.

(3)   Heat absorption by gases in the material substrate as they
      percolate to the surface char region.

(4)   Surface reradiation.

(5)   Transpiration of gases from the ablating surface into the
      boundary layer.

(6)   Convection.[4]

2.2   Ablator Surface Energy Balance

In its simplest form, the energy balance at the ablating surface
is essentially[3]

$$\dot{q}_{hw} = \dot{q}_c + \dot{q}_s + \dot{q}_t + \dot{q}_{rr} \qquad (2\text{-}1)$$

22

with all terms as defined in the following pages. Figure 2.1 illustrates this surface energy balance. Specific material properties and the thermal environment to which each material is subjected will determine the actual amount of energy expended by each mechanism.
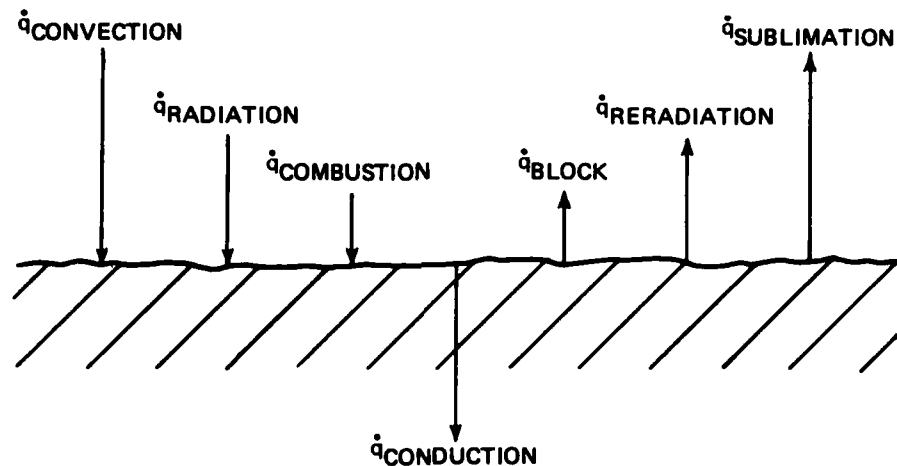
Figure 2.1. Ablator surface energy balance.[3]

2.2.1 Thermal Input

Heat transfer to the ablating surface occurs by the mechanisms of convection, radiation, and combustion, all of which are included in a reference hot-wall heat flux value, $\dot{q}_{hw}$, defined as the thermal flux incident to a nonablating surface at the ablative surface temperature. The hot-wall heat flux is described mathematically as[1]

$$\dot{q}_{hw} = \dot{q}_{cw} \left[\frac{h_e - h_{hw}}{h_e - h_{cw}} \right] \qquad (2\text{-}2)$$

where

h_e = gas enthalpy at the boundary layer edge

23

h_{hw} = gas enthalpy at the ablative surface temperature

h_{cw} = gas enthalpy at a cold wall

$\dot{q}_{cw}$ = cold-wall heat flux measured by the water-cooled calorimeter

2.2.2 Internal Heat Conduction

In the initial phases of heating below the material ablation temperature, the ablator behaves as a heat sink, conducting all of the energy absorbed at the surface into the substrate, where it is stored by the effective heat capacity of the material. Since the rate of heat penetration into the material initially exceeds the rate of surface removal, the process is considered to be transient ablation.[4] Once steady-state ablation is attained, the transfer of heat from the surface region into the substrate takes on the form of steady conduction

$$\dot{q}_c = \frac{d}{dx}\left[k\,\frac{dt}{dx}\right] \tag{2-3}$$

where

x = depth from ablator surface

k = thermal conductivity

T = temperature

2.2.3 Sublimation

As the ablator is heated to higher temperatures, it undergoes complex phase changes and chemical reactions, such as vaporization and sublimation. The total energy flux absorbed by these material phase changes and chemical reactions is described by[4]

$$\dot{q}_s = f_v m\, h_s \tag{2-4}$$

24

where

f_v = the fraction of the material which has undergone a phase change or reaction

m = mass of material

h_s = effective heat of reaction which is a function of the material and the environment to which it is subjected

2.2.4 Transpirational Cooling

Gaseous products formed during the ablation process are injected into the hot boundary layer. The gases absorb heat by sensible temperature rise as they percolate through this high temperature environment, carrying off some of the heat originally destined for the ablating surface.[4] The amount of this transpiration or heat blocking effect is approximated by

$$\dot{q}_t = f_v \, m \, B \, (h_e - h_{hw}) \qquad (2-5)$$

where B = the transpiration number, a function of the molecular weight of undissociated air, and the average molecular weight of injected vapors.[4]

2.2.5 Surface Reradiation

Depending on the material properties and the incident heat flux, a substantial portion of the heat input to an ablator may be dissipated by surface reradiation. The total amount of thermal reradiation is a function of the ablating surface temperature, the environment, and the surface emittance, and is described by

$$\dot{q}_{rr} = \sigma \varepsilon T_s^4 \qquad (2-6)$$

25

where

ε = ablator surface emissivity

σ = Stefan-Boltzmann constant, $4.806 \times 10^{-13} \dfrac{Btu}{ft^2-s-°F^4}$

T_s = ablative surface temperature

From the equation, it is quite apparent that the total surface reradiation becomes significant at high values of surface temperature. Ablative plastics that char in response to heating exhibit maximum beneficial effects of surface reradiation, temperatures ranging from 1000°F to over 5500°F being characteristic of their highly emissive carbonaceous surface chars.[4]

2.3 Transient Ablation

In the previous section, the internal conduction term took the form specified assuming steady-state ablation had been achieved. When modeling a high heat flux ablation process such as atmospheric reentry, energy released from the thermal and chemical reactions during the transient ablation phase is assumed to be negligible compared to that released during the steady-state phase. This assumption is valid primarily because the high heat flux ensures an extremely short time span for the transient process, as can be seen in the mathematics of Eq. (2-7). Models of the steady-state ablation process normally appear as closed-form solutions to integral equations, using assumed exponential profile approximations to accurately predict surface recession, mass loss, and in-depth temperature response.

Considering the transient ablation problem complicates matters significantly, as expected. When modeling low heat flux environments, the transient phase cannot be ignored since steady-state ablation may never be realized during short duration test runs. To determine which

26

regime the thermal evaluations conducted here fall into, the heating
time required to reach steady-state ablation can be determined by[4]

$$t_{ss} = \alpha \left(\frac{1}{V_w}\right)^2 = \alpha \left(\frac{\rho Q^*_{cw}}{\dot{q}_{cw}}\right) \qquad (2\text{-}7)$$

where

α = thermal diffusivity

V_w = linear rate of ablation

ρ = material density

Q^*_{cw} = cold wall heat of ablation

$\dot{q}_{cw}$ = cold wall heating rate

For the low heat flux environment applicable to this evaluation,
typical values of these quantities for one candidate material tested
(Firex panel specimen 27) are

$$\alpha = 1.02 \times 10^{-6} \frac{ft^2}{s}$$

$$\rho = 78.03 \frac{lbm}{ft^3}$$

$$Q^*_{cw} = 5.07 \times 10^3 \frac{Btu}{lbm}$$

$$\dot{q}_{cw} = 10.2 \frac{Btu}{ft^2\text{-}s}$$

yielding a steady-state ablation onset time of 1538 seconds. This
clearly places the 45- and 200-second thermal tests conducted here in
the transient ablation regime.

27

To accurately predict the thermal response of candidate ablators in this transient environment, while also accounting for surface recession or expansion, pyrolysis gas generation and flow rates, mass loss, and material property variations with temperature, a sophisticated model was necessary. Implicit finite difference techniques are generally employed in the transient regime to solve the energy equation and transient heat conduction equation. The accuracy of these techniques is dependent on the user's ability to predict thermophysical property variations with temperature and time.

Lieutenant Richard A. Schwarting, in his concurrent thesis work[19], attempted to model this process of transient ablation in low heat flux environments. Adopting a finite difference computer simulation program entitled STAB II[3], developed at the Manned Space Center, Houston, he modified it to model intumescent ablators subjected to the environment encountered in this thermal testing program. A short description of the simulation program follows.

2.4   STAB II Computer Simulation Program

The STAB II computer simulation was developed to determine the transient in-depth response of a one-dimensional, charring ablation thermal protection system subjected to a given hyperthermal environment.[3] The analytical model considers both an ablation material and a backup structure. The ablation material is considered to be composed of three distinct regions; char, reaction and virgin material. STAB II has the capability of considering up to twelve different materials composing the backup structure, with or without air gaps between materials. The boundary condition for thermal input at the external surface may be in the form of a heating rate or temperature history. The output of the model includes performance parameters, such as in-depth temperature-time histories and surface recession rates.

The basic ablation process modeled by the program is the pyrolysis of ablative material in the reaction zone which, in its simplest

28

form, is described by the expression[3]

$$\text{Virgin material} \rightarrow \text{gas} + \text{char} \qquad (2\text{-}8)$$

The calculation of the in-depth temperature response required the solution of an energy equation of the form[3]

$$\rho c_p \left(\frac{\partial T}{\partial \tau}\right) = \frac{\partial}{\partial x}\left(K\frac{\partial T}{\partial x}\right) + \sum_i \dot{m}_i c_{p_{g_i}} \left(\frac{\partial T}{\partial x}\right) + \sum_j \nu_j H_{v_j}\left(\frac{\partial \rho_j}{\partial \tau}\right) + \sum_k Q_k(x)$$

$$(2\text{-}9)$$

where

$$\rho c_p \left(\frac{\partial T}{\partial \tau}\right) = \text{rate of energy storage}$$

$$\frac{\partial}{\partial x}\left(K\frac{\partial T}{\partial x}\right) = \text{heat conduction}$$

$$\sum_i \dot{m}_i c_{p_{g_i}} \left(\frac{\partial T}{\partial x}\right) = \text{heat convected by pyrolysis gases}$$

$$\sum_j \nu_j H_{v_j}\left(\frac{\partial \rho_j}{\partial \tau}\right) = \text{rate of heat absorption due to thermochemical reaction of the ablative material constituents}$$

$$\sum_k Q_k(x) = \text{possible additional modes of heat absorption or liberation not other-wise accounted for}$$

This equation applies to materials experiencing one-dimensional heat transfer.

In solving the energy balance, boundary conditions at each of the three interfaces must be described. The boundary conditions at the

ablator front surface were illustrated in Figure 2.1 and described analytically as [3]

$$Gq_{hw} + q_{radiation} + q_{combustion} - q_{reradiation} - q_{sublimation} = -K\frac{\partial T}{\partial x}\bigg|_{x=0}$$

$$(2-10)$$

where

$$Gq_{hw} =$$ hot wall convective flux corrected for the effects of mass injection into the boundary layer

$$q_{radiation} =$$ incident radiative heat flux

$$q_{combustion} =$$ heat liberated at the surface due to combustion of char constituents with boundary layer gaseous species

$$q_{reradiation} =$$ heat flux reradiated from surface

$$q_{sublimation} =$$ energy absorbed dur to char sublimation

$$K\frac{\partial T}{\partial x}\bigg|_{x=0} =$$ conduction at ablator surface

At the second interface, that being the ablator/backup structure bondline, the boundary condition is pure conduction, and described by [3]

$$-K\frac{\partial T}{\partial x}\bigg|_{x=L} = -K_{bs}\frac{\partial T}{\partial x}\bigg|_{x=L}$$

$$(2-11)$$

Finally, the boundary condition at the backup structure/environment interface can be chosen to be adiabatic or radiative to the environment.

Numerical difference forms of the energy equation and boundary conditions are programmed into STAB II for compilation of temperature-time profiles and surface recession.

Ablator pyrolysis gas production ($\dot{m}_g$) is calculated using an Arrhenius kinetic rate expression of the form[3]

$$\frac{\partial \rho}{\partial t} = K_0 \left(\frac{\rho - \rho_c}{\rho_v - \rho_c} \right)^n e^{\frac{-E}{RT}} \qquad (2\text{-}12)$$

where the pre-exponential coefficient and activation energy values may be determined using thermogravimetric analysis (TGA) techniques.[20]

31

CHAPTER 3

MATERIAL CHARACTERIZATION

3.1 Introduction

Successful selection of the most promising ablative material of
the countless available must be preceded by their characterization and
evaluation in an appropriate hyperthermal environment. The vast assort-
ment of materials were first analytically screened to determine their
basic thermal insulative characteristics and properties and potential for
use in the specified environment. Selection of candidate materials pos-
sessing the best apparent insulative qualities was based on solution of a
semi-infinite solid heat conductance equation of the form

$$T = \frac{2\dot{q}\sqrt{\alpha t}}{k} \text{ ierfc } \frac{x}{2\sqrt{\alpha t}} \qquad (3\text{-}1)$$

with assumed boundary condition of constant heat flux, $\dot{q} \frac{Btu}{ft^2\text{-}s}$ [18]. The
most promising candidate materials were then experimentally evaluated to
determine material performance in simulated application environments.

The materials tested in this evaluation can be divided into two
broad categories, charring and intumescent ablators. The charring abla-
tors include Dynatherm S-885, S-886, DE-350, DE-370, Fiberfrax, and
Avcoat 893-5 cork sheet. The intumescent ablators include Firex, Flex-
fram 605, Chartek 59, and Flamarest 1600B. Specifics of each material
will be discussed later in this chapter, after a brief description of the
characteristics of the two ablator types.

32

3.2   Charring Ablators

In general, charring ablators are composite reinforced, organic polymers, the most common being elastomers and plastics. Thermosetting polymers (high degree of cross linking) readily facilitate surface char formation upon heating in a hyperthermal environment.[17] Charring ablators, via endothermic decomposition processes, provide effective thermal protection to substrate materials throughout a wide range of heat fluxes. The major mechanisms of heat insulation of the charring ablator include:

(1)   Heat absorption of the virgin material due to low values of diffusivity and conductivity, and high value of specific heat.

(2)   Latent heat absorption during the endothermic decomposition process which forms low molecular weight pyrolysis gases.

(3)   Transpirational cooling, whereby pyrolysis gases percolate to the surface of the ablator and on into the boundary layer, absorbing heat from the ablator as well as reducing the convective heat transfer from the environment to the surface char.

(4)   Reradiation of heat flux from the high temperature surface char to the environment.

These thermal effects are combined into a single parameter termed the effective heat of ablation, a function of both the material and the environment, which is of considerable importance when comparing charring ablators for a given task.

The physical aspects of the charring ablator decomposition process are illustrated in Figure 3.1. Initially, the material behaves as a heat sink, absorbing all of the incident heat flux. The low value of thermal diffusivity of the virgin ablator causes the heat to be entrained in a thin surface region, thereby rapidly increasing the surface temperature. At the charring ablator reaction temperature, the endothermic decomposition process occurs, releasing low-atomic-weight pyrolysis gases and

33

forming the surface char. The char produced is generally of sufficient mechanical strength to survive high shear stresses, thereby allowing the use of charring ablators in severe convective environments such as atmospheric reentry.

**DISTINCT REGIONS AND MODES
OF ENERGY TRANSPORT**

FULLY CHARRED REGION
- CONDUCTION
- CONVECTION
- GAS-CHAR REACTIONS
    - COKING
    - CARBON-SILICA

REACTION ZONE
- PYROLYSIS
- CONDUCTION
- CONVECTION

VIRGIN MATERIAL
- CONDUCTION

BACKUP STRUCTURE
- CONDUCTION
- RADIATION
- CONVECTION

**CABIN ENVIRONMENT BOUNDARY
CONDITION**
- ADIABATIC
- RADIATION
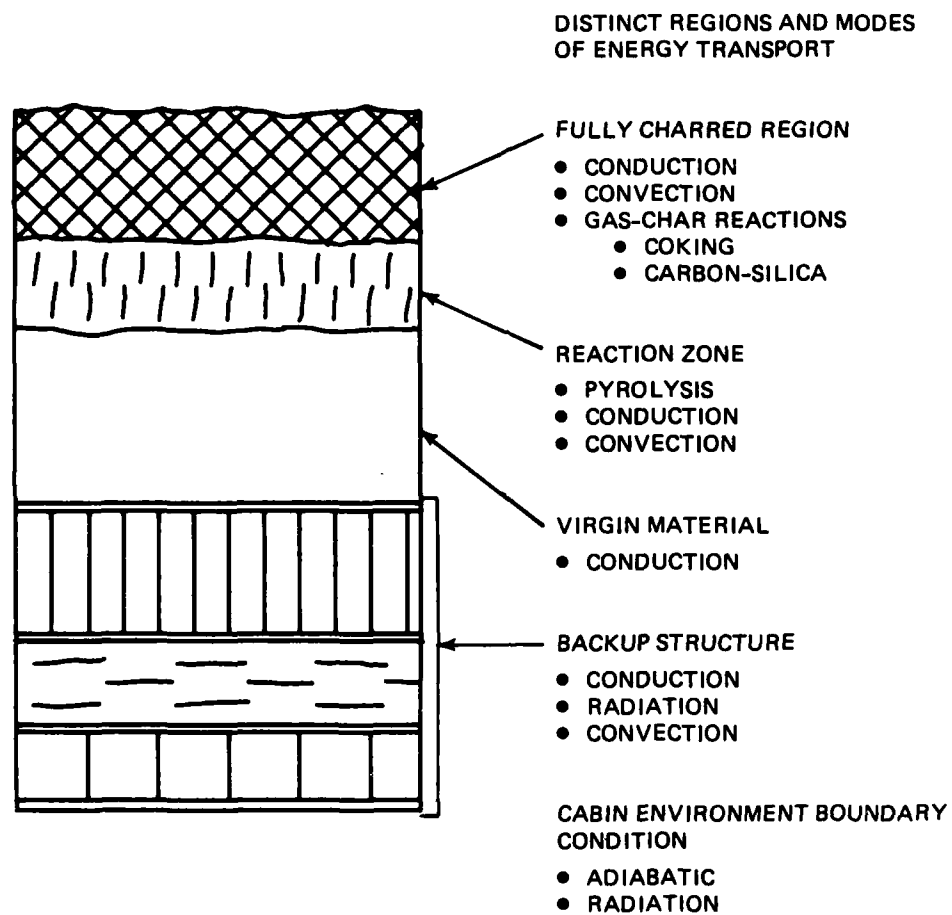
Figure 3.1. Physical model of a charring ablator.[3]

34

3.3   Intumescent Ablators

Intumescent ablators are characterized by their unique heat insu-
lating mechanism of forming a foam-like zone through enlargement or swel-
ling of the virgin material under the action of heat. As in charring
materials, low values of thermal diffusivity result in the incident heat
being entrained close to the surface of the material, causing a rapid
rise in the temperature of the surface region. When intumescent reaction
temperature is reached, a pyrolysis zone is generated, in which hot gases
produced by the decomposition process percolate to the material surface.

The physical aspects of the intumescent ablator decomposition
process are illustrated in Figure 3.2. Upon heating, the ablator expands
up to fifty times its original thickness, forming a cocoon-like insula-
ting char, substantially reducing the thermal conductivity of the mate-
rial. This char tends to be fragile, possessing poor mechanical
strength, generally able to remain intact only in environments of negli-
gible velocities. Therefore, intumescent ablators are commonly applied
on surfaces which will experience primarily a low radiant heat flux with
little or no convective influence. The outstanding thermal insulative
performance of intumescent ablators in low heat flux environments, cou-
pled with their generation of only small amounts of toxic combustion
gases when heated, makes them ideally suited in commercial applications
as fire-retardant coatings for metals, plastics, wood, and other mate-
rials.[27]

3.4   Ablator Behavioral Differences

There are several distinct differences in behavior between char-
ring and intumescent ablators, perhaps the most striking one being that
the intumescent decomposition reaction is exothermic (heat releasing),
while the charring decomposition reaction is endothermic (heat absorb-
ing).[5] The heat releasing effect of the intumescent reaction, which
can degrade the substrate insulation protection, can be countered by the

35
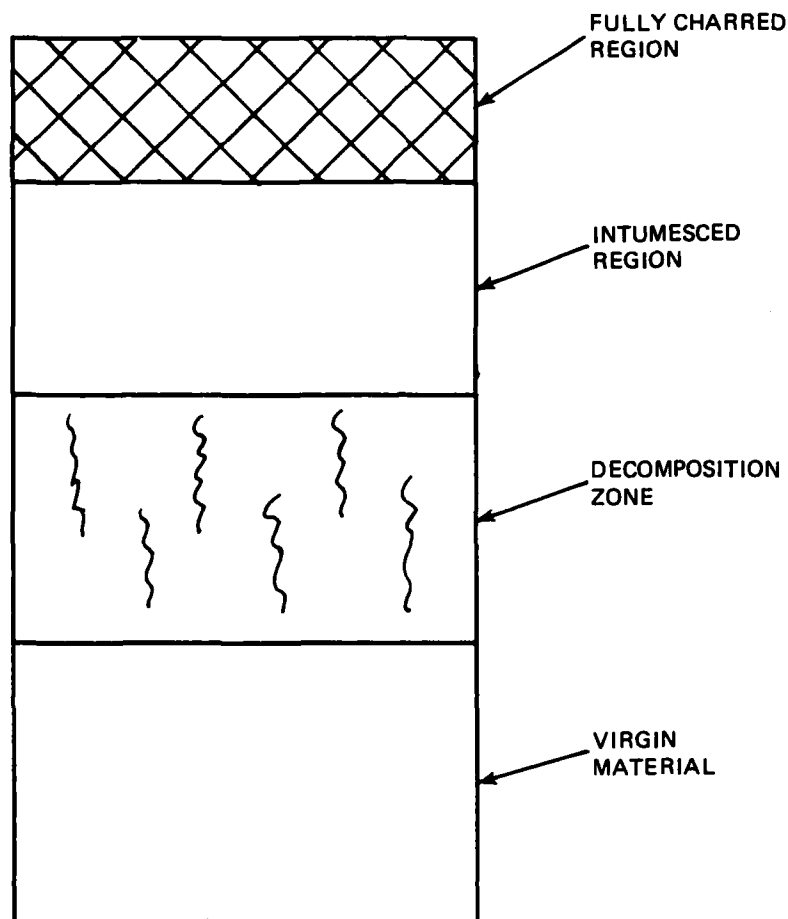
Figure 3.2. Physical model of an intumescent ablator.

addition of endothermic inorganic filler material so as to improve the overall thermal performance of the intumescent ablator.[5]

Charring and intumescent ablators also show marked differences in their thermal property (k, c_p, α) responses to increasing temperature. The result of the charring reaction with increasing temperature, is an increase in the value of thermal conductivity, with a corresponding decrease in the value of specific heat, as shown in Figures 3.3 and 3.4.
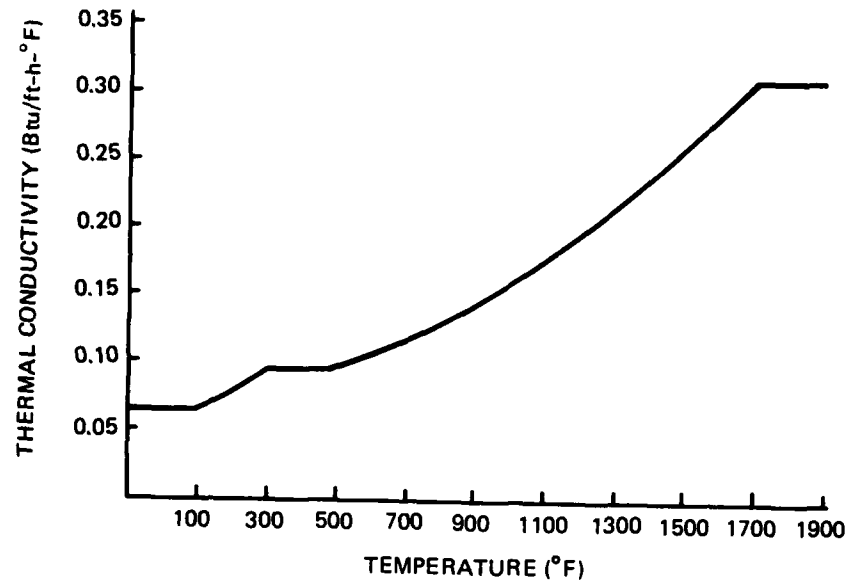
Figure 3.3. Effect of temperature on the thermal conductivity
value of a charring ablator (DE-370).
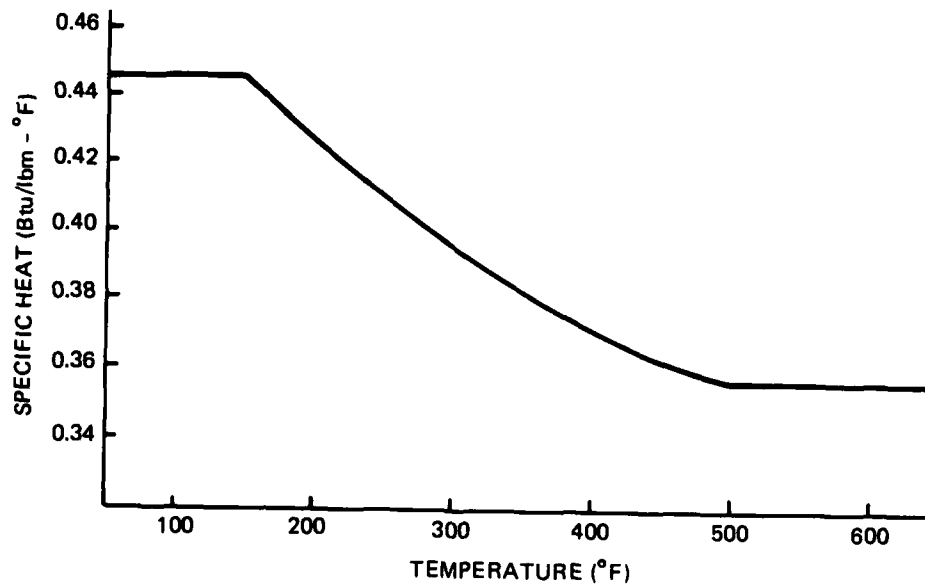
Figure 3.4. Effect of temperature on the specific heat value
of a charring ablator (DE-350).

37

respectively.[10,12] Conversely, in an intumescent reaction, with in-
creasing temperature, there is a decrease in the value of thermal conduc-
tivity, with a corresponding increase in the value of specific heat, as
shown in Figures 3.5 and 3.6, respectively.[7,31]

Thus, since thermal diffusivity is directly proportional to con-
ductivity and inversely proportional to specific heat; as the temperature
is increased, the thermal diffusivity of a charring ablator increases,
while that of an intumescent ablator decreases.

A final contrast between the two ablator types concerns the tem-
perature level at which the ablation reaction occurs. The reaction tem-
perature for charring ablators is generally in the range of 400 to
500°F, whereas the intumescent reaction occurs in the neighborhood of
250°F.[7,10,31] Therefore, for low heat flux environments, the lower
temperature of reaction of the intumescent ablator is of great insulative
value, whereas in the higher heat flux environments, the large value of
heat of reaction for the charring ablator provides the high degree of
insulation effectiveness, outweighing the fact that the reaction occurs
at a somewhat higher temperature.

3.5   Candidate Ablative Materials

In the thermal evaluation conducted here, the single most impor-
tant factor in determining the net worth of a candidate ablative material
is its ability to offer thermal protection to a backup structure, such as
an aluminum casing, when subjected to a radiant, low heat flux environ-
ment. In addition to this parameter, other factors contribute signifi-
cantly to the selection criteria. These factors include material toxi-
city, moldability, machinability, adhesion to backup structure, hydro-
lytic stability, and mechanical and thermal properties. Tables 3.1
through 3.3 contain summaries of material characteristics for each candi-
date ablator evaluated, and brief descriptions of each material type
follow here.

38
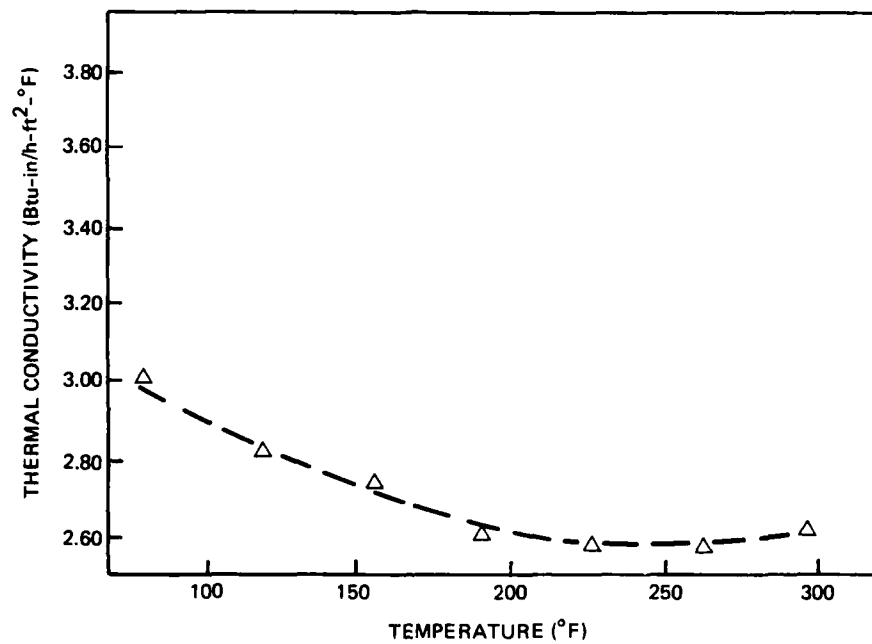
Figure 3.5. Effect of temperature on the thermal conductivity
value of an intumescent ablator (Flexfram).
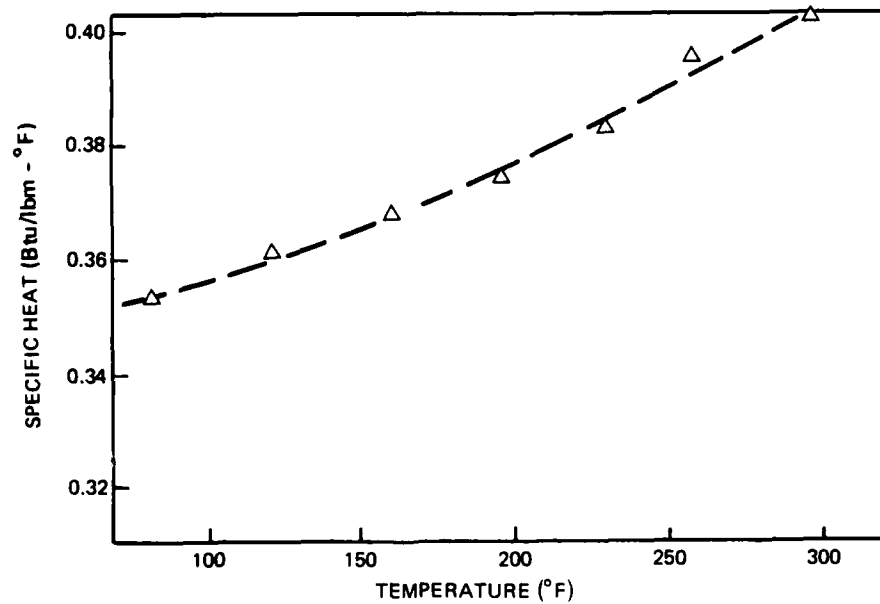
Figure 3.6. Effect of temperature on the specific heat
value of an intumescent ablator (Flexfram).

39

Table 3.1. Candidate ablator thermal
properties (vendor supplied).

Material	$k \times 10^{-6}$ $(\frac{Btu}{s\text{-}ft\text{-}°F})$	c_p $(\frac{Btu}{lbm\text{-}°F})$	ρ $(\frac{lbm}{ft^3})$	Q^* $(\frac{Btu}{lbm})$	$\alpha \times 10^{-6}$ $(\frac{ft^2}{s})$
FIREX	37.5	0.47	77.76	—	1.03
FLEXFRAM	69.44	0.35	85.53	2130	2.32
FIBERFRAX	13.88	—	40.0	—	—
CHARTEK	30.5	0.20	75	—	2.03
DE-350	22.22	0.446	68.64	—	0.726
DE-370	18.61	0.375	62.0	2812	0.800
S-885	17.36	—	39.31	—	—
S-886	20.83	—	45.6	—	—
1600B	—	—	83.03	—	—
CORK	11.94	0.471	34.0	—	0.746

3.5.1 Firex RX-2373 (Pfizer, Inc.)

Firex is a modified epoxy binder filled with thermally active
materials that form cooling gases when exposed to temperatures above
350°F. When exposed to heat in the approximate range of 1000 to 5000°F,
a surface char forms which insulates by transpirational cooling and re-
radiation.[6] Firex is composed of a two-part system, with a 24-hour
curing time at room temperature. When thoroughly mixed, the material may
be applied by spraying, troweling or pouring. Adhesion to aluminum du-
ring molding was found to be excellent, as advertised. Molding of void-
free specimens necessitated deaerating the mixture for a period of ap-
proximately ten minutes to avoid entrapped air bubbles. All mixing was

Table 3.2. Candidate ablator mechanical properties (vendor supplied).

Material	Specific Gravity	Tensile Strength ($lb/in.^2$)	Lap shear Strength ($lb/in.^2$)	Hardness (D scale)
FIREX	1.25	810	680	65
FLEXFRAM	1.37	400	—	65
FIBERFRAX	0.64	—	—	—
CHARTEK	1.20	960	1740	68
DE-350	1.1	240	360	<40
DE-370	1.0	3000	2000	<40
S-885	0.63	40	<100	<40
S-886	0.73	40	<100	<40
1600B	1.33	—	—	—
CORK	0.55	330		

performed under a ventilated hood because of the extremely rancid odor given off by the components when combined.

3.5.2 Flexfram 605 (Fiber Materials, Inc.)

Flexfram is a rubber modified epoxy, fortified with fibers and pigments to enhance erosion and flame resistance.[7] It is composed of a two-part system that self-cures within 20 to 30 minutes after mixing, with full cure taking place in 24 hours at room temperature. When mixed, the material may be applied with stiff brush or trowel. Flexfram showed excellent adhesive bond strength when applied to an aluminum backup structure. Flexfram has been approved by the U.S. Navy as an ablative coating for use on shipboard missile launchers.

Table 3.3. Fabrication characteristics of candidate ablative materials.

Material	Mixing Ratio	Pot Life	Cure Cycle	Moldability	Bondability to Aluminum (6061)	Machinability	Porosity	Thinning Agent	Application Methods	Remarks
Dynatherm DE-350	100:86:35 pbw A:B:C	2 h	24 h @ 75°F	Excellent	Excellent	Excellent	Negligible	—	(1) Transfer molding (2) Spray (if thinned down)	(1) Mechanical stirring recommended (2) Vacuum mix to increase density
Dynatherm DE-370	2:1 pbw A:B	2 h	(1) 24 h @ 75°F or (2) 2-4 h @ 140°F	Excellent	Excellent	Excellent	Very Little	"DE-370 thinner"	(1) Trowel (2) Injection molding (3) Transfer molding	Mechanical stirring recommended
Flamarest 1600B	100:3 pbw A:B	1-2 h	4 days @ 75°F	Poor (molds in 0.25-inch thickness range fail to cure completely)	Good	Good	Negligible	Methylene Chloride	Spray	(1) Mechanical mixing required (2) Spray application recommended with 1-3 mil thickness recommended (3) Some shrinkage during cure (4) Component B hazardous
Fiberfrax	Single Component	—	24 h @ 75°F	Poor	Extremely Poor	Poor	Some present due to entrapped air	—	Trowel	Once cured, very brittle and difficult to machine
Flamemaster S-885	100:10 pbw A:B	—	—	Good	Poor	Poor (rubber-like consistency)	Slight	Toluene or methyl ketone	Trowel	(1) Easily peeled off aluminum plate (2) Difficult to machine because not rigid

Table 3.3 Fabrication characteristics of candidate ablative materials. (Continued)

Material	Mixing Ratio	Pot Life	Cure Cycle	Moldability	Bondability to Aluminum (6061)	Machin- ability	Porosity	Thinning Agent	Application Methods	Remarks
Flamemaster S-886	100:10 pbw A:B	–	–	Excellent	Poor	Poor (rubber-like consistency)	Slight	Toulene or methyl ketone	Trowel	(1) Easily peeled off aluminum plate (2) Difficult to machine because not rigid
Firex 2373	130:100 pbw A:B	20 min.	(1) 2 days @ 72°F or (2) 16 h @ 118°F	Good	Excellent	Excellent (good if voids present)	Some present, can be reduced with vacuum mixing	Acetone	(1) Spray (2) Trowel (3) Pour	(1) Vacuum mixing recommended to minimize porosity (2) Mechanical stirring (3) Short pot life requires quick molding
Chartek 59	65:35 pbw A:B	30-45 min.	24 h	Good (high viscosity makes molding difficult)	Excellent	Good (void presence detrimental)	Some present	Methylene chloride	(1) Spray (2) Trowel	Without thinning, extremely difficult to mold without void formation
Flexfram	1:1 pbv A:B	20-30 min.	24-36 h @ 70°F	Excellent	Excellent	Excellent	Negligible	–	(1) Brush (2) Trowel	Mechanical stirring recommended

3.5.3 Chartek 59 (Avco Corp.)

Chartek 59 is a solvent-free epoxy mastic coating, designed for spray application, but capable of being applied by trowel if necessary.[8] Chartek is composed of a two-part system which fully cures in 24 hours at room temperature. In a fire environment, Chartek will intumesce to a thickness 4-6 times greater than the applied thickness to form an insulating, cocoon-like char which protects the substrate. Adhesive bonding to aluminum was found to be excellent.

3.5.4 Flamarest 1600B (Avco Corp.)

1600B is a filled, amine-cured intumescent epoxy coating containing flame retardant fillers.[9] It is packaged as a two-component system, one part being hazardous in nature, and applied by spraying. In a fire environment, 1600B intumesces 50 to 100 times application thickness to form a low-density char that insulates the substrate from the fire. A 20-mil coating will cure completely in 24 hours at room temperature. Adhesion of 1600B to aluminum was found to be quite good.

3.5.5 Dynatherm DE-350 (Flamemaster Corp.)

DE-350 is a silicone modified, epoxy polyamide ablative coating compound.[10] It is composed of a three-part system, component C being hazardous in nature. Application methods include transfer molding and spraying, with a full cure time of 24 hours at room temperature. Adhesion to aluminum was found to be excellent.

3.5.6 Dynatherm DE-370 (Flamemaster Corp.)

DE-370 is a lightweight, rigid epoxy-based compound, which is composed of a two-part system.[12] Application techniques include trowelling, injection/transfer molding, and spraying. DE-370 cure time is 24 hours at room temperature, and bond quality to aluminum was excellent.

3.5.7 Dynatherm S-885 (Flamemaster Corp.)

S-885 is a low density, silicone rubber-based ablative coating, composed of a two-part system.[13] It can be applied by spray, trowel or transfer/compression molding techniques, with a curing time of 24 hours at room temperature. The bonding quality to aluminum was poor in all specimens molded. The flexible, rubber nature of S-885 caused it to be peeled easily from the backup material.

3.5.8 Dynatherm S-886 (Flamemaster Corp.)

S-886 is similar in composition and charact.ristics to S-885, with only a small increase in density. As with S-885, there is poor adhesion between S-886 and the aluminum backup structure.

3.5.9 Fiberfrax LDS Moldable (Carborundum Co.)

Fiberfrax consists of ceramic fibers dispersed in a sticky water-based refractory silica binder requiring only drying to produce a hard surfaced, low thermal conductivity insulation.[15] Fiberfrax may be applied by troweling or with a caulking gun. When fully cured, the specimens were found to be hard and brittle in nature. Adhesion to aluminum was found to be poor, 80% of the samples molded having separated from the aluminum backup material with no force applied.

3.5.10 Avcoat 893-5 Cork (Avco Corp.)

Avcoat Cork-Silicone 893-5 is an elastomeric silicone-based material filled with uniformly granulated cork particles.[16] It is applied by sheet bonding, and therefore lends itself well to protection of planar surfaces. No attempt was made to bond the cork sheet to an aluminum backup structure.

CHAPTER 4

EVALUATION FACILITY

4.1   Introduction

In selecting a testing facility for the evaluation of the most
promising candidate ablative materials, the following considerations
were taken into account:

(1)   The availability and cost of the material to be charact-
      erized.

(2)   The extent and accuracy of the information desired.

(3)   The environmental conditions to be simulated.

(4)   Uniformity and reproducibility of the test medium.

(5)   The ability to accurately calibrate the testing apparatus.

The choice of testing apparatus was based primarily on the given
environmental condition of incident radiative heat flux of approximately
10 Btu/ft^2-s, 45-second burn duration, with negligible convective influ-
ence.

Candidate ablative material evaluation testing was conducted in
the Thermal Laboratory at The Charles Stark Draper Laboratory, Inc.,
Cambridge, Massachusetts. Each experiment was conducted under a vented
hood specifically designed for thermal testing. Ventilated hood features
included a two-speed ventilation fan, overhead lighting, asbestos side
shielding and electrical outlets for heat source power. The ventilation
assembly ensured any toxic gaseous products would be swept away without
disturbing any ongoing laboratory work.

Several components of the testing apparatus were common to all three series of tests conducted, and these units shall be described before continuing on to the specialized equipment required for individual tests. Basically, the testing apparatus consists of a heat source, specimens of various types suited to specific needs, specimen holders, means of recording backface, substrate and surface temperatures and a means of recording incident radiative heat flux. Major components of the test apparaturs appear in Figure 4.1.
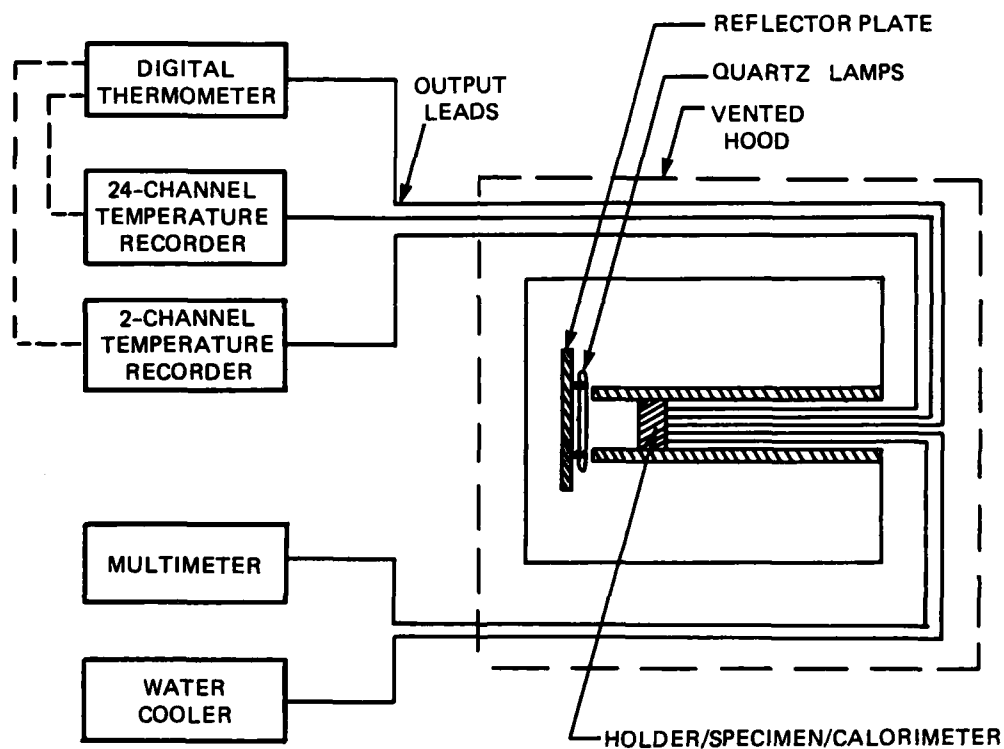
Figure 4.1. Equipment arrangement for calorimeter and backface/ substrate temperature measurements.

47

4.2   Thermal Testing Apparatus

4.2.1 Heat Source

A heat source capable of generating a flux of 10 Btu/ft^2-s was required to simulate given environmental conditions. The source consisted of a bank of nine 500-watt quartz lamps, mounted vertically on an aluminum reflecting plate, as depicted in Figure 4.2. A heat flux of 10 Btu/ft^2-s was measured at a distance of 2 inches from the center of the bank of lamps. A plot of heat flux versus distance from source center, normal to the source, appears in Figure 4-3. At a fixed distance from the lamp bank, the incident measured heat flux decreases rapidly with increasing distance from the bank centerline. Plots of this variation both horizontally and vertically, appear in Figures 4.4 and 4.5, at fixed distances of 2.1 inches and 4.2 inches from the heat source.

4.2.2 Water-Cooled Calorimeter

Because the calorimeter surface temperature is much less than the ablation temperature of the specimens, the water-cooled calorimeter is used to determine the cold-wall heat transfer rate, $\dot{q}_{cw}$. The calibration curve for the calorimeter appears in Figure 4.6. Cooling water is supplied to the calorimeter by a water cooler, manufactured by Atlas Engineering Company. Cooling water inlet temperature was kept at approximately 60°F, and cooling water flow rate maintained at 0.3 gallon per minute.

4.2.3 Hewlett Packard 3490A Multimeter

The digital multimeter displays millivolts read directly from the water-cooled calorimeter input leads. Using the calorimeter calibration curve, millivolts are converted to heat flux units of Btu/ft^2-s.

48

SPECIMEN
HOLDER ———   ——— QUARTZ LAMP BANK

——— CENTERLINE GUIDERAILS

FRONT VIEW

——— QUARTZ LAMP BANK

——— SPECIMEN HOLDER
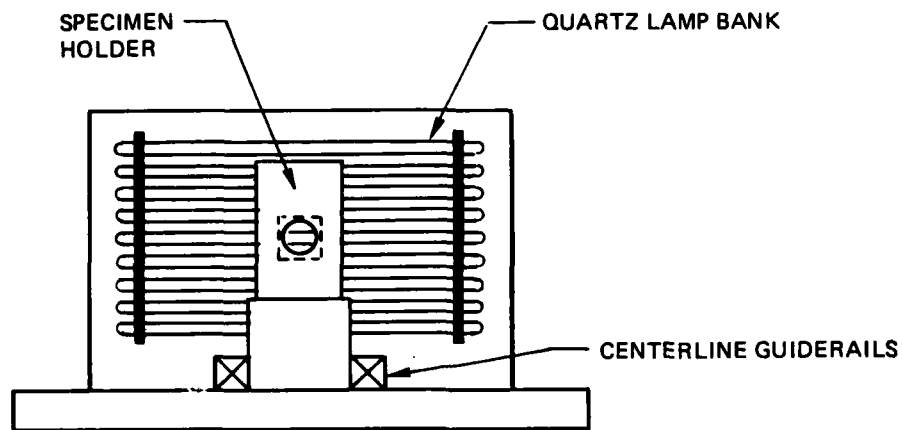
——— CENTERLINE
GUIDERAILS
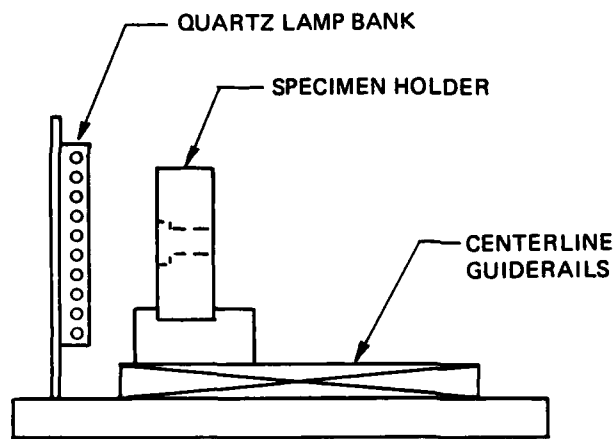
SIDE VIEW

Figure 4.2.   Experimental setup: heat source, panel specimen holder,
              centerline guiderails.

4.2.4 <u>Temperature Measuring Devices</u>

4.2.4.1 <u>Bristol Series 73A-550 24-Channel Temperature Recorder</u>

The sampling function of the recorder consists of an electronic
programming unit and a mechanically-driven print mechanism which samples
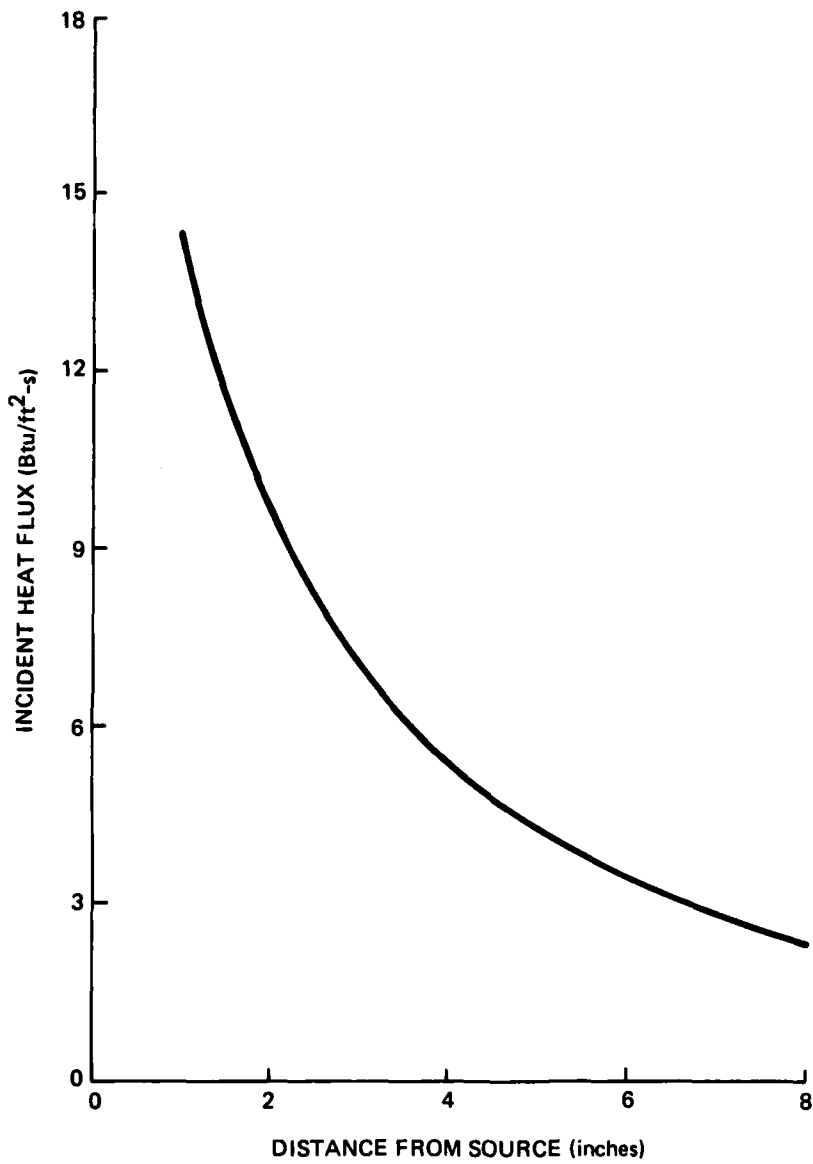
Figure 4.3. Incident heat flux versus distance from center of quartz lamp bank. Measurements taken along normal to source center.
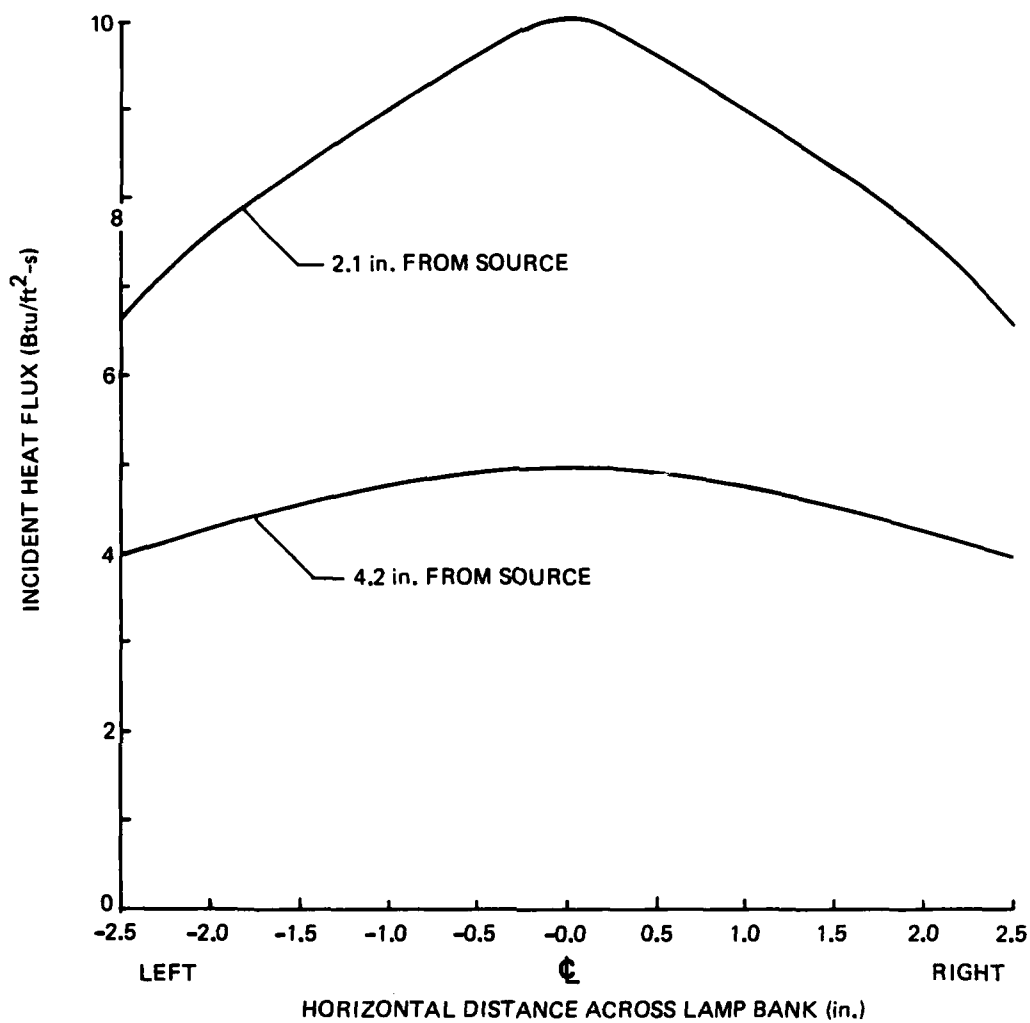
Figure 4.4. Heat flux distribution at indicated distance from heat
source as horizontal position of calorimeter is varied
across lamp bank.

24 channels. Unwanted channels are deleted from the scanning cycle by
defeat switches on a side control panel. Each temperature profile print-
out is coded by the number of the corresponding input channel. The temp-
erature recorder prints output on a standard 12-inch roll chart in the
temperature range 0°F-200°F.
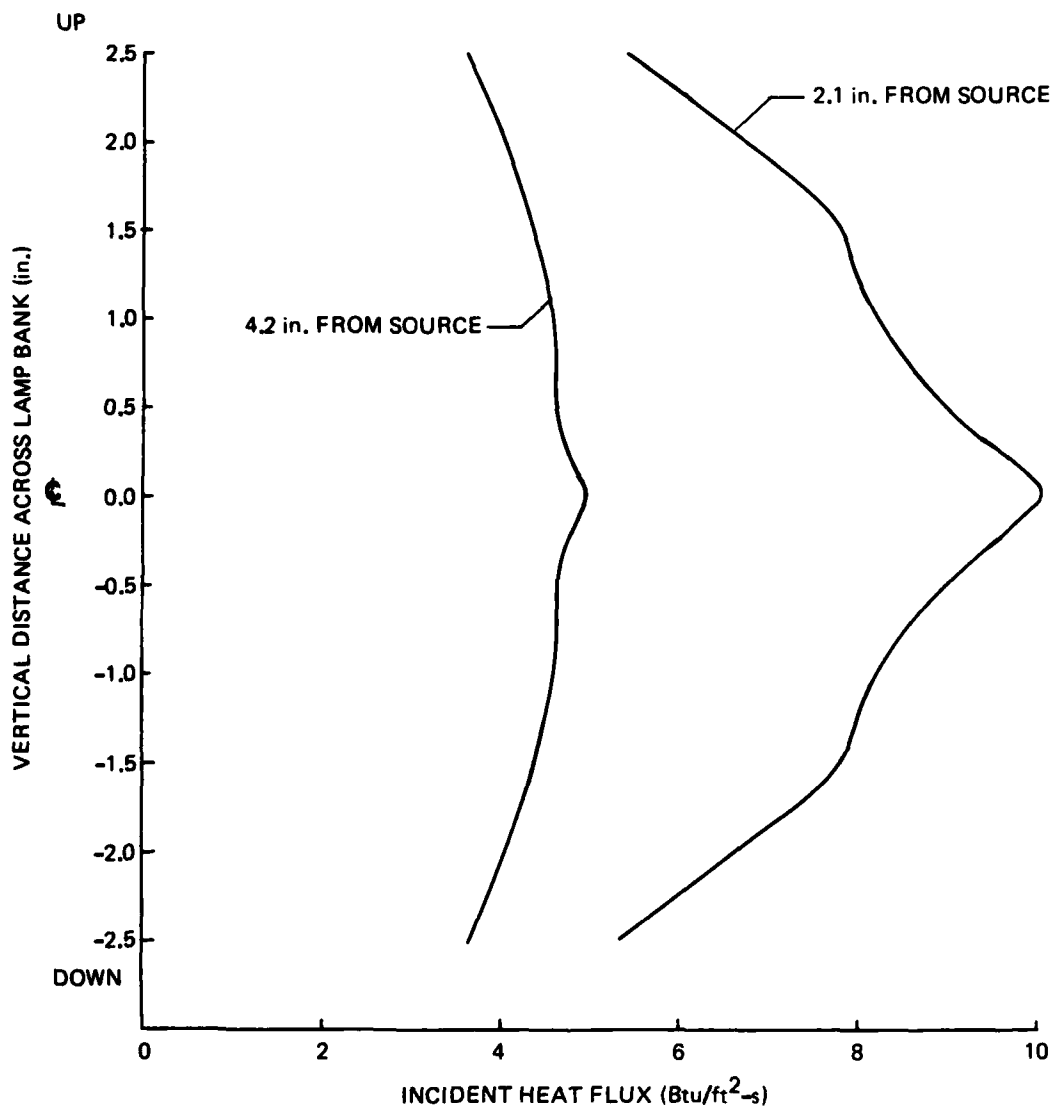
Figure 4.5. Heat flux distribution at indicated distances from heat
           source as vertical position of calorimeter is varied
           across lamp bank.

4.2.4.2 Bristol Model 570 Temperature Recorder

This two-channel pen recorder continuously monitors temperatures
in the range 0°F-350°F. Temperature profile output appears on a standard
12-inch roll chart.
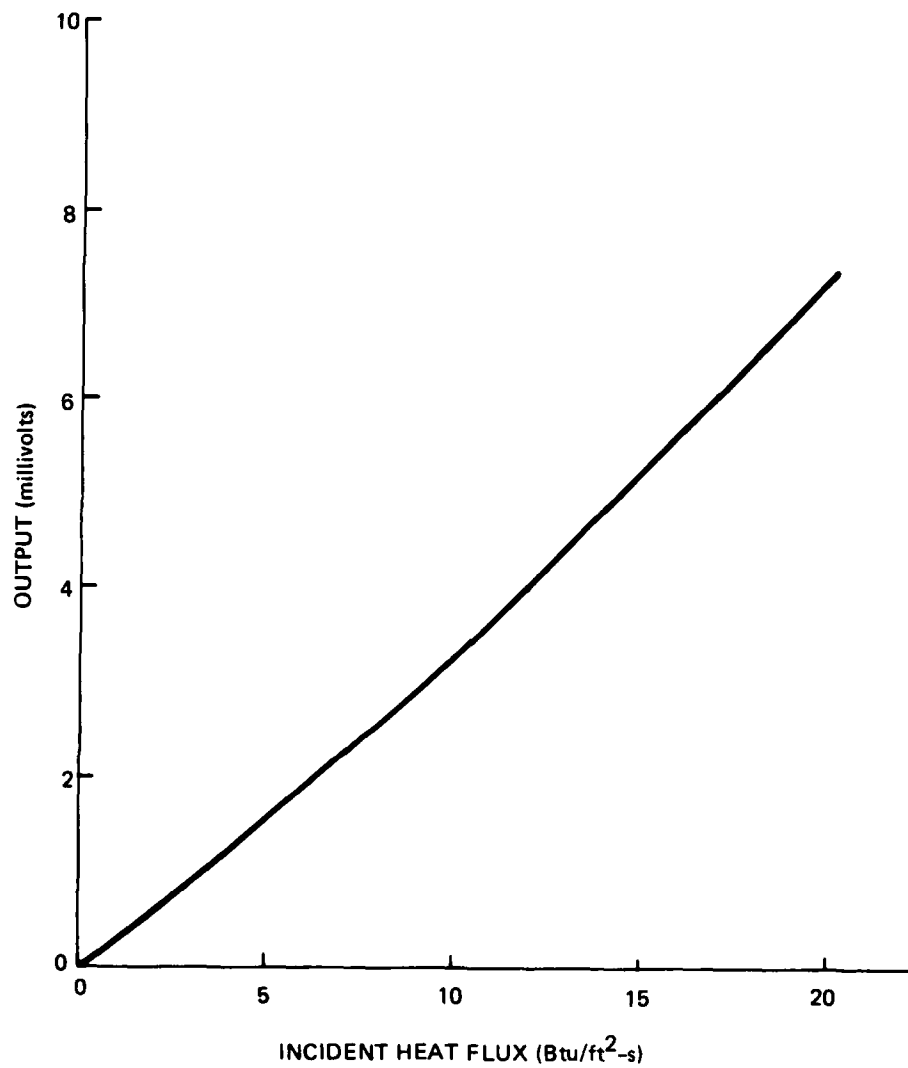
Figure 4.6.   Calorimeter calibration curve.

4.2.4.3 Omega 2176A Digital Thermometer

The 10-channel digital thermometer is used to monitor numerous temperature sources by dialing the selector switch to the appropriate channel.

4.2.4.4 Omegascope[TM] Infrared Pyrometer Model OS-2000A

The Omegascope[TM] is a computerized hand-held or tripod-mounted, noncontact thermometer for measuring surface temperatures. The Omega-scope[TM] collects the infrared energy emitted by the specimen during a burn, and its self-contained microprocessor computes the object's surface temperature four times per second.[11] The eight-bit microprocessor performs all calculations required for a direct readout of temperature, including self-calibration, when the trigger is pulled. It also calculates and stores in memory the maximum, minimum and average temperatures of a series of measurements. The Omegascope[TM] OS-2000A has a range of -20° to 2500°F. A 1.3 × sighting scope is bore-sighted to the pyrometer, improving its aiming precision to target center. Field of view data for the OS-2000A is contained in Figure 3.2 of Reference 11.

4.2.4.5 Copper-Constantan Thermocouple

Backface and substrate temperatures were monitored continuously using copper-constantan thermocouples (24 gage) wired directly to the strip chart recorders. Thermocouple attachment schemes will be discussed in the following chapter under test specimen descriptions. All thermocouple leads were protected from incident radiant flux by shielding with multiple layers of aluminum foil.

4.2.5 Specimen Holder

The specimen or calorimeter is supported in this insulative fixture, the type of holder depending on the specific test being conducted.

4.2.5.1 Panel Specimen and Calorimeter Holder

A single specimen holder was designed to accommodate both the 2 × 2 × 0.250-inch specimen and the water-cooled calorimeter. A schematic of the holder appears in Figure 4.7 and photographs of the fixture holding a test specimen and the calorimeter appear in Figure 4.8 and 4.9,

54
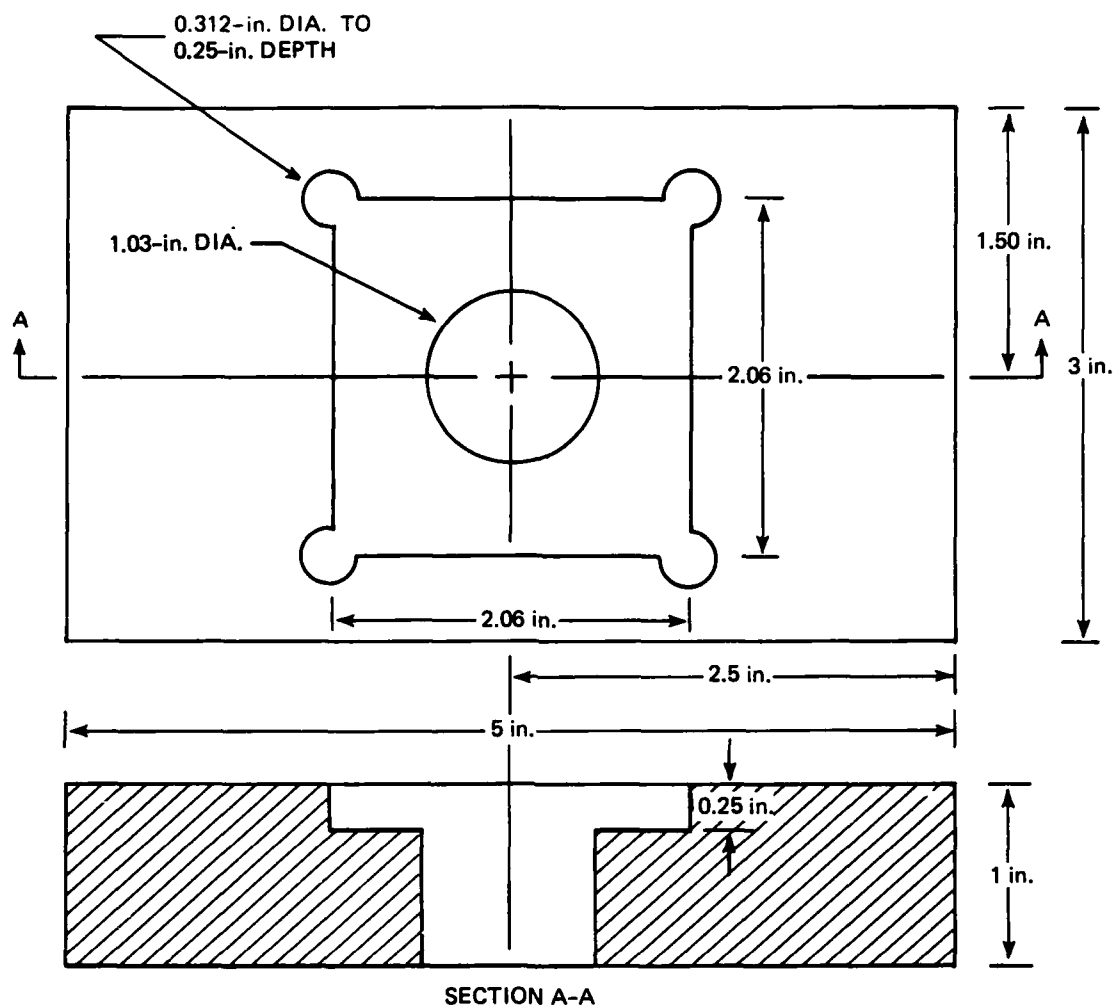
Figure 4.7. Asbestos holder for calorimeter and panel specimens.

respectively. The fixture is constructed from four 0.25-inch thick
asbestos sheet boards bolted together. It is supported in a standard
vise and arranged in such a fashion that it can be moved inward and out-
ward, normal to the heat source between centerlined guide rails (Fig-
ure 4.2), to ensure specimen alignment and to facilitate heat flux
calibration between the calorimeter and the source bank. The holder is
designed in such a way that the front face acts as a reference point for
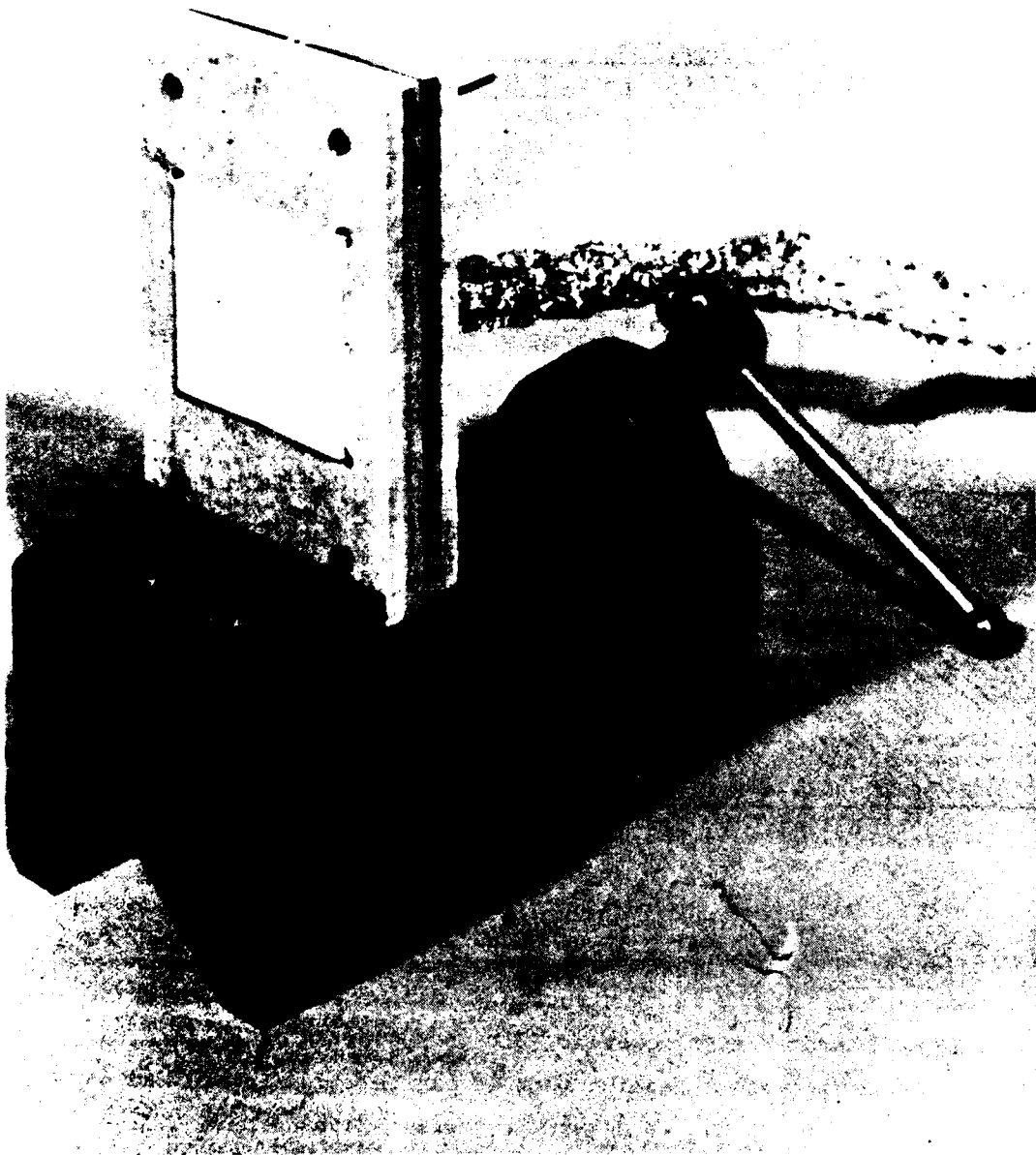
Figure 4.8. Firex panel test specimen mounted in asbestos holder.

Figure 4.9. Water-cooled calorimeter mounted in asbestos holder.

all measurements. Both the panel specimen and the calorimeter, when
inserted into the holder, have their front faces flush with the front
face of the holder. Once the holder/vise combination is fixed in place
in the guides using a clamping mechanism, the heat flux is measured with
the calorimeter, after which the test specimen is inserted for a burn
at a known heat flux.

4.2.5.2 Cylindrical Specimen Holder

Two different fixtures were used during cylindrical specimen
test runs. The first was a 3 × 5 × 2-inch fiberboard block built up
from 0.5-inch thick sheets manufactured by Johns Mansville. The second
consists of a 6-inch diameter cylindrical slug of the same material
being tested, Figure 4.10. The goal was to achieve one dimensional
heat flow in the cylinder specimen. Once one-dimensional flow is at-
tained, direct correlation between experimentally measured temperatures
and STAB II computer predicted temperatures can be made.
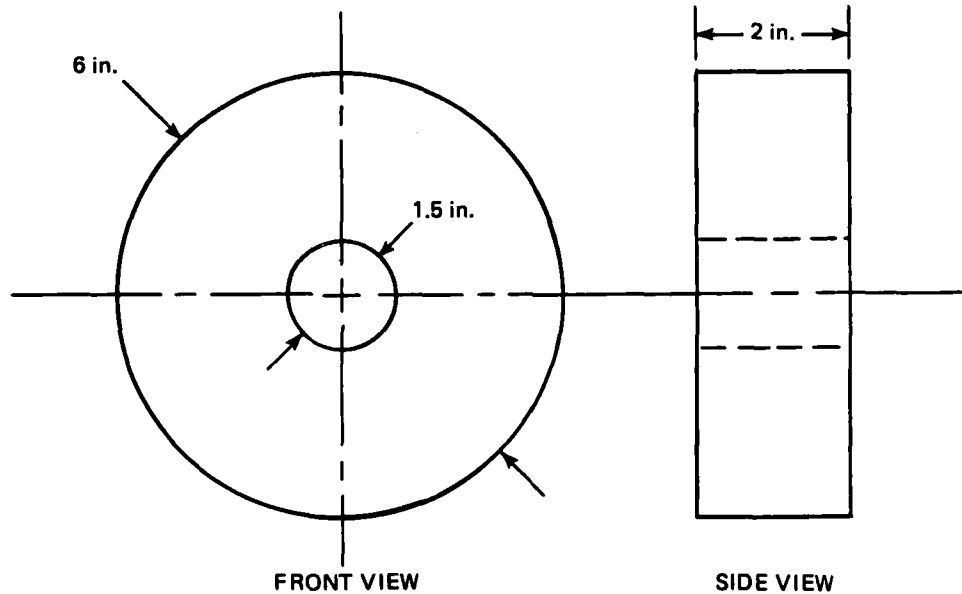
Figure 4.10. Cylinder test specimen holder (same material as
specimen being tested).

CHAPTER 5

THERMAL EVALUATION TEST PROCEDURES

5.1   Introduction

        Experimental evaluation facilities were described in detail in
the preceding chapter. The actual experimental procedures involving
these facilities will be delineated in this chpater, including specimen
preparation, specific temperature measurements, and detailed pretest,
test, and post-test procedures.

5.2   Materials Processing and Specimen Fabrication

        The insulative quality and thermal properties of an ablative
plastic are affected to a great extent by processing variables and fab-
rication procedures. Specimen preparation instructions concerning mix-
ing ratios, thinning agent addition, evacuation requirements, stirring
techniques, pot life, and curing time, play an important role in deter-
mining the ablative properties of the fully cured sample. In addition,
post-curing temperature level and duration can further alter the thermo-
physical properties of the ablator. For example, while post-curing a
phenolic resin results in removal of residual solvent and unpolymerized
resin, vaporization of the water of reaction and promotion of further
polymer cross-linking, it also promotes certain detrimental effects in-
cluding the removal of some material which may aid in heat absorption,
increased porosity, and possible nonuniform and unpredictable shrinkage.[4]

        In the cases of each of the candidate ablative materials studied
in this experiment, mixing and curing instructions supplied by respective

vendors and/or government agencies were strictly adhered to. A summary
of processing characteristics for each material studied appears in
Table 3.3 of Chapter 3.

Several facets of the specimen fabrication process were common
to most of the materials. For multicomponent mixtures, each individual
component was thoroughly stirred prior to being combined with other com-
ponents, ensuring homogeneity of individual parts, as well as consistency
in final product output. Stirring of all mixtures was accomplished
mechanically utilizing a slow-speed drill press and standard paint stir-
rer attachment. Material components were mixed under the protection of
a vented hood certified for use with toxic materials, several of the
individual components having been hazardous in nature. In cases where
extended pot life allowed, mixtures were deaerated under a standard bell
jar vacuum chamber to eliminate the possibility of void formation during
the specimen curing phase. Problems encountered during the mixing phase
are detailed for each material in Table 3.3.

Upon completion of mixing, candidate ablators were molded using
the standard molds fabricated for each specimen type. The panel speci-
men mold, illustrated in Figure 5.1, was machined from a Teflon slab to
a depth of 0.250 inch. Fully cured specimens were easily removed from
the mold in much the same manner that ice cubes are removed from a tray.
Cylindrical specimens were molded in 5-inch long, 1.25-inch inside-
diameter plexiglass tubes. Once fully cured, standard sized cylindrical
specimens were then machined from these molds to the specifications de-
tailed in the following section.

5.3   Test Specimen Specifications

Test specimen dimension specifications, as well as thermocouple
locations and attachment schemes, shall be discussed by individual
specimen type.

SECTION A-A
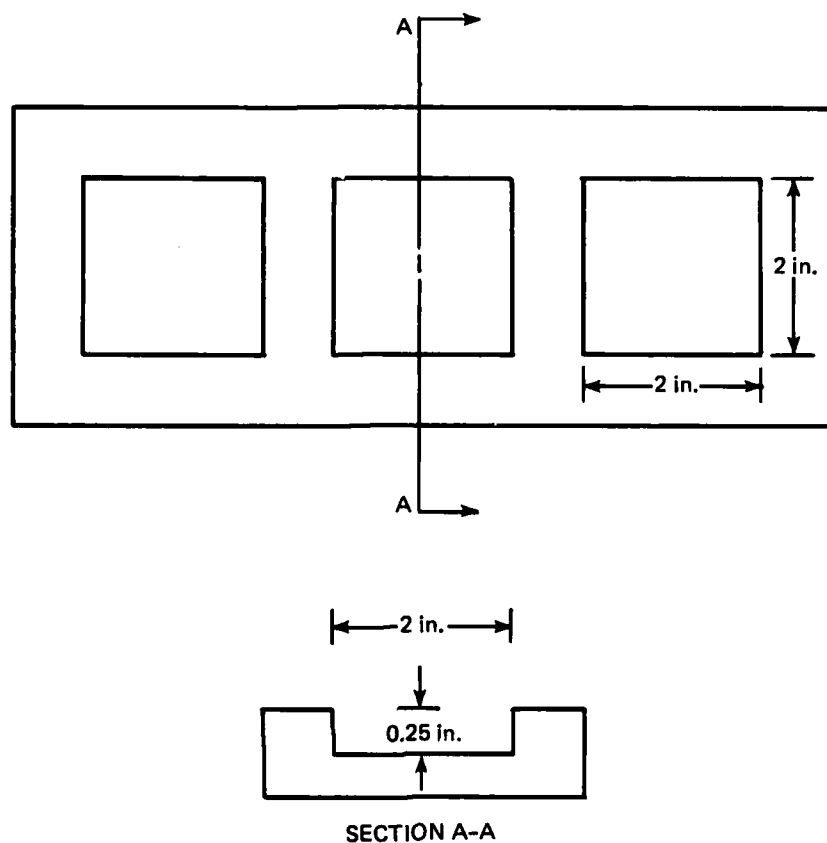
Figure 5.1. Panel specimen Teflon mold.

5.3.1 2 × 2 × 0.25-inch Panel Test Specimen

A sketch of the flat panel test specimen appears in Figure 5.2, and typical molded specimens appear in Appendix F. A 1 × 1 × 0.0625-inch 6061-aluminum backing plate is embedded, centered, in the specimen rear surface, its backface being coincident with the backface of the specimen (Figure 5.3). Once fully cured, specimens were removed from the Teflon molding tray and machined to a 0.250-inch thickness. This standard panel thickness facilitated ease of data correlation between candidate materials by removing specimen thickness as one of the variables. Specimens were then weighed, and backface instrumented with thermocouples.

61
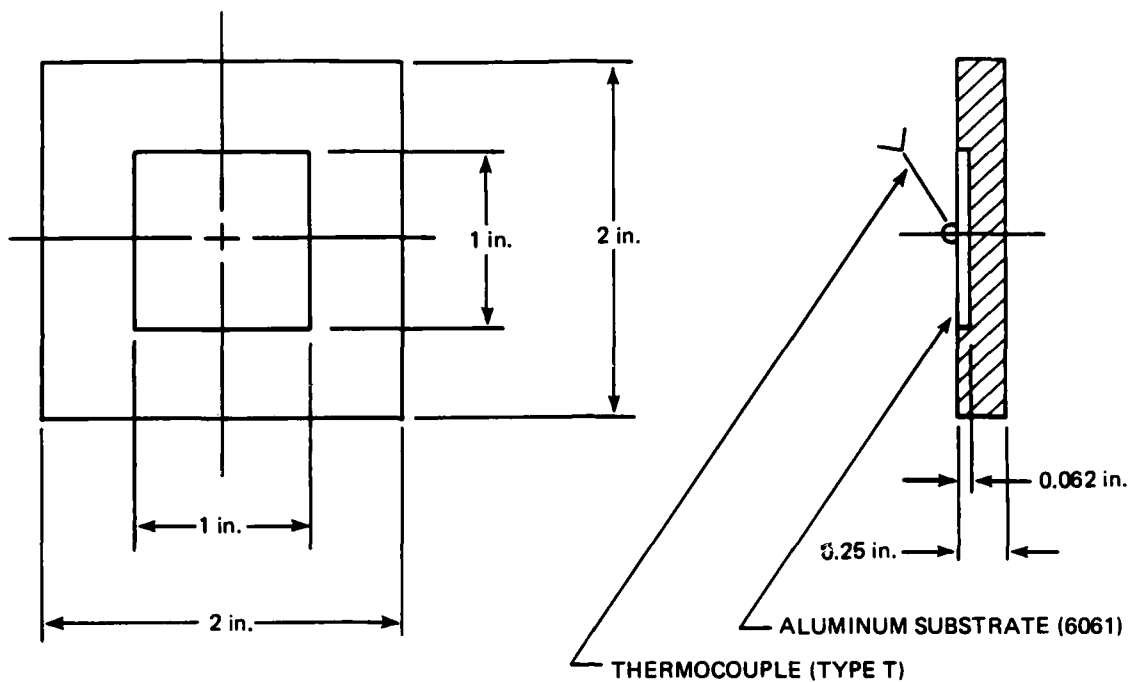
Figure 5.2. Standard panel test specimen.

A copper-constantan thermocouple was mounted to the aluminum
backing plate by means of Scotch brand aluminum tape. The aluminum
backing plate was cleaned thoroughly with acetone and then alcohol prior
to both specimen molding and backface thermocouple attachment to ensure
high quality bonding between specimen and backplate, and thermocouple
and backplate.

5.3.2 Cylindrical Specimen

The standard cylindrical test specimen is illustrated in Fig-
ure 5.4, and a typical machined specimen appears in Figure 5.5. Once
fully cured, the cylindrical specimens were machined from the plexiglass
mold and drilled for thermocouple implantation. Each specimen was instru-
mented with six thermocouples at depths of 1/16, 1/8, 1/4, 1/2, 1, and

62
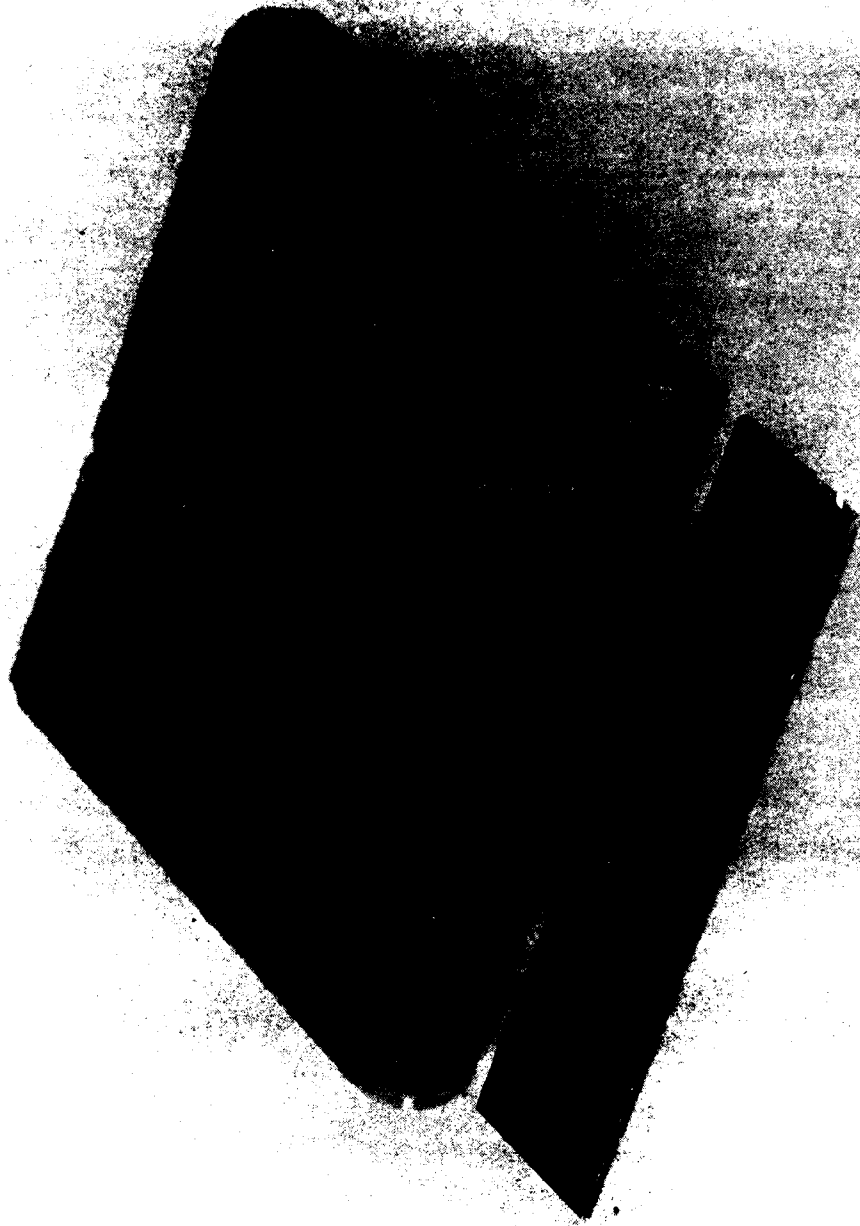
Figure 5.3. Backface of panel test specimen showing embedded aluminum backplate.

63
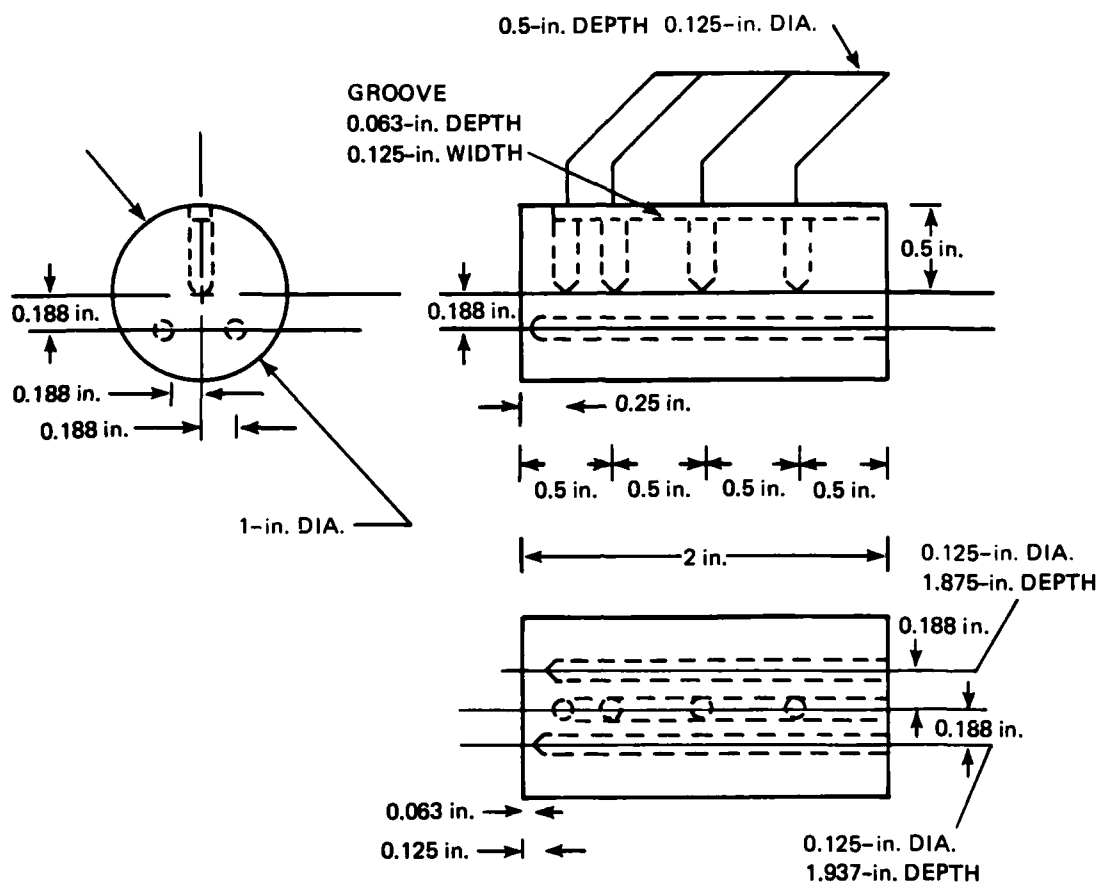
Figure 5.4. Cylindrical test specimen.

1-1/2 inches from the front face. The four rear thermocouples are located on the specimen centerline, as depicted in Figure 5.4, with leads entering from the top of the specimen. Thermocouples at 1/16 inch and 1/8 inch were inserted from the rear face of the specimen, off centerline. Once instrumented, the holes drilled for thermocouple insertion were then filled with the same material as the specimen and set to cure in an attempt to eliminate erroneous temperature readings because of voids or lack of thermocouple bonding at desired depth. Once fully cured, the specimen was then wrapped in 0.25-inch thick cork sheet insulation and inserted into the specimen holder described previously.

64

THERMOCOUPLE LEAD GROOVE

1/8 in.

1/16 in.

1-1/2 in.

1 in.

1/2 in.

1/4 in.
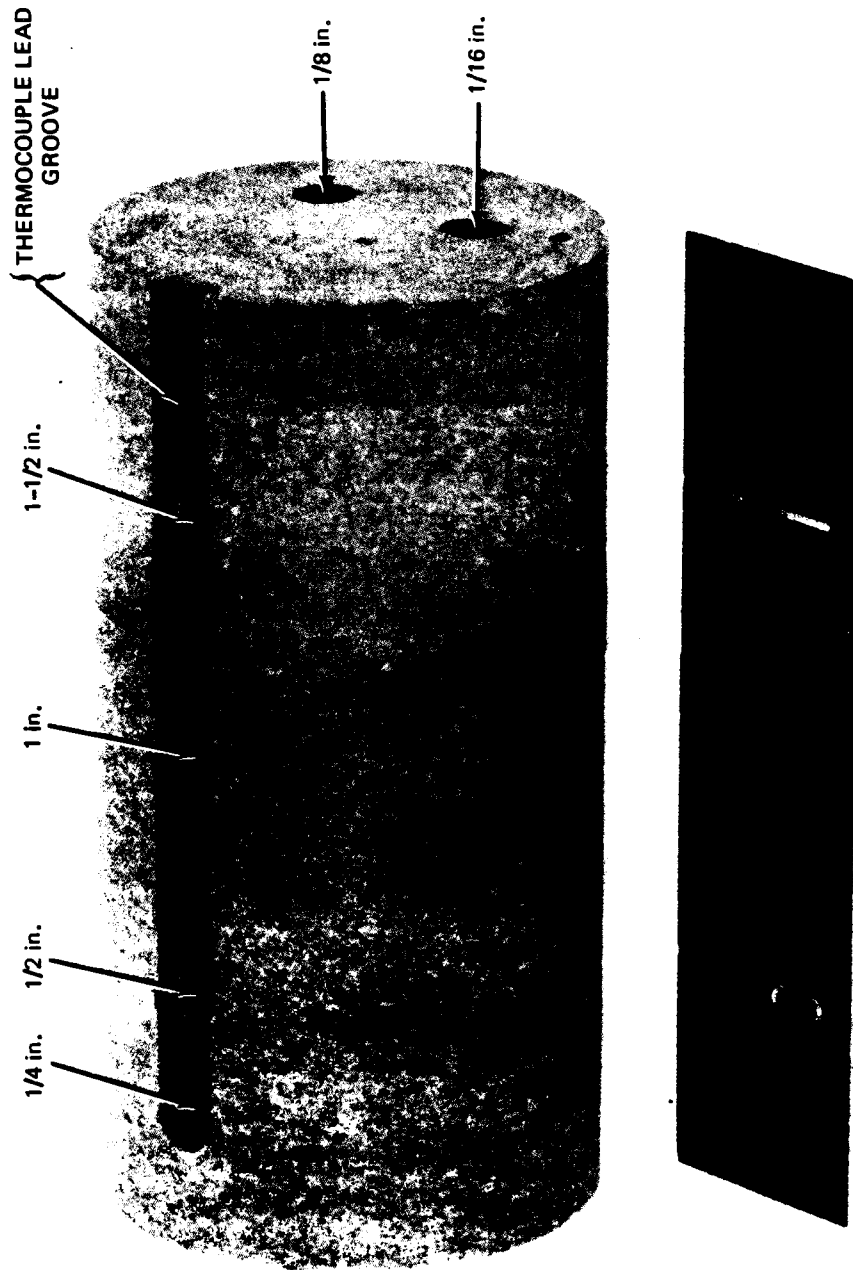
Figure 5.5. DE-370 cylinder test specimen for measurement of substrate temperatures at indicated depths from front face.

Since knowledge of exact thermocouple location was necessary for accurate temperature profile predictions, all cylindrical specimens were x-rayed to pinpoint thermocouple junction locations. Actual thermocouple depths for each specimen are found in Table 5.1. As is evident from the data in the table, actual and assumed locations differed quite dramatically in several instances, justifying the need for exact depth measurement using x-ray techniques. The most noticeable deviations from assumed locations occurred at the 1/16- and 1/8-inch thermocouple locations. Because of the erratic data obtained at these thermocouple locations, due primarily to actual junction depth, poor contact between thermocouple and test material and possible geometric effects, the only data retained for correlation with the computer simulation model were those recorded at the centerline thermocouple locations (1/4-, 1/2-, 1-, and 1-1/2 inch depths).

5.3.3 Surface Temperature Specimen

The surface temperature specimen is a 1-inch thick, 6-inch diameter cylindrical slab, as illustrated in Figure 5.6. There were no thermocouples implanted in this specimen nor on the back, the only measurement of concern being the surface temperature. The flat front face of the specimen was aligned normal to the incident heat flux.

5.4 Thermal Evaluation Testing

The screening environment used in the evaluation program consisted of a 10 Btu/ft^2-s heat flux generated by a vertical bank of nine 500-watt quartz lamps. The incident flux was directed normal to the test specimen surface in all test runs. Test procedures common to the different types of tests shall be discussed here, after which procedures applicable to each specific test shall be delineated.

5.4.1 General Test Procedures

Prior to thermal evaluation testing, the heat flux described above was determined with the water-cooled calorimeter. Centerline

Table 5.1. Cylinder specimen thermocouple locations (distance in inches from front face of specimen).

ACTUAL THERMOCOUPLE LOCATIONS

SPECIMEN # ASSUMED THERMOCOUPLE LOCATION	C-1	C-2	C-3	C-4	C-10	C-11	C-20	C-21	C-30	C-31	C-40	C-41	C-50	C-51	C-60	C-61	C-70	C-71	D-1	D-2
0.0625	0.115*	0.07	0.12*	0.12*	0.10*	0.08*	0.10*	0.045*	0.13*	0.04*	0.04*	0.08*	0.06	0.06	0.08*	0.09*	0.10*	0.32*		
0.125	0.14	0.14	0.18*	0.19*	0.16*	0.17*	0.125	0.13	0.27*	0.135	0.08*	0.10	0.13	0.13	0.10	0.15	0.13	0.40*		
0.250	0.14*	0.20	0.27	0.27	0.22	0.25	0.24	0.20	0.30	0.20	0.17*	0.24	0.24	0.22	0.15*	0.18*	0.17*	0.20		
0.500	0.42	0.46	0.49	0.49	0.50	0.51	0.48	0.44	0.52	0.47	0.41	0.44	0.45	0.46	0.40	0.46	0.41	0.48		
1.000	0.97	0.95	1.00	1.04	1.00	1.00	1.00	0.94	1.00	0.97	1.02	0.98	0.99	1.00	0.96	1.00	0.96	0.96		
1.500	1.45	1.45	1.50	1.58	1.51	1.50	1.54	1.50	1.52	1.48	1.46	1.48	1.50	1.50	1.47	1.48	1.50	1.46		
0.500 right																			0.50	0.47
0.500 center																			0.48	0.47
0.500 left																			0.50	0.47

*More than 20% from assumed thermocouple location

67
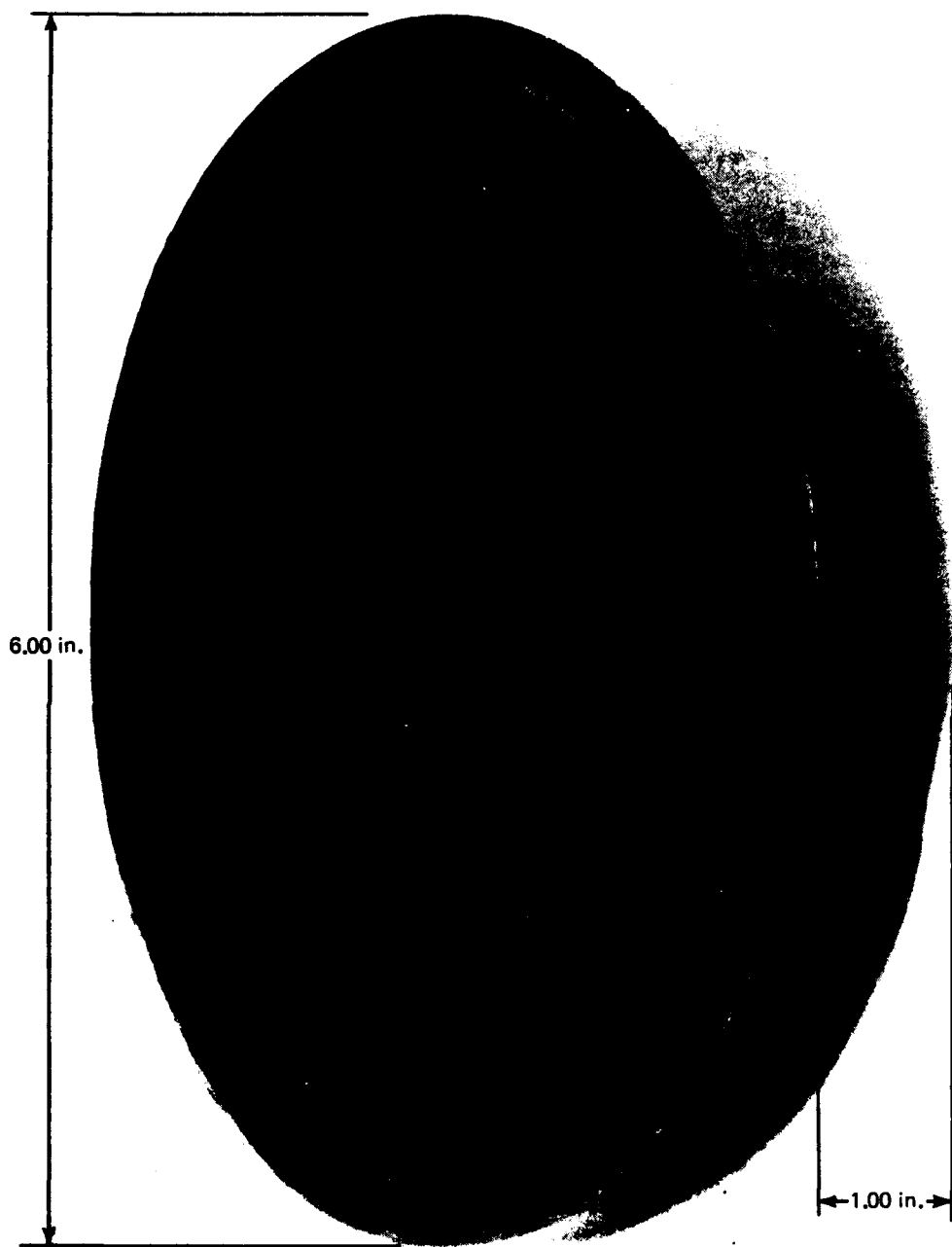
Figure 5.6.   Flexfram specimen for pyrometer surface temperature
            measurements.

68

alignment of the holder assembly with respect to the heat source was maintained by the installed guide rails previously described. The source-to-specimen distance was adjusted to obtain the desired incident heat flux, after which three independent readings were averaged to determine the specific test run heat flux. It proved necessary to take this measurement before each and every test run because of a deleterious effect the pyrolyzing gases had on the lamps.

As the gases percolated to the surface during specimen decomposition, a layer of deposits was formed on both the quartz lamps and the aluminum reflecting plate, causing a noticeable decrease in measured heat flux between pretest and post-test readings. As a result, flux measurements taken before and after each test were averaged to determine the average incident heat flux experienced by the test specimen. After every other test run, the lamp assembly was partially dismantled, and both the lamps and the aluminum reflecting plate were thoroughly cleaned to remove the built-up decomposition products deposited during testing.

Prior to insertion into its holder, each test specimen was measured to determine initial weight and linear dimensions. Once the specimen was mounted in place, thermocouple leads were shielded from the radiant heat using portable insulation and then connected to temperature recorders. Initial thermocouple temperatures, as well as ambient temperature, were recorded and the timer initialized.

During all test runs, it was necessary to ensure the ventilated hood was in operation due to generation of rancid, and possibly toxic byproducts formed when each insulating material decomposed. All temperatures were monitored continuously for a minimum period of 1800 seconds.

Upon completion of thermal testing, each specimen was carefully removed from its holder to ensure the fragile char would remain intact. Post-test weights and dimensions were recorded to determine mass loss and surface expansion/recession. Finally, visual observations pertinent to the specimen test were recorded, and burned specimens photographed.

Specific test procedures tailored to meet the needs of each specimen type shall be described in the pages to follow.

5.4.2 2 × 2 × 0.250-inch Panel Test Specimen

After completing the test-run-heat-flux calibration, the calorimeter was removed from the asbestos holder, and the panel specimen inserted. After passing the thermocouple leads through the holder, insulation plugs were inserted behind the specimen to block any radiant heat flux incident to the specimen backface which would have created erroneous temperature measurements.

Test specimens were then subjected to a heat flux of approximately 10 Btu/ft^2-s for a 45-second period, resulting in a time-integrated heat input of 450 Btu/ft^2. Backface temperature was monitored on both the digital thermometer and the strip chart recorder for a period of 1800 seconds. Specimen weight and physical dimensions were measured and recorded upon completion of testing. Experimental test run data are presented and evaluated in Chapter 6.

5.4.3 Cylinder Test Specimen

After removal of the calorimeter assembly, the cylinder specimen and holder were mounted at the prescribed distance from the heat source to obtain the desired incident flux. The cylinder backface was insulated to eliminate incident flux at locations other than the front face of the specimen.

All cylinder tests were run using specimen holders of the same material as the test sample in order to achieve one-dimensional heat flow through the specimen.

To test the one-dimensionality of the cylinder specimen under observation, two special test cylinders were fabricated to specifications shown in Figure 5.7. Three thermocouples were mounted at a common depth from the front surface, 0.5 inch, across the diameter of the cylinder.

70
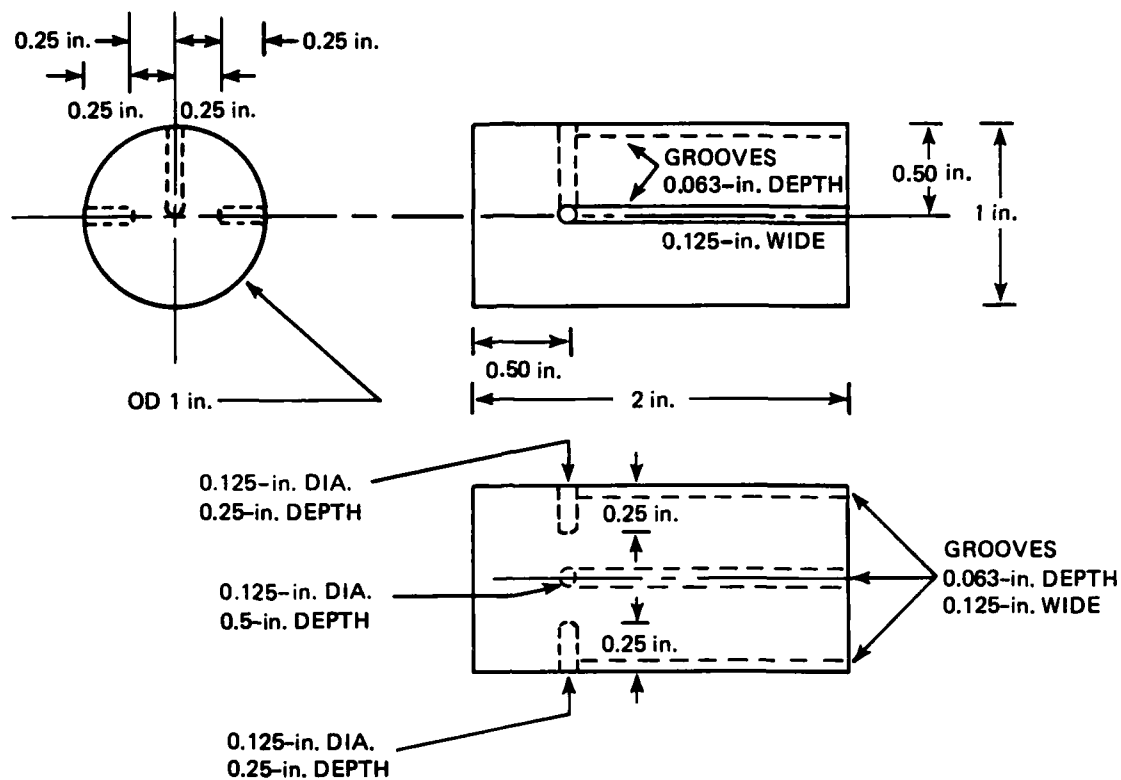
Figure 5.7. One-dimensional heat flow test specimen.

One test was conducted under a 200-second burn condition using a fiber-board insulation holder; (Figure 5.8), the results of the temperature-time traces appear in Figure 5.9. Temperature-time profiles of a similar test, using instead a holder of the same material as the test specimen, Figure 5.10, are plotted in Figure 5.11. Comparison of Figures 5.9 and 5.11 shows clearly the deviation (3.45% at peak) from one-dimensionality of the first test using the fiberboard holder, and the reasons for the selection of holders of identical material to the test specimen for subsequent evaluations.

Cylinder substrate temperatures were monitored on both the digital thermometer and the 24-channel strip chart recorder for a period of

71
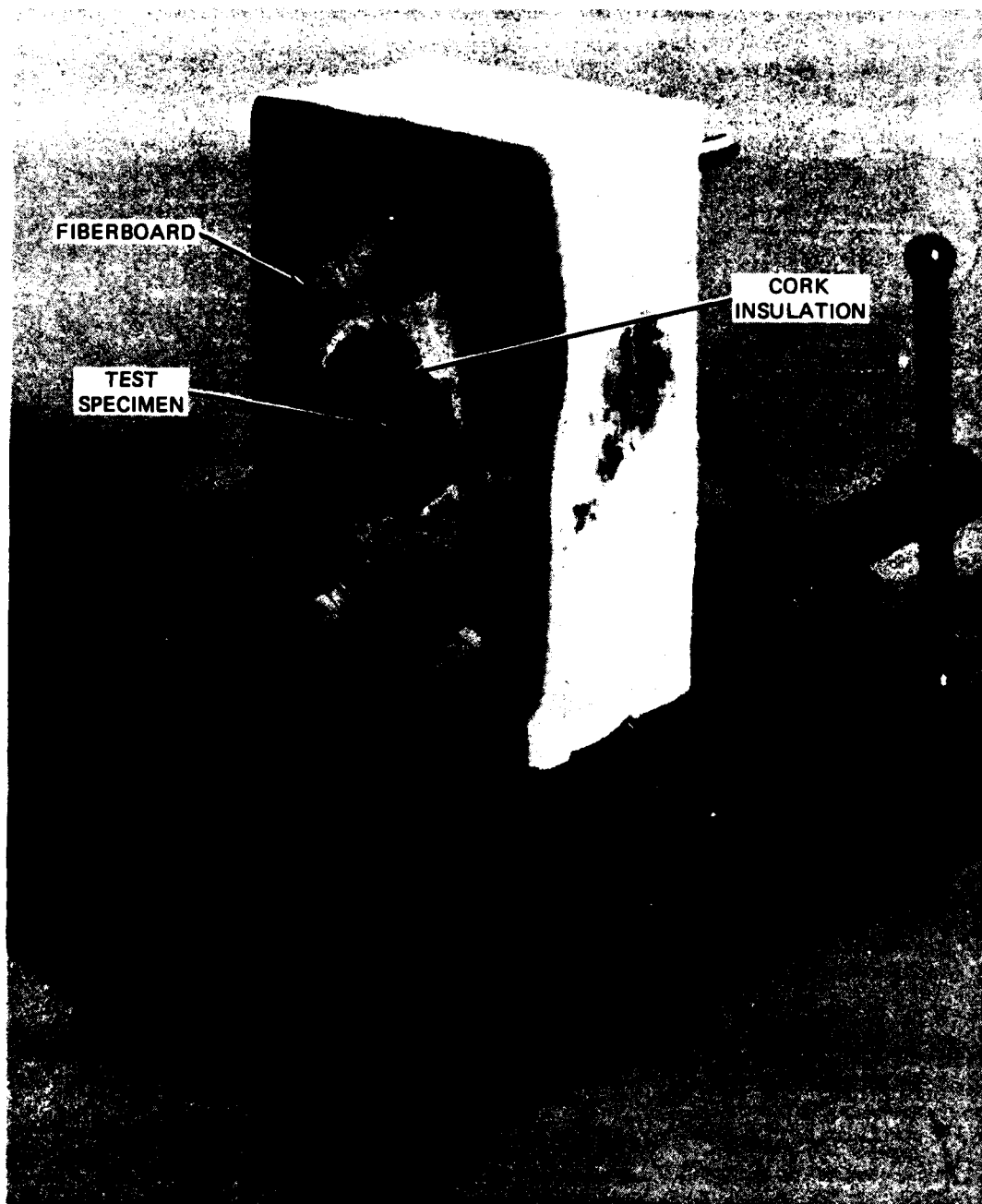
Figure 5.8. Cylinder test specimen mounted in fiberboard holder.
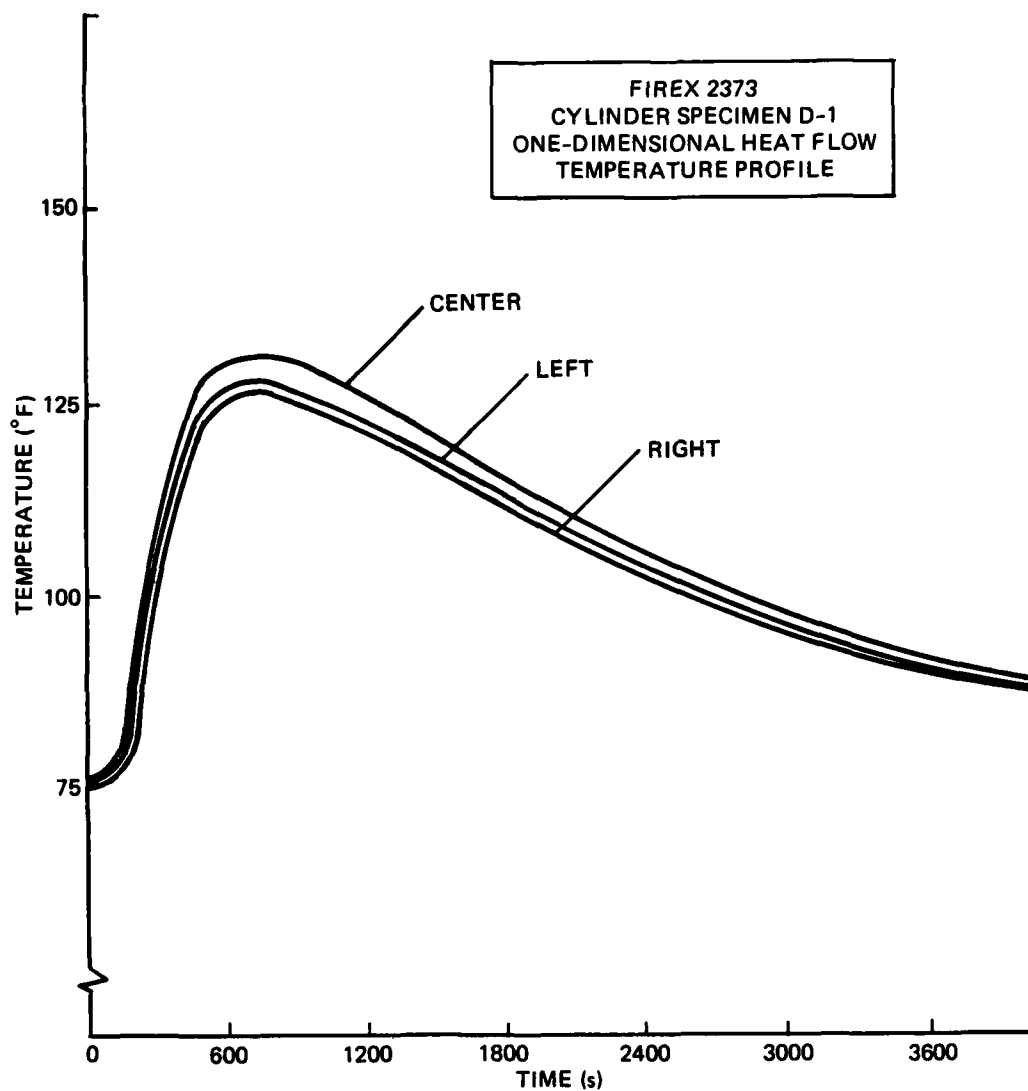
Figure 5.9. Experimental temperature profiles for Firex 2373 one-
dimensional heat flow cylinder specimen D-1, thermo-
couple depths 0.5 in. across diameter at locations
indicated, 10 Btu/ft^2-s heat flux, 200-s burn dura-
tion, fiberboard holder.

3000 seconds. A series of tests were conducted on each material under a
45-second burn duration, and another series under a 200-second burn dura-
tion. With incident heat fluxes of approximately 10 Btu/ft^2-s, the two
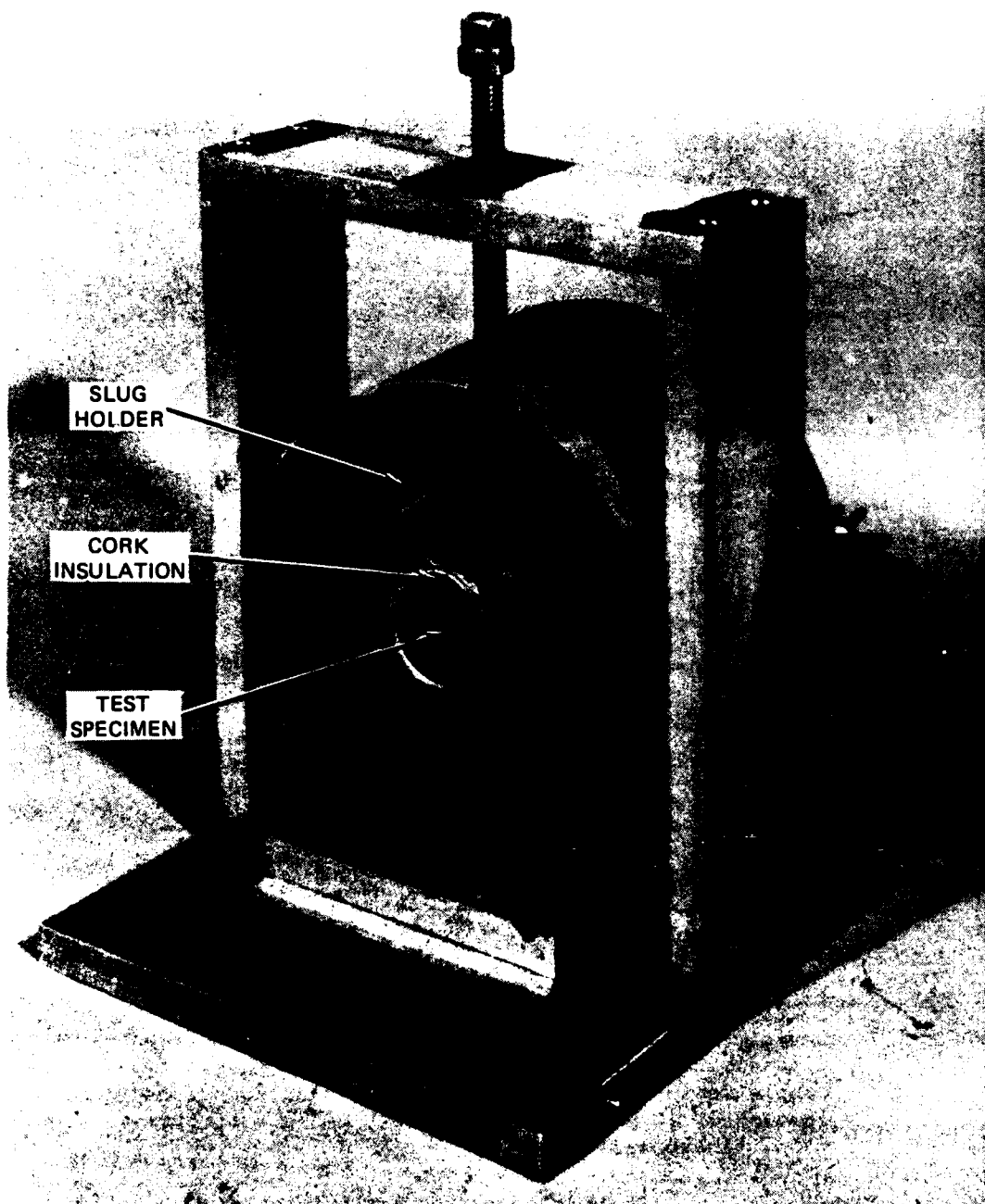
Figure 5.10. Dynatherm DE-370 cylinder specimen mounted in slug holder of identical material.

FIREX 2373
CYLINDER SPECIMEN D-2
ONE-DIMENSIONAL HEAT FLOW
TEMPERATURE PROFILE

LEFT,RIGHT,CENTER
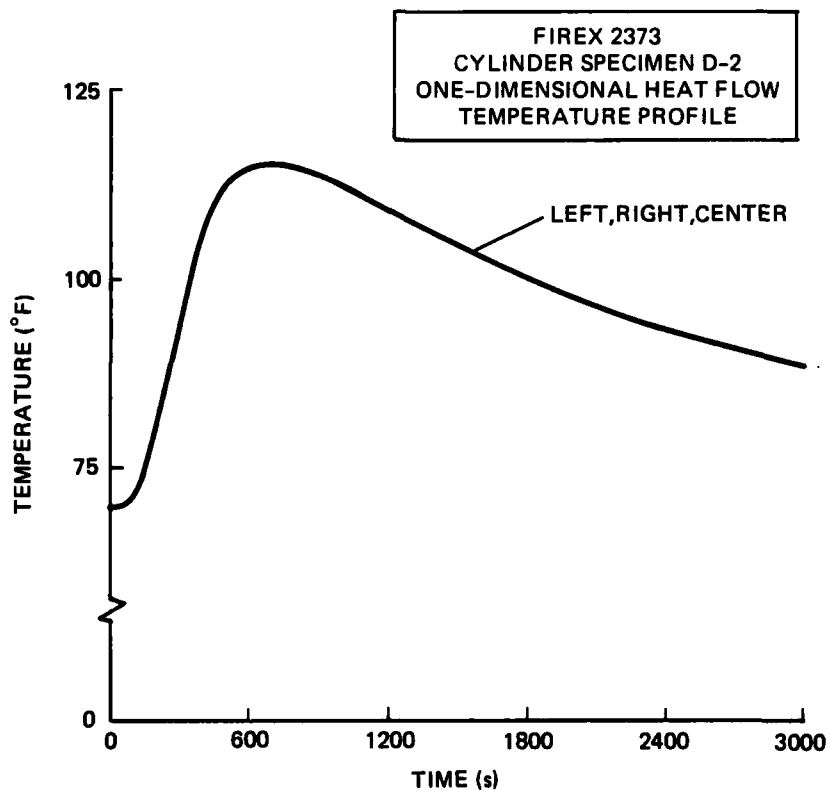
Figure 5.11. Experimental temperature profiles for Firex 2373 one-
dimensional heat flow, cylinder specimen D-2, thermo-
couple depths 0.5 in. across diameter at locations
indicated, 10 Btu/ft^2-s heat flux, 200-s burn duration,
Firex 2373 slug holder.

tests yielded time integrated heat fluxes of 450 and 2000 Btu/ft^2, re-
spectively. Specimen physical dimensions were measured and recorded
upon completion of testing. Experimental test run data are presented in
the following chapter.

5. .4 Surface Temperature Specimen

After heat flux calibration was accomplished, the surface temp-
erature specimen was mounted normal to the lamp assembly, at the prescribed

distance from the heat source to obtain the desired 10 Btu/ft^2-s incident flux. Surface temperatures were monitored continuously for a period of 300 seconds using the Omegascope^{TM} OS-2000A infrared pyrometer.

As the test setup depicted in Figure 5.12 illustrates, the pyrometer-to-specimen distance was maintained at the focal distance, 39 inches, and the pyrometer was aligned at a 45° angle to the specimen surface. Surface temperature measurements are independent of the angle between the axis line-of-sight and the target as long as the target fills the projected field-of-view. The minimum target size required to fill the 99-percent energy cone field-of-view was thus determined from the geometry of the setup (see Figure 3.6 of Reference 11). For a 45° target angle at the 39-inch focal distance, the area being measured is an ellipse 2.60 × 3.68 inches.

Short Axis: 2.60 inches

Long Axis: $\dfrac{2.60 \text{ in.}}{\sin 45°}$ = 3.68 inches

Therefore, the 6-inch diameter specimen previously described is easily large enough to accommodate the entire target area required.

Surface temperature test runs were conducted on each material to obtain data to be correlated with the STAB II computer simulation model predictions. Each test specimen was subjected to an approximate heat flux of 10 Btu/ft^2-s for a 45-second burn duration, resulting in an integrated heat input of 450 Btu/ft^2. An assumed emissivity of 0.95 was input to the Omegascope^{TM} microprocessor for computation of the surface temperature. Experimental test run data are presented in the following chapter.
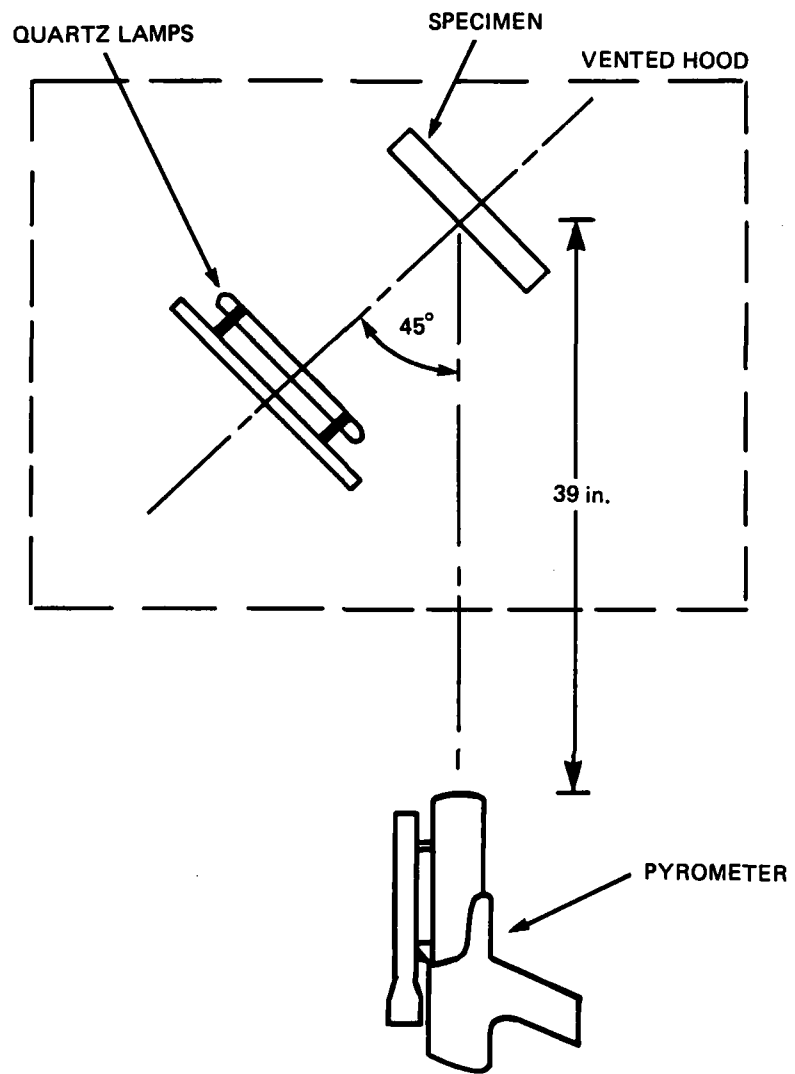
Figure 5.12.   Equipment arrangement for surface temperature
              measurements (overhead view).

77

CHAPTER 6

EXPERIMENTAL RESULTS

6.1   Introduction

The experimental results of the various tests conducted are in-
tended to lead to the logical selection of the most promising ablative
material, of the candidates available, for use in the specifically defined,
low heat flux environment. Thermal insulation performance is the govern-
ing factor in choice of ablator, although various other quantitative and
qualitative observations have an effect on the final decision.

Many of the data tables and figures presented later in the chapter
and in the appendices are based on:

(1)   Temperatures and temperature rates read directly from
traces obtained during testing.

(2)   Physical specimen measurements and observations recorded
before and after each individual test run.

(3)   Various calculations designed to lend a quantitative basis
to the material selection process.

Clarification of specific data reduction techniques shall be discussed,
where appropriate, in the sections to follow.

6.2   Panel Specimen Tests

6.2.1 Purpose

The primary goal of the panel tests was to obtain a relative ranking of the materials, based on several performance criteria, including

(1)   Maximum backface temperature rise.

(2)   Time to reach an indicated temperature level (e.g., 150°F).

(3)   Thermophysical material properties.

(4)   Analytically determined performance indices.

6.2.2 Preliminary Calculations

6.2.2.1 Mass Flux Transfer Rate

The mass transfer is equal to the difference between initial mass and final mass, divided by the test duration. The mass transfer rate is further divided by the exposed surface area to give the mass flux transfer as

$$\dot{m} \;=\; (\omega_i - \omega_f)/tA \;\left(\frac{lbm}{ft^2\text{-}s}\right) \tag{6-1}$$

where

ω_i = initial specimen weight, lbm

ω_f = final specimen weight, lbm

A = exposed surface area of specimen, ft^2

t = time, s

6.2.2.2 Cold-Wall Heat of Ablation

The cold-wall heat of ablation is defined as the incident cold-wall heat dissipated per unit mass of material ablated, as follows

79

$$Q^{*}_{cw} \ = \ \dot{q}_{cw/\dot{m}} \quad (Btu/lbm) \qquad\qquad (6\text{-}2)$$

where

$\dot{q}_{cw}$ = heat transfer rate from the test environment to a
cold wall, $Btu/ft^{s}\text{-}s$

$\dot{m}$ = total mass flux transfer, $lbm/ft^{2}\text{-}s$

6.2.3 Test Data and Results

6.2.3.1 General

Tables A-1 through A-12 of Appendix A contain all pertinent data related to each individual test run, categorized by material type. Backface temperature histories for each panel specimen tested are illustrated in Figures C-1 through C-12 of Appendix C, grouped again by material type. Close inspection of the temperature-time traces for a given material indicates a relatively high degree of reproducibility of data.

6.2.3.2 Temperatures

A summary of the panel specimen temperature measurements is presented in Table 6.1. Upon averaging values in this table for each specimen type, a relative performance ranking is obtained for each thermal parameter listed. As Table 6.2 illustrates, the materials can be ranked, based on their thermal performance, from 1, indicating best performer, to 10, indicating worst performer. In this particular ranking scheme, Firex easily outdistanced the competition by sweeping top honors in all four categories.

This observation is further corroborated by the data presented in Figure 6.1, a collective plot of representative temperature histories selected for each material from the figures of Appendix C. It is easily seen that Firex not only experiences a much lower maximum backface temperature rise than all others, but also takes on the order of twice as long to reach that peak.

80

Table 6.1. Summary of panel specimen temperature measurements.

Material	Sample Number	Heat Flux (Btu/ft^2-s)	Maximum Backface Temp. (°F)	Time to Max. Backface Temp. (s)	$(\frac{dT}{dt})_{t=45}$ (°F/s)	$(\frac{dT}{dt})_{t=100}$ (°F/s)
FLEXFRAM	4	10.11	266.8	132	1.85	0.85
FLEXFRAM	5	9.95	272.4	135	2.72	0.86
FLEXFRAM	217	9.97	291.4	125	2.78	0.82
FIREX	7	10.2	143.8	177	1.11	0.67
FIREX	8	10.09	149.4	195	0.88	0.47
FIREX	9	10.06	148.4	195	0.83	0.49
FIREX	11	10.04	153.8	190	0.71	0.10
FIREX	27	10.2	152.6	260	1.03	0.13
FIREX	29	10.2	143.4	280	0.89	0.45
FIREX	39	9.58	148.0	240	1.03	0.39
FIREX	40	9.58	149.0	300	1.10	0.54
FIREX	201	9.95	158.6	186	0.83	0.31
FIREX	202	9.85	150.0	195	1.04	0.36
FIREX	205	10.0	150.0	128	0.79	0.21
FIREX[1]	32	9.9	145.0	195	0.78	0.49
FIREX[1]	33	10.0	143.0	210	0.78	0.43
FIREX[1]	36	9.95	145.2	145	0.93	0.20
FIBERFRAX	14	10.04	224.6	120	2.08	0.59
FIBERFRAX	17	9.9	219.2	110	2.17	0.33
DE-370	103	10.13	230.8	155	1.98	0.67
DE-370	218	9.95	242.8	135	2.40	0.63
DE-370	220	10.27	247.2	120	2.50	0.67
DE-350	107	10.13	244.0	115	1.69	0.22
DE-350	221	9.96	211.2	170	0.87	0.36
DE-350	224	9.97	221.6	150	1.37	0.69
S-886	152	10.16	250.0	155	1.45	1.63
S-886	153	10.29	251.8	173	1.21	1.54

Table 6.1. Summary of panel specimen temperature measurements. (Continued)

Material	Sample Number	Heat Flux (Btu/ft^2-s)	Maximum Backface Temp. (°F)	Time to Max. Backface Temp. (s)	$(\frac{dT}{dt})_{t=45}$ (°F/s)	$(\frac{dT}{dt})_{t=100}$ (°F/s)
S-885	135	9.95	185.0	180	0.87	0.80
S-885	213	10.09	214.0	135	1.33	1.09
S-885	215	9.95	203.6	145	1.26	1.11
CHARTEK	148	10.0	193.0	155	1.33	0.99
CHARTEK	210	10.19	193.6	150	1.36	0.51
CHARTEK	211	9.99	197.0	165	1.43	0.75
1600B	112	10.04	205.0	188	1.17	0.99
1600B	114	10.0	227.8	125	—	0.47
1600B	117	10.0	231.8	135	1.45	0.85
CORK[2]	47	10.19	236.4	144	2.66	0.45
CORK[2]	54	9.95	220.0	145	1.53	1.01
CORK[2]	62	9.96	228.6	140	1.95	0.58
FIREX[2]	306	10.06	140.0	280	0.74	0.43
FIREX[2]	307	10.06	140.8	300	0.79	0.45
FIREX[2]	308	10.0	139.5	290	0.74	0.47

Notes: (1) FIREX specimens coated with environmental vinyloid topcoat.

(2) Specimens with no aluminum backplate.

Table 6.2 Relative ranking of panel specimen materials using temperature-based indices.

Material	$T_{BF_{max}}$ (°F)	$t_{T_{max}}$ (s)	$\dfrac{dT}{dt}$ t=45 (°F/s)	$\dfrac{dT}{dt}$ t=100 (°F/s)
Firex	1	1	1	1
Flexfram	10	9	10	8
Fiberfrax	5	10	8	3
DE-350	6	6	4	2
DE-370	8	8	9	4
S-885	3	4	2	9
S-886	9	2	5	10
Chartek	2	3	6	6
1600B	4	5	3	7
Cork	7	7	7	5

Data tables in Appendix A were further reduced, using the simplified calculations detailed in Section 6.2.2, to obtain cold-wall heat of ablation values. These values appear in Table 6.3 for each material test specimen.

FLEXFRAM (5)
S-886 (153)
DE-370 (218)
DE-350 (224)
1600B (112)
CHARTEK (211)
CORK^2 (62)
FIBERFRAX (17)
S-885 (215)
FIREX (27)
FIREX^1 (32)
FIREX^2 (307)

TEMPERATURE (°F)
TIME (s)
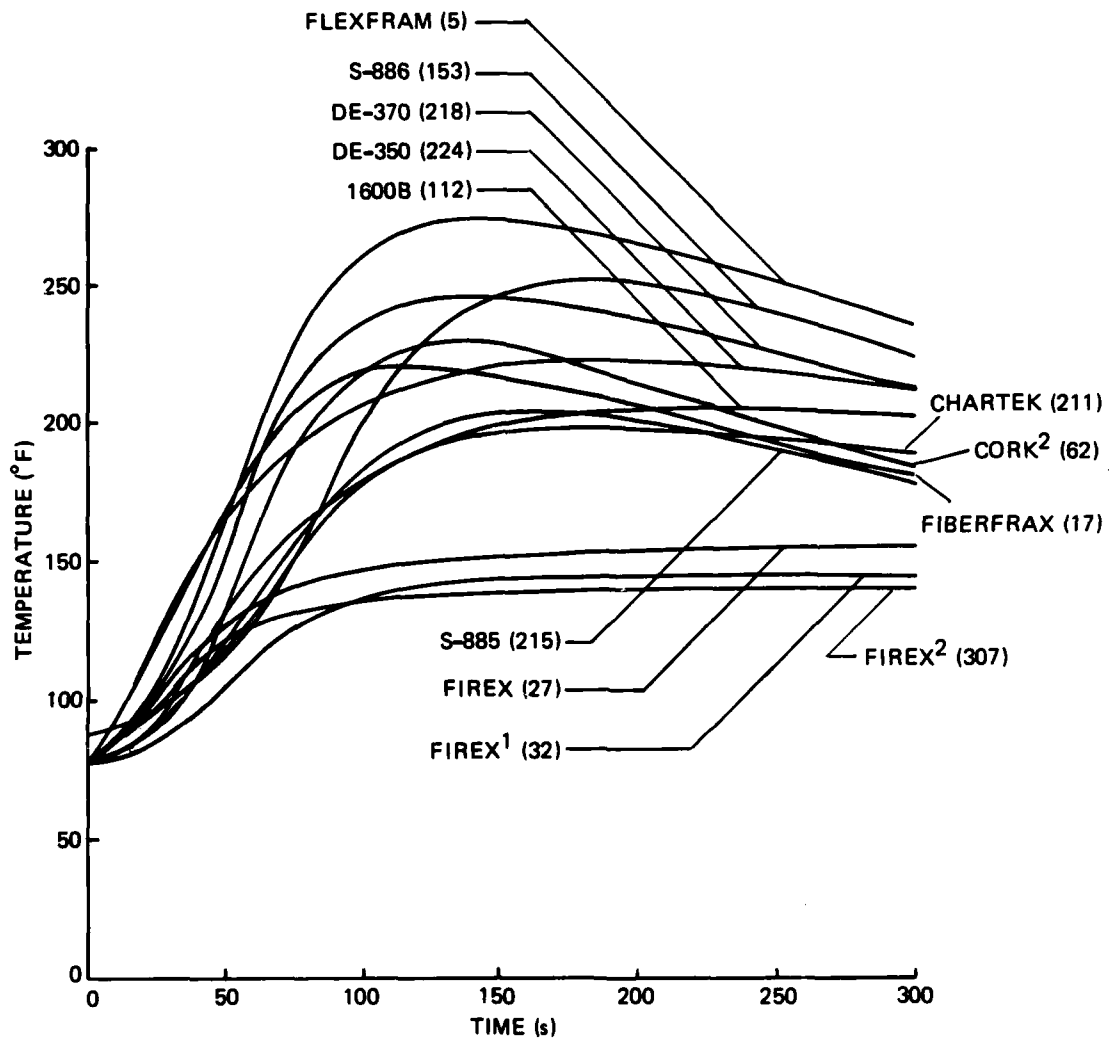
NOTES: (1)   FIREX WITH VINYLOID COATING.
        (2)   SPECIMENS WITHOUT ALUMINUM BACKPLATE.

Figure 6.1.   Panel specimen backface temperature responses for
              all materials tested.   (XXX) indicates specimen number.

Table 6.3. Summary of cold-wall heats of ablation.

Material	Sample Number	Cold-wall Heat Flux (Btu/ft^2-s)	Mass Flux Transfer Rate (lbm/ft^2-s)	Cold-Wall Heat of Ablation (Btu/lbm)
FLEXFRAM	4	10.11	2.98×10^{-3}	3.39×10^{3}
FLEXFRAM	5	9.95	2.94×10^{-3}	3.39×10^{3}
FLEXFRAM	217	9.97	2.87×10^{-3}	3.47×10^{3}
FIREX	7	10.2	1.11×10^{-3}	9.17×10^{3}
FIREX	8	10.09	1.27×10^{-3}	7.94×10^{3}
FIREX	9	10.06	1.26×10^{-3}	7.98×10^{3}
FIREX	11	10.04	9.28×10^{-4}	1.08×10^{4}
FIREX	27	10.2	2.01×10^{-3}	5.07×10^{3}
FIREX	29	10.2	1.44×10^{-3}	7.09×10^{3}
FIREX	39	9.58	1.22×10^{-3}	7.86×10^{3}
FIREX	40	9.58	9.82×10^{-4}	9.76×10^{3}
FIREX	201	9.95	2.51×10^{-3}	3.96×10^{3}
FIREX	202	9.85	2.34×10^{-3}	4.20×10^{3}
FIREX	205	10.0	1.63×10^{-3}	6.14×10^{3}
FIREX[1]	32	9.9	2.76×10^{-3}	3.59×10^{3}
FIREX[1]	33	10.0	2.87×10^{-3}	3.48×10^{3}
FIREX[1]	36	9.95	2.58×10^{-3}	3.85×10^{3}
FIBERFRAX	14	10.04	9.22×10^{-5}	1.09×10^{5}
FIBERFRAX	17	9.9	8.66×10^{-5}	1.14×10^{5}
DE-370	103	10.13	2.02×10^{-3}	5.03×10^{3}
DE-370	218	9.95	1.95×10^{-3}	5.10×10^{3}
DE-370	220	10.27	2.25×10^{-3}	4.56×10^{3}
DE-350	107	10.13	9.97×10^{-4}	1.02×10^{4}
DE-350	221	9.96	1.05×10^{-3}	9.50×10^{3}
DE-350	224	9.97	1.11×10^{-3}	8.99×10^{3}
S-886	152	10.16	3.19×10^{-3}	3.18×10^{3}

Table 6.3. Summary of cold-wall heats of ablation. (Continued)

Material	Sample Number	Cold-Wall Heat Flux (Btu/ft^2-s)	Mass Flux Transfer Rate (lbm/ft^2-s)	Cold-Wall Heat of Ablation (Btu-lbm)
S-886	153	10.29	3.91×10^{-3}	2.63×10^{3}
S-885	135	9.95	2.38×10^{-5}	4.18×10^{5}
S-885	213	10.09	3.77×10^{-5}	2.67×10^{5}
S-885	215	9.95	3.39×10^{-5}	2.94×10^{5}
CHARTEK	148	10.0	6.43×10^{-4}	1.55×10^{4}
CHARTEK	210	10.19	9.75×10^{-4}	1.05×10^{4}
CHARTEK	211	9.99	8.74×10^{-4}	1.14×10^{4}
1600B	112	10.04	2.79×10^{-3}	3.59×10^{3}
1600B	114	10.0	1.77×10^{-3}	5.66×10^{3}
1600B	117	10.0	2.48×10^{-3}	4.04×10^{3}
CORK[2]	47	10.19	2.43×10^{-3}	4.20×10^{3}
CORK[2]	54	9.95	2.33×10^{-3}	4.28×10^{3}
CORK[2]	62	9.96	2.48×10^{-3}	4.02×10^{3}
FIREX[2]	306	10.06	1.75×10^{-3}	5.75×10^{3}
FIREX[2]	307	10.06	1.33×10^{-3}	7.56×10^{3}
FIREX[2]	308	10.0	1.40×10^{-3}	7.13×10^{3}

NOTES: (1) FIREX specimens coated with environmental vinyloid topcoat.

(2) Specimens with no aluminum backplate.

6.2.3.3 Weights

Before and after each test run, samples were weighed to deter-
mine weight loss for the mass flux rate calculation. Table 6.4 contains
a summary of weight measurements taken on all test specimens. This
data is further reduced to a percentage weight loss summary, by material
type, as illustrated in Figure 6.2.
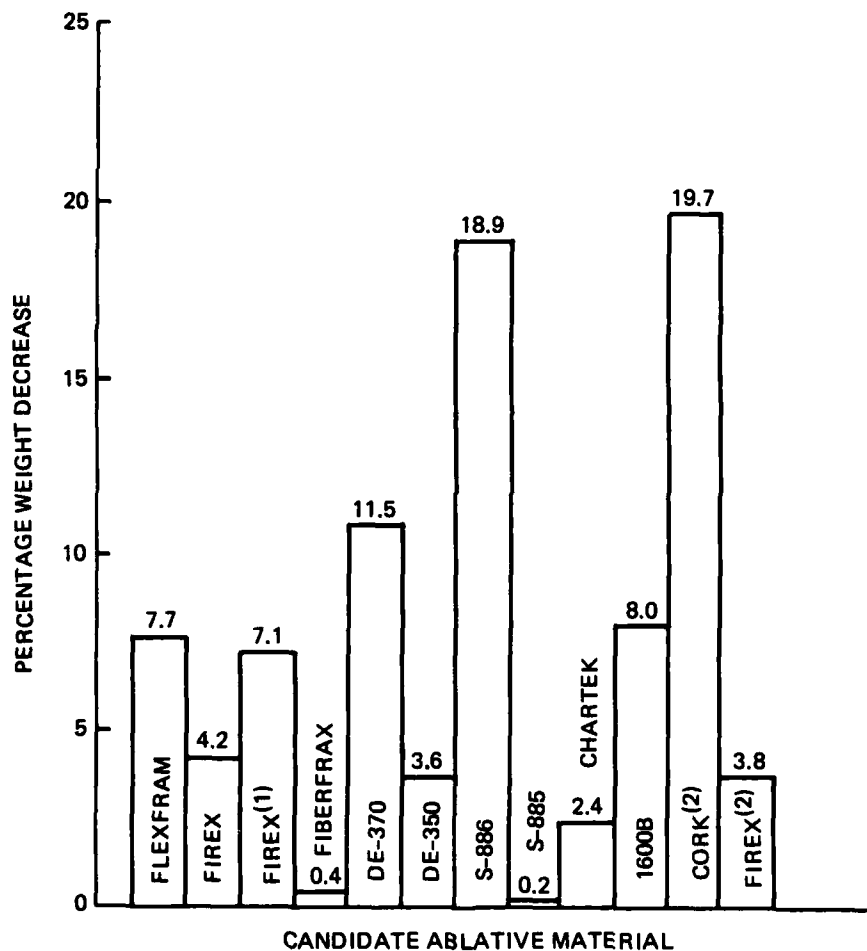

NOTES: (1) FIREX SPECIMENS COATED WITH ENVIRONMENTAL VINYLOID TOPCOAT
          (2) SPECIMENS WITH NO ALUMINUM BACKPLATE

Figure 6.2. Average panel specimen weight changes.

87

Table 6.4. Summary of panel specimen weight measurements.

Material	Sample Number	Initial Weight (grams)	Final Weight (grams)	Weight Decrease (grams)	% Weight Decrease
FLEXFRAM	4	24.5158	22.8248	1.6910	7.78
FLEXFRAM	5	24.7802	23.1157	1.6645	7.56
FLEXFRAM	217	23.6472	22.0179	1.6293	7.85
FIREX	7	23.6093	22.9788	0.6305	3.03
FIREX	8	22.9693	22.2486	0.7207	3.57
FIREX	9	22.9569	22.2424	0.7145	3.54
FIREX	11	22.0985	21.5723	0.5262	2.72
FIREX	27	24.6310	23.4905	1.1405	5.23
FIREX	29	26.2151	25.4000	0.8151	3.85
FIREX	39	26.4322	25.7404	0.6918	2.93
FIREX	40	26.1463	25.5898	0.5565	2.39
FIREX	201	22.0273	20.6029	1.4244	7.44
FIREX	202	22.5123	21.1838	1.3285	6.77
FIREX	205	22.7436	21.8199	0.9237	4.65
FIREX[1]	32	23.6003	22.0366	1.5637	7.55
FIREX[1]	33	25.6876	24.0577	1.6299	7.15
FIREX[1]	36	24.8818	23.4170	1.4648	6.64
FIBERFRAX	14	14.6609	14.6086	0.0523	0.44
FIBERFRAX	17	15.8745	15.8254	0.0491	0.38
DE-370	103	13.6350	12.4919	1.1431	10.65
DE-370	218	12.6231	11.5178	1.1053	11.35
DE-370	220	13.0393	11.7611	1.2782	12.58
DE-350	107	17.5640	16.9986	0.5654	3.85
DE-350	221	19.7778	19.1836	0.5942	3.52
DE-350	224	21.1081	20.4797	0.6284	3.45
S-886	152	13.1745	11.3602	1.8143	17.61
S-886	153	13.7524	11.5345	2.2179	20.39

Table 6.4. Summary of panel specimen weight measurements. (Continued)

Material	Sample Number	Initial Weight (grams)	Final Weight (grams)	Weight Decrease (grams)	% Weight Decrease
S-885	135	13.0628	13.0493	0.0135	0.13
S-885	213	13.2236	13.2022	0.0214	0.21
S-885	215	12.8245	12.8053	0.0192	0.19
CHARTEK	148	21.9827	21.6179	0.3648	1.90
CHARTEK	210	22.8113	22.2583	0.5330	2.77
CHARTEK	211	22.1824	21.6866	0.4958	2.57
1600B	112	21.3202	19.7380	1.5822	8.59
1600B	114	18.9762	17.9750	1.0012	6.21
1600B	117	18.1241	16.7192	1.4049	9.21
CORK[2]	47	6.8624	5.4865	1.3759	20.05
CORK[2]	54	6.9440	5.6249	1.3191	18.99
CORK[2]	62	7.0109	5.6070	1.4039	20.02
FIREX[2]	306	21.1367	20.1447	0.9920	4.69
FIREX[2]	307	21.1726	20.4178	0.7548	3.57
FIREX[2]	308	24.7692	23.9738	0.7954	3.21

NOTES: (1) FIREX specimens coated with environmental vinyloid topcoat.

(2) Specimens with no aluminum backplate.

6.2.3.4 Thicknesses

Pretest and post-test thickness measurements were also taken on each specimen, the data appearing in Table 6.5. This data is further simplified to a percentage thickness increase summary, by material type, as depicted in Figure 6.3. It is noted that Firex and 1600B show a very large thickness change because of their intumescent nature of swelling upon heating. This swelling is indicative of good thermal protection for an intumescent ablator. It is further noted that Flexfram and Chartek, although also being intumescents, experienced thickness changes of the same order of magnitude as the charring ablators, suggesting only minor intumescence.

6.3   Cylinder Specimen Tests

6.3.1 Purpose

The primary purpose of the cylinder tests was to provide in-depth, one-dimensional heat flow temperature histories of all materials for direct correlation of data with computed values obtained from an analytical simulation model.

6.3.2 Test Data and Results

6.3.2.1 General

Tables B-2 through B-9 of Appendix B contain all experimental data pertinent to each individual test run. Substrate temperature histories at depths of 1/4-, 1/2-, 1-, and 1-1/2 inches for each cylinder specimen are illustrated in Appendix D, Figures D-1 through D-10, for 200-second burn duration tests, and in Appendix E, Figures E-1 through E-8, for 45-second burn duration tests.

Table 6.5. Summary of panel specimen dimensions.

Material	Sample Number	Initial Thickness (inches)	Final Thickness (inches)	Thickness Increase (inches)	% Thickness Increase
FLEXFRAM	4	0.250	0.284	0.034	13.6
FLEXFRAM	5	0.250	0.284	0.034	13.6
FLEXFRAM	217	0.250	0.276	0.026	10.4
FIREX	7	0.250	0.330	0.080	32.0
FIREX	8	0.250	0.320	0.070	28.0
FIREX	9	0.250	0.323	0.073	29.2
FIREX	11	0.250	0.287	0.037	14.8
FIREX	27	0.250	0.338	0.088	35.4
FIREX	29	0.250	0.349	0.099	39.6
FIREX	39	0.253	0.323	0.070	27.8
FIREX	40	0.254	0.320	0.066	25.9
FIREX	201	0.250	0.284	0.034	13.6
FIREX	202	0.250	0.284	0.034	13.6
FIREX	205	0.250	0.289	0.039	15.6
FIREX[1]	32	0.250	0.344	0.094	37.6
FIREX[1]	33	0.250	0.359	0.109	43.6
FIREX[1]	36	0.250	0.362	0.112	44.8
FIBERFRAX	14	0.250	0.250	0.0	0.0
FIBERFRAX	17	0.250	0.250	0.0	0.0
DE-370	103	0.250	0.279	0.029	11.6
DE-370	218	0.250	0.328	0.078	31.2
DE-370	220	0.250	0.279	0.029	11.6
DE-350	107	0.250	0.250	0.0	0.0
DE-350	221	0.250	0.252	0.002	0.8

Table 6.5. Summary of panel specimen dimensions. (Continued)

Material	Sample Number	Initial Thickness (inches)	Final Thickness (inches)	Thickness Increase (inches)	% Thickness Increase
DE-350	224	0.250	0.268	0.018	7.2
S-886	152	0.250	0.307	0.057	22.8
S-886	153	0.250	0.279	0.029	11.6
S-885	135	0.250	0.250	0.0	0.0
S-885	213	0.250	0.250	0.0	0.0
S-885	215	0.250	0.250	0.0	0.0
CHARTEK	148	0.250	0.292	0.042	16.8
CHARTEK	210	0.250	0.279	0.029	11.6
CHARTEK	211	0.250	0.281	0.031	12.4
1600B	112	0.250	1.813	1.563	625.2
1600B	114	0.250	1.539	1.289	515.6
1600B	117	0.250	1.406	1.156	462.4
CORK[2]	47	0.250	0.281	0.031	12.4
CORK[2]	54	0.250	0.279	0.029	11.6
CORK[2]	62	0.250	0.279	0.029	11.6
FIREX[2]	306	0.250	0.328	0.078	31.2
FIREX[2]	307	0.250	0.324	0.074	29.6
FIREX[2]	308	0.250	0.310	0.060	24.0

NOTES: (1) FIREX specimens coated with environmental vinyloid topcoat.
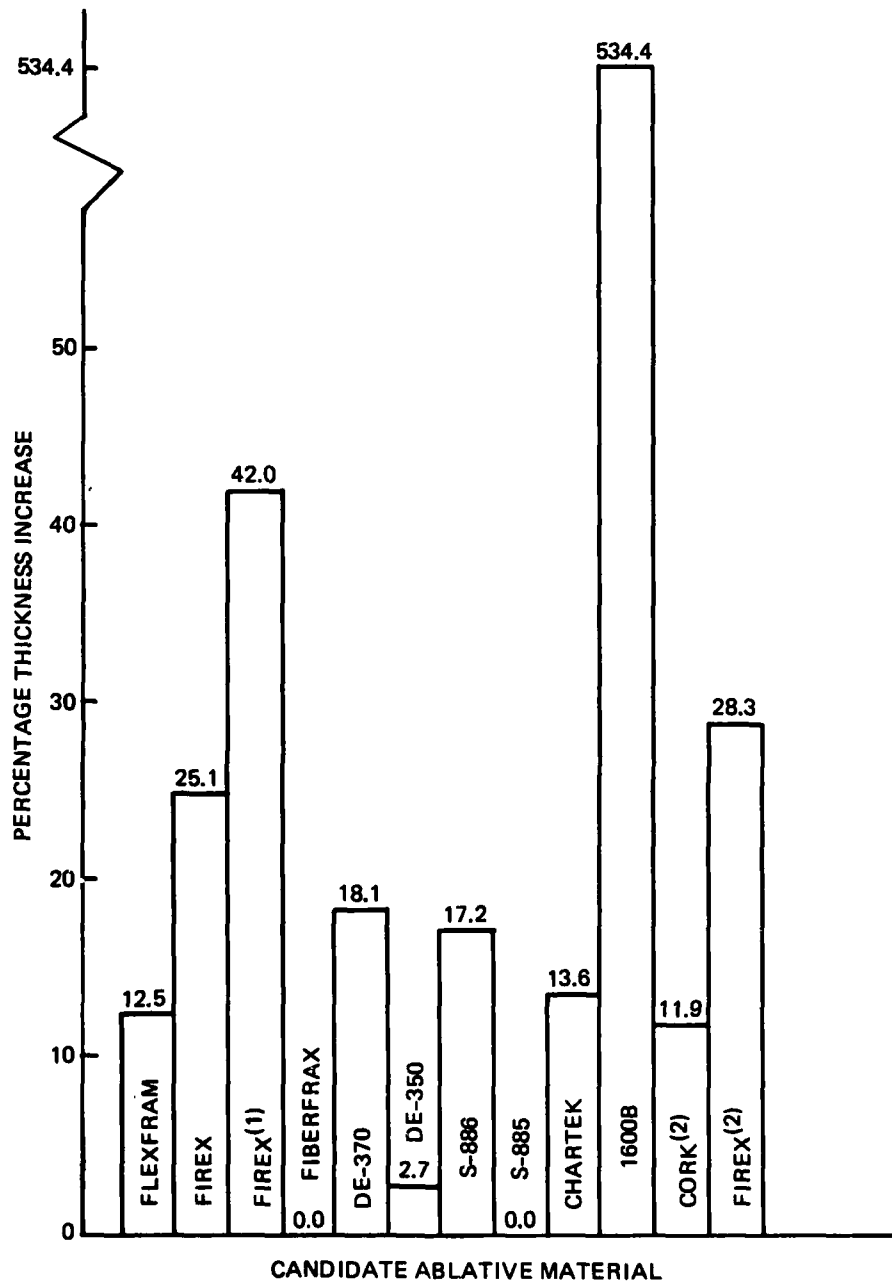
(2) Specimens with no aluminum backplate.

Figure 6.3. Average panel specimen thickness changes.

NOTES: (1) FIREX SPECIMENS COATED WITH ENVIRONMENTAL VINYLOID TOPCOAT
          (2) SPECIMENS WITH NO ALUMINUM BACKPLATE

6.3.2.2 Temperatures

6.3.2.2.1 200-second Burn

A summary of cylinder specimen substrate temperature measurements for the 200-second burn duration tests is presented in Table 6.6. As the data illustrates, Firex outperforms the other materials at the 1/4- and 1/2-inch depths, and although DE-350 experiences a slightly lower temperature rise at the 1- and 1-1/2-inch depths, (1% and 5% difference, respectively), Firex still takes a much longer time to reach that peak (30% and 20% longer, respectively).

6.3.2.2.2 45-second Burn

Table 6.7 contains a similar summary of substrate temperature measurements for the 45-second burn duration test runs. Once again, Firex demonstrates superior thermal protection performance at all substrate measurement points, both in magnitude of temperature rise and in the time required to reach that maximum.

A comparison of experimental versus computed values for a temperature-time trace, at ? inch depth, appears in Figure 6.4 for a Firex sample. As the plot illustrates, good data correlation was obtained for the full time range of 600 seconds, with almost coincident temperature peaks. The computed values were generated using the STAB II computer simulation model previously described in Chapter 2.

6.3.2.3 Lengths

Pretest and post-test length measurements were also taken on each cylinder specimen, the results appearing in Table 6.8. This data is further reduced to the percentage length increase summary found in Figure 6.5. Once again, examination of the data presented here leads to the same conclusion concerning ablator intumescence as previously discussed in Section 6.2.3.4.

Table 6.6. Summary of cylinder specimen substrate temperature measurements (200-s burn duration).

Material	Sample Number	Max. Temp. at 1/4-in. Depth (°F)	Time of Max. Temp. at 1/4-in. Depth (s)	Max. Temp. at 1/2-in. Depth (°F)	Time of Max. Temp. at 1/2-in. Depth (s)	Max. Temp. at 1-in. Depth (°F)	Time of Max. Temp. at 1-in. Depth (s)	Max. Temp. at 1-1/2-in. Depth (°F)	Time of Max. Temp. at 1-1/2-in. Depth (s)
FIREX	C-1	180.0	.00	147.8	840	124.0	1415	111.2	1793
	C-2	158.8	401	129.3	689	106.1	1225	93.9	1667
	C-4	146.0	347	123.0	767	106.6	1903	96.5	2114
DE-350	C-10	199.0	313	150.6	580	111.2	1106	95.4	1526
S-885	C-20	350.4	300	236.2	470	164.7	884	132.3	1175
FLEXFRAM	C-30	280.2	320	204.2	497	146.8	1429	122.2	1850
S-886	C-40	369.0	280	238.8	470	165.0	660	132.5	1083
DE-370	C-51	340.0	265	211.4	476	155.1	1134	125.8	1167
CHARTEK	C-60	243.4	315	189.8	552	147.0	991	123.0	1436
1600B	C-70	258.8	290	189.4	635	142.6	1208	118.0	1706
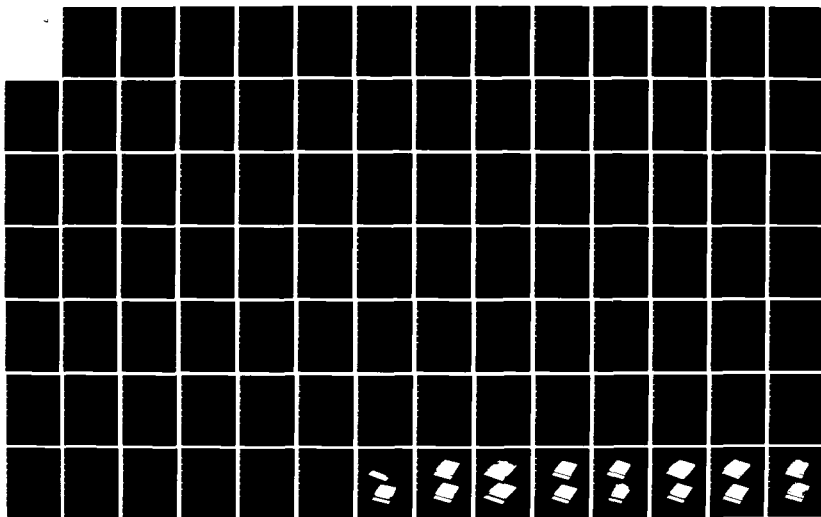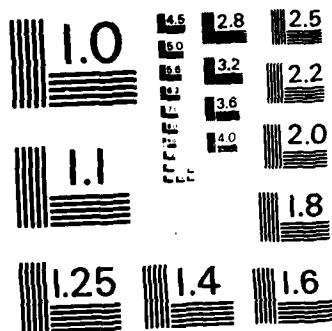
MICROCOPY RESOLUTION TEST CHART

NATIONAL BUREAU OF STANDARDS-1963-A

Table 6.7. Summary of cylinder specimen substrate temperature measurements (45-s burn duration).

Material	Sample Number	Max. Temp. at 1/4-in. Depth (°F)	Time of Max. Temp. at 1/4-in. Depth (s)	Max. Temp. at 1/2-in. Depth (°F)	Time of Max. Temp. at 1/2-in. Depth (s)	Max. Temp. at 1-in. Depth (°F)	Time of Max. Temp. at 1-in. Depth (s)	Max. Temp. at 1-1/2-in. Depth (°F)	Time of Max. Temp. at 1-1/2-in. Depth (s)
FIREX	C-3	117.8	304	106.8	538	92.8	1096	86.2	1631
DE-350	C-11	143.1	268	117.1	627	97.6	1386	88.5	1616
S-885	C-21	184.8	129	140.0	347	109.8	767	94.6	1129
FLEXFRAM	C-31	188.0	140	138.0	330	108.4	823	97.2	1260
S-886	C-41	160.0	197	131.8	361	106.0	784	95.0	1230
DE-370	C-50	156.1	144	113.8	389	94.5	900	87.0	1688
CHARTEK	C-61	148.5	143	114.8	275	92.2	830	86.2	1451
1600B	C-71	161.0	164	120.0	478	99.0	1683	89.5	1904
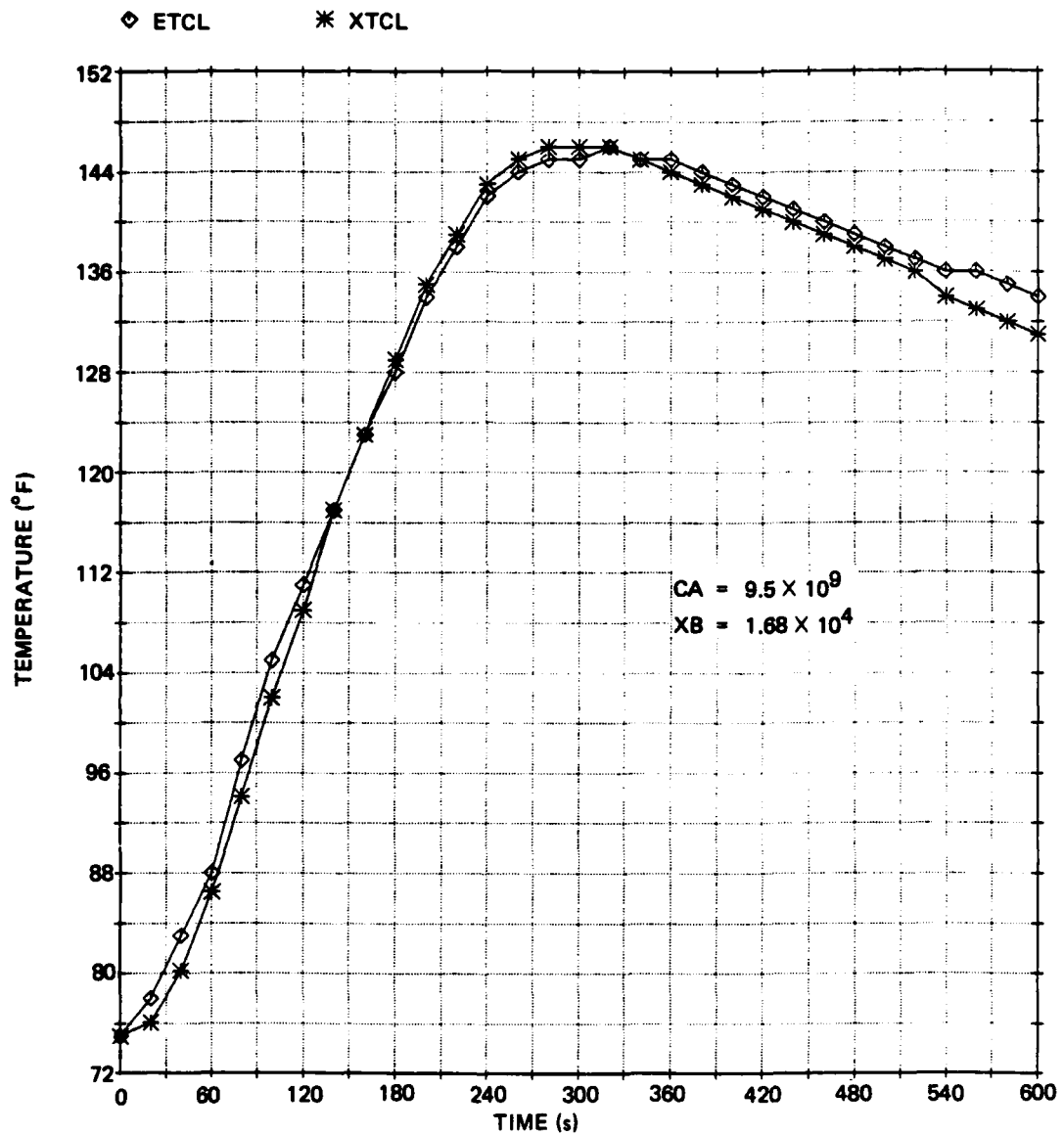
Figure 6.4.   Comparison of experimental and computer-generated
              temperature profiles for Firex, 1/4-inch depth,
              45-second burn duration, 10 Btu/ft^2-s heat flux.

Table 6.8. Summary of cylinder specimen length measurements.

Material	Sample Number	Initial Length (inches)	Final Length (inches)	Length Increase (inches)	% Length Increase
FIREX	C-1	2.00	2.33	0.33	16.5
	C-2	2.00	2.325	0.325	16.25
	C-3	2.00	2.290	0.290	14.5
	C-4	2.00	2.3125	0.3125	15.63
	D-1	2.00	2.30	0.30	15.0
	D-2	2.00	2.33	0.33	16.5
DE-350	C-10	2.00	2.195	0.195	9.75
	C-11	2.00	2.086	0.086	4.30
S-885	C-20	2.00	2.211	0.211	10.55
	C-21	2.00	2.085	0.085	4.25
FLEXFRAM	C-30	2.00	2.102	0.102	5.10
	C-31	2.00	2.078	0.078	3.9
S-886	C-40	2.00	2.3125	0.3125	15.63
	C-41	2.00	2.110	0.110	5.5
DE-370	C-50	2.00	2.025	0.025	1.25
	C-51	2.00	2.031	0.031	1.50
CHARTEK	C-60	2.00	2.152	0.152	7.60
	C-61	2.00	2.055	0.055	2.75
1600B	C-70	2.00	3.3125	1.3125	65.63
	C-71	2.00	2.55	0.55	27.50
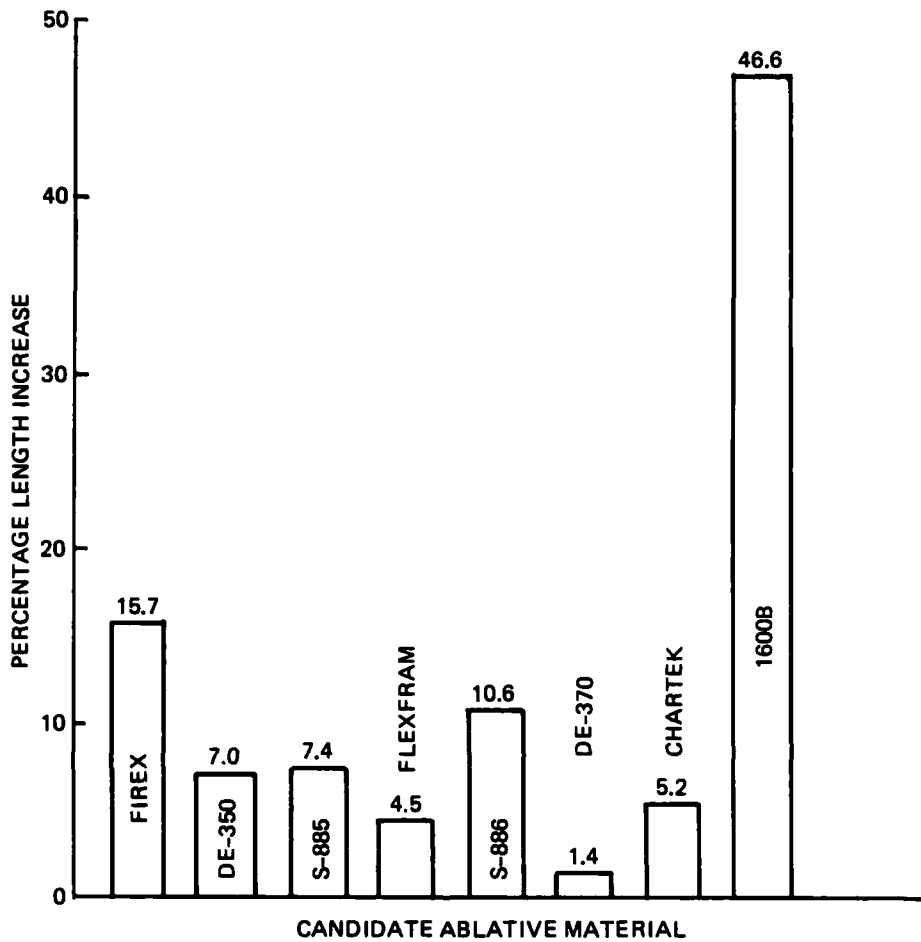
Figure 6.5. Average cylinder specimen length changes.

6.4   Surface Temperature Specimen Tests

6.4.1   Purpose

The purpose of the series of surface temperature specimen tests was to obtain temperature-time profiles of all materials for direct correlation of data with computed values obtained from the STAB II computer model.

6.4.2 Test Data and Results

Surface temperature histories for each material appear in Figures 6.6a and 6.6b. Congestion of data precluded plotting of all materials on a single graph. It is noted that Firex performs well in this test also, second only to the Fiberfrax sample.

6.5 Observations

6.5.1 General

Observations made during thermal testing and during specimen examination after testing are detailed in this section for each material, under two different categories

(1)   Ablator panel specimens exposed to a 45-second burn duration.

(2)   Ablator cylinder specimens exposed to a 200-second burn duration.

A summary of the burn characteristics for each material under these two test conditions is presented in Table 6.9. Appendix F contains photographs of representative panel specimens, before and after testing, while post-test photographs of cylinder specimens are in Appendix G.

Each material shall be considered separately; some of the observations discussed include post exposure appearance, char qualitative assessment, profile changes, and smoke generation.

6.5.2 Specific Material Tests

6.5.2.1 Firex RX-2373

6.5.2.1.1 Panel (Figure F-1)

The 45-second burn condition resulted in negligible smoke generation and the formation of only a light, bubbly char over the entire exposed surface. The uniform char appeared to possess a high degree of

100
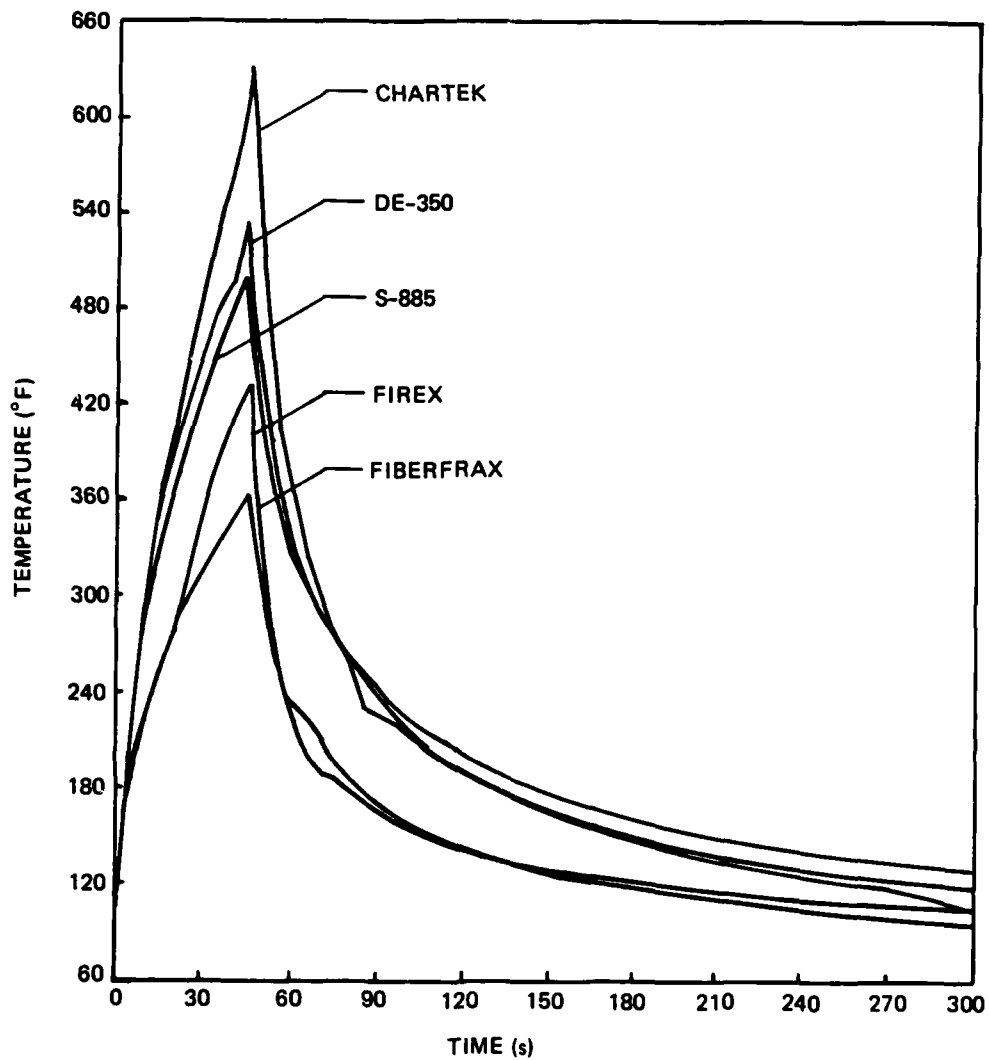
Figure 6.6a. Surface temperatures of candidate ablative materials
subjected to 10 Btu/ft^2-s incident heat flux, assumed
emissivity 0.95, pyrometer angle of attack 45°.

mechanical strength, experiencing no degradation during post-test handling
and measurement. A high degree of swelling was evident in that the
specimen became lodged in the asbestos holder, requiring prying to be
freed. The only profile change noted was the high degree of swelling

101
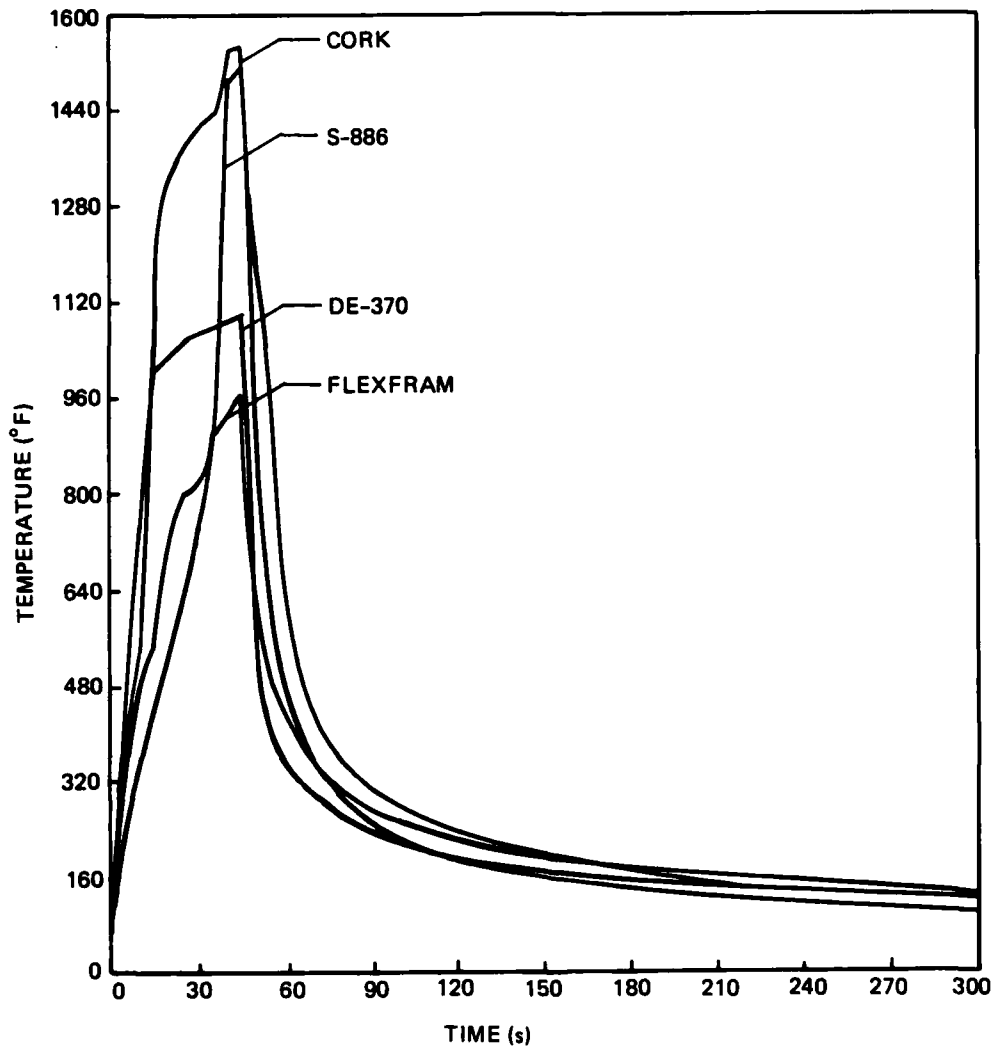
Figure 6.6b. Surface temperatures of candidate ablative materials subjected to 10 Btu/ft^2-s incident heat flux, assumed emissivity of 0.95, pyrometer angle of attack 45°.

in the surface region, with no warping evident. A rather rancid odor was given off as a result of burning, necessitating the use of the vented hood assembly.

Table 6.9. Burn characteristics of candidate ablative materials.

Test Material	Specimen Type	Exposure Time (s)	Smoke Generation	Loss of Adhesion to Aluminum	Surface Char Formation	Surface Droplet Formation	Deformation	Average Temp. Rise at 1/4 inch (°F)	Remarks
Dynatherm DE-350	Panel	45	Moderate White	None	Brittle, flaky char over 80% of surface	None	Slight Warping	225.6	Sizzling sound noted
	Cylinder	200	Moderate White	N/A	Heavy, strong deeply cracked char	None	N/A	199.0	(1) Flames present during test. (2) Some surface discoloration (blue tint)
Dynatherm DE-370	Panel	45	Heavy white smoke	None	Thick, fragile uniform char over entire surface	None	Negligible	240.3	Nonuniform char formation
	Cylinder	200	Heavy white, then heavy black smoke	N/A	Fragile char, minor cracking	None	N/A	340.0	(1) Soot deposited on lamps (2) Flames present during test
FIREX 2373	Panel	45	Negligible	None	Moderate bubbly char over entire surface	None	Large amt. of swelling (had to be pried from holder)	149.7	(1) Residue deposited on quartz lamps (2) Rancid smell upon burning
	Cylinder	200	Some	N/A	Deep, fragile uniform char	Yes, over entire surface, avg. dia. 0.05 in.	N/A	161.6	Rancid smell upon burning
CHARTEK 59	Panel	45	Slight	None	Some in center of specimen	None	Slight swelling near specimen surface	194.5	Sizzling sound noted
	Cylinder	200	Black smoke	N/A	Thick, brittle, deeply cracked char	None	N/A	243.4	Sizzling sound noted

Table 6.9. Burn characteristics of candidate ablative materials.
(Continued)

Test Material	Specimen Type	Exposure Time (s)	Smoke Generation	Loss of Adhesion to Aluminum	Surface Char Formation	Surface Droplet Formation	Deformation	Average Temp. Rise at 1/4 inch (°F)	Remarks
Flamarest 1600B	Panel	45	Heavy black	None	Extremely thick but fragile	None	None	221.5	(1) Char depth 5-6 times specimen thickness (2) Popping & sizzling sound noted.
	Cylinder	200	Heavy black	N/A	Extremely thick, fragile ashy char	None	N/A	258.8	Ashes deposited on lamps
Fiberfrax	Panel	45	None	None	None	None	None	216.9	Only mild surface discoloration observed, appears reusable
	Cylinder	–	–	–	–	–	–	–	Not tested
Flamemaster S-885	Panel	45	None	Peeled off aluminum upon removal of thermocouple	None	None	None	208.8	Only mild surface discoloration observed, appears reusable
	Cylinder	200	Some	N/A	Thick, fragile, white char, no mechanical strength	Large, white droplets over entire surface, but more concentrated at top of specimen face. Avg. diam. 0.12 in.	N/A	350.4	Some droplets were deposited on holder as much as 2 in. above specimen

Table 6.9. Burn characteristics of candidate ablative materials. (Continued)

Test Material	Specimen Type	Exposure Time (s)	Smoke Generation	Loss of Adhesion to Aluminum	Surface Char Formation	Surface Droplet Formation	Deformation	Average Temp. Rise at 1/4 inch (°F)	Remarks
Flamemaster S-886	Panel	45	Moderate white	Peeled off aluminum upon removal of thermocouple	Moderately thick, fragile char, some of which peeled off surface during and after test	None	None	250.9	One specimen fell off aluminum plate during test run
	Cylinder	200	Some	N/A	Thick, soft, fragile, deeply cracked, no mechanical strength	Large droplets, more concentrated at top of specimen face, avg. dia. 0.14 in.	N/A	369.0	Ashes deposited on lamps
FIREX 2373 with Vinyloid Coating	Panel	45	Heavy white smoke	None	Black, thin char over 100% of surface, some cracking	None	Large amount of swelling (had to be pried from holder)	144.4	Vinyloid coating caused smoke generation
	Cylinder	–	–	–	–	–	–	–	Not tested
Flexfram 605	Panel	45	Moderate white smoke	None	Black, thick, strong, uniform char over entire surface	None	Moderate swelling (had to be pried from holder)	276.9	(1) Char has high mechanical strength (2) Rancid smell upon burning
	Cylinder	200	Moderate white smoke	N/A	Black, thick, strong, uniform char over entire surface	None	N/A	280.2	(1) Char has high mechanical strength (2) Rancid smell upon burning
Cork	Panel	45	Heavy white smoke	–	Black, thick, strong char over entire surface, deep surface cracks	None	High degree of warping after burn, bent outward at center	229.0	Tested with no aluminum backplate
	Cylinder	–	–	–	–	–	–	–	Not tested

6.5.2.1.2 Cylinder (Figure G-1)

Under the 200-second burn, a deep, fragile, uniform char was formed with some concurrent smoke generation. The entire exposed surface was also riddled with material droplets of approximately 0.05-inch average diameter formed during the burn. Once again, the burn produced rather odiferous byproducts.

6.5.2.1.3 Vinyloid Topcoat (Figure F-2)

Several panel specimens were painted with a special environ t coating prior to testing. Results were similar to the normal panel ests with four exceptions:

(1) Temperature rise was on the order of 3.5% less for the vinyloid-coated specimens.

(2) Thickness increase was on the order of 80% greater for the vinyloid-coated specimens.

(3) An extremely heavy, white smoke was generated for the entire burn duration.

(4) A black, crisp, thin char was formed over the entire exposed surface with some surface cracking observable.

6.5.2.2 Flexfram 605

6.5.2.2.1 Panel (Figure F-4)

Panel burns resulted in the generation of a moderate amount of white smoke, and the formation of a black, thick char uniformly over the exposed surface. The char exhibited good mechanical strength during all post-test handling evolutions. Being an intumescent, it also experienced a moderate amount of swelling in the surface region, and had to be pried from the holder, as did Firex. A pungent odor was also given off, requiring use of the vented hood.

6.5.2.2 Cylinder (Figure G-3)

The same observations made for the panel case are applicable here. There was no surface droplet formation, the char generated being thick, strong, and uniform over the exposed surface.

6.5.2.3 Chartek 59

6.5.2.3.1 Panel (Figure F-3)

The burning sample experienced only a slight degree of smoking, and formed a slight, nonuniform char in the center of the exposed surface. A slight swelling, the only profile change noted, was experienced near the specimen surface, but not enough to require prying from the holder. A sizzling sound was also noted in the latter half of the burn period.

6.5.2.3.2 Cylinder (Figure G-2)

Quite different results were obtained under the 200-second burn period experienced by the cylinder specimen. The generation of a moderate amount of black smoke accompanied the formation of a thick, brittle, deeply-cracked surface char. The char was uniform in thickness, and there were no surface droplets present. Once again, the sizzling sound was heard during almost the entire test duration.

6.5.2.4 Flamarest 1600B

6.5.2.4.1 Panel (Figure F-5)

The 45-second burn resulted in heavy, black smoke and ash generation. An extremely fragile, cocoon-like (hollow) char, on the order of five to six times the original thickness of the specimen enveloped the entire panel surface. The char possessed negligible mechanical strength, and easily separated from the specimen during post-test handling. There were no profile changes or deformations detectable. Popping and sizzling sounds were heard throughout the burn duration.

107

6.5.2.4.2 Cylinder (Figure G-4a, b)

The observations made during the 200-second burn are very similar to those of the previous section. Char formation was similar, with no surface droplet formation. The longer burn resulted in a large amount of floating ash products.

6.5.2.5 Dynatherm DE-350

6.5.2.5.1 Panel (Figure F-6)

A moderate amount of white smoke was generated with the accompanying formation of a brittle, flaky char over approximately 80% of the exposed surface. A profile change, in the form of a slight warping, was found during post-test inspections. Here, again, a sizzling sound was noted during testing.

6.5.2.5.2 Cylinder (Figure G-5)

During the 200-second burn, the specimen smoked moderately white, and formed a heavy, strong, deeply-cracked char. Some discoloration (blue tint) was evident on the specimen surface. There were no surface droplets formed; however, there were flames present during the test run.

6.5.2.6 Dynatherm DE-370

6.5.2.6.1 Panel (Figure F-7)

Heavy white smoke was generated as a thick, brittle, uniform char formed over the entire specimen surface. Although brittle, the char held up well under post-test handling. A negligible amount of warpage was detected.

6.5.2.6.2 Cylinder (Figure G-6)

Long period burning resulted in the generation of heavy white smoke, which was followed by heavy black smoke. A uniform, brittle char

formed which experienced minor surface cracking. There was no surface droplet formation. Flames were observed during testing, and a black soot was deposited on the quartz lamps.

6.5.2.7 Dynatherm S-885

6.5.2.7.1 Panel (Figure F-8)

The 45-second burn resulted in no smoke or char generation, only a mild surface discoloration being detectable. There was no physical deformation apparent, however, upon post-test handling during removal of the backface thermocouple, the specimen was easily peeled off the aluminum backplate. This lack of adhesion to aluminum is reason enough to eliminate S-885 from further consideration as a candidate material.

6.5.2.7.2 Cylinder (Figure G-7)

Some smoke was generated under the long burn, with the formation of a thick, fragile, white char of negligible mechanical strength. The char included the formation of large white droplets (average diameter 0.12 inch) over the entire surface, but more concentrated at the top of the specimen face. Some of these white droplets were deposited on the holder, as much as two inches above the specimen. The surface char easily dislodged during post-test handling, being completely removed from the virgin material.

6.5.2.8 Dynatherm S-886

6.5.2.8.1 Panel (Figure F-9)

Moderate white smoke generation accompanied the formation of a moderately thick, extremely fragile char, some of which peeled off the specimen surface during the test. The flaky char possessed absolutely no mechanical strength, and what little remained at the end of test was removed during post-test handling. Once again, upon removal of the back-face thermocouple, the specimen was easily peeled off the aluminum

backplate. In fact, one specimen actually fell off the plate during a test run. In view of its bonding problems to aluminum, S-886 would be eliminated from further consideration as a candidate material.

6.5.2.8.2 Cylinder (Figure G-8)

Results of this test are similar to those for the S-885 cylinder test. A thick, soft, flaky, deeply-cracked char possessing no mechanical strength was formed over the entire specimen surface. Large surface droplets (average diameter 0.14 inch) accompanied the char formation, once again showing a higher concentration at the top of the specimen face. During this test, ashes were found to be deposited on the quartz lamp assembly.

6.5.2.9 Fiberfrax LDS Moldable

6.5.2.9.1 Panel (Figure F-10)

The panel specimen experienced almost no noticeable physical change, with the single exception of a slight surface discoloration, suggesting this material may find use in applications requiring a reusable material.

6.5.2.9.2 Cylinder

Due to the fact that a cylinder specimen could not be molded with sufficient mechanical strength (too brittle) to be machined, no cylinder specimen was tested for this material.

6.5.2.10 Avcoat 893-5 Cork

6.5.2.10.1 Panel (Figure F-11)

The 45-second burn condition resulted in heavy, white smoke generation and the formation of a black, thick, deeply-cracked char spread uniformly over the specimen surface. The char was strong, allowing easy post-test handling of the specimen. This material suffered a high degree

110

of warping, with the specimen center bent outward. The warping may have been due, in part, to the fact that the cork specimens were tested with no aluminum backplate, which would have offered a certain amount of rigidity to the panel.

6.5.2.10.2 Cylinder

There were no cork cylinder specimens tested because of the nature of the material provided for testing, that being 1/4-inch thick cork sheet.

6.6   Material Performance Indices

In an effort to make the material selection process as quantitative as possible, various effectiveness measurements describing ablative thermal behavior can be employed. Possible criteria suggested in the literature include the rate of backface temperature rise, the time required to reach burn-through (when using a flame as the heat source), the effective heat of ablation of the material, pseudodiffusivity, and various insulative indices designed to account for the intended material application.[2,4,22,23] It should be apparent that a material which is a good thermal insulator will require a long period of time to reach a relatively low backface temperature. This was the basis of ranking the materials by temperature measurement alone, as previously outlined in Section 6.2.3.2.

Two additional indices of performance shall be described for use in relatively ranking the candidate materials. These indices are:[29]

(1)   The pseudodiffusivity, defined as

$$\alpha_{\Delta T} = L^2/t_{\Delta T} \quad (ft^2/h) \tag{6-3}$$

111

where

L = initial specimen length, ft

$t_{\Delta T}$ = the time interval for the backface temperature to increase a specified increment ΔT above its initial value, s

(2)   The cold-wall heat of insulation, defined as

$$q_I^* = \frac{\dot{q}_{cw}\, t_{\Delta T}}{\rho L} \qquad (6\text{-}4)$$

where

$\dot{q}_{cw}$ = cold-wall heat flux, Btu/ft^2-s

ρ = material density, lbm/ft^3

The pseudodiffusivity is a convenient index of insulative perform-ance for materials in which the heat propagation is controlled primarily by conduction rather than by ablation. The cold-wall heat of insulation, on the other hand, is a convenient index for materials in which quasi-steady ablation is attained. For the purposes of this evaluation, the former appears to be the most promising parameter, although values for the latter shall also be computed and tabulated.

A summary of all material performance indices considered is con-tained in Table 6.10, including the simple temperature indices used in the previous relative ranking. It is noted that although Firex ranked number one using solely the temperature rise, rise-rate, and time to peak, it ranks fourth using the pseudodiffusivity value at $\Delta T = 50°F$. However, it is also noted that within reasonable experimental error, the top five contenders in the pseudodiffusivity column (30% spread in values) fall close enough together to be grouped into a single unit, ranking at the top of the list.

Combining this observation with previous rankings based on tem-perature indices alone, Firex RX-2373 remains the best candidate ablator for the 10 Btu/ft^2-s radiative heat flux environment specified.

112

Table 6.10. Material performance indices.

Material (Specimen Number)	ρ (lbm/ft³)	$\dot{q}_{cw}$ (Btu/ft²-s)	$T_{BF\ MAX}$ (°F)	$t_{BF\ MAX}$ (s)	$t_{\Delta T=50}$ (s)	$t_{\Delta T=100}$ (s)
Firex (27)	78.03	10.2	152.6	260	45	-(1)
Flexfram (5)	85.53	9.95	272.4	135	33.6	55.2
Fiberfrax (17)	40.00	9.9	219.2	110	31.2	55.2
Chartek (211)	74.91	9.99	197.0	165	43.2	88.8
DE-350 (224)	68.67	9.97	221.6	150	19.2	52.3
DE-370 (218)	62.43	9.95	242.8	135	26.4	48.0
S-885 (215)	39.33	9.95	203.6	145	47.5	52.5
S-886 (153)	45.45	10.29	251.8	173	62.4	91.2
1600B (112)	83.03	10.04	205.0	188	25	57.5
Cork (62)	34.34	9.96	228.6	140	45.6	67.2

Notes: (1) Maximum backface temperature never reached 100° above ambient.

113

Table 6.10. Material performance indices. (Continued)

Material (Specimen Number)	$\alpha_{\Delta T=50}$ (ft²/h)	$\alpha_{\Delta T=100}$ (ft²/h)	$\dot{q}^*_{I_{\Delta T=50}}$ (Btu/lbm)	$\dot{q}^*_{I_{\Delta T=100}}$ (Btu/lbm)	Q^*_{cw} (Btu/lbm)	$\left(\frac{dT}{dt}\right)_{t=45}$ (°F/s)	$\left(\frac{dT}{dt}\right)_{t=100}$ (°F/s)
Firex (27)	0.035	–	282.35	–	5.07×10^3	1.03	0.13
Flexfram (5)	0.047	0.028	401.2	659.1	3.39×10^3	2.72	0.86
Fiberfrax (17)	0.050	0.028	173.35	306.69	1.14×10^5	2.17	0.33
Chartek (211)	0.036	0.018	276.54	568.43	1.14×10^4	1.43	0.75
DE-350 (224)	0.081	0.030	133.81	364.48	8.99×10^3	1.37	0.69
DE-370 (218)	0.059	0.033	201.96	367.21	5.10×10^3	2.40	0.63
S-885 (215)	0.033	0.030	576.81	637.53	2.94×10^5	1.26	1.11
S-886 (153)	0.025	0.017	678.12	991.10	2.63×10^3	1.63	1.54
1600B (112)	0.063	0.027	145.10	333.74	3.59×10^3	1.17	0.99
Cork (62)	0.034	0.023	634.84	935.56	4.02×10^3	1.95	0.58

It is interesting to note that although all of the candidate materials could not be relatively ranked using a distinct index, the thermal performance of the intumescent materials tested could be ranked according to their virgin thermal diffusivities, the lowest diffusivity corresponding to the lowest backface temperature rise. Because this occurs for the four intumescents here does not validate the use of thermal diffusivity as a possible factor. Further testing of a large number of intumescent ablators would be required to verify its use as a performance index.

6.7   Sources of Error

There are a number of experimental and environmental parameters which may have affected the precision and accuracy of the thermal tests conducted. Some of the possible sources of error in this series of tests include, but are not limited to:

(1)   A varying heat flux during test runs due to pyrolysis products being deposited on the heat source.

(2)   Variations in the off-centerline heating rates as discussed in Chapter 4.

(3)   Variations in thermocouple junction location.

(4)   Response lag of the thermocouple temperature behind the local material temperature.

(5)   Distortions in the temperature field within the material due to the presence of voids in the specimen, as well as heat conduction along the embedded thermocouple wire.

(6)   Variations in bond strength of backface thermocouples to aluminum backplates resulting in nonuniform contact coefficients.

(7) Poor bonding between backplate and specimen resulting in lower backface temperature readings.

(8) Minor convective influence introduced by the ventilation hood assembly.

CHAPTER 7

SHIPBOARD APPLICATION OF ABLATIVE MATERIALS

7.1   Introduction

        Ablative materials have been used on board U.S. Navy vessels for a
number of years to enhance overall shipboard combat capability in any
number of ways, depending on ship type (i.e., conventional surface ship,
aircraft carrier, or submarine). The thermal protection requirements of
each ship type vary, and therefore, the type of ablative materials designed
to fit those needs will similarly vary. Current uses of ablative materials
in the shipboard environment tend to fall into two general categories:

        (1)   Those concerned with controlling and/or preventing the spread
                of on board fires.

        (2)   Those dedicated to ensuring that the combat capability of a
                specific shipboard weapon system is fully realized and unim-
                paired during system operation.

Many of the test programs conducted to date in an effort to identify abla-
tive materials certified for use in the severe naval environment have been
accomplished at the Naval Weapons Center (NWC), China Lake, California; the
Center for Fire Research (CFR), National Engineering Laboratory, National
Bureau of Standards; and the Naval Surface Weapons Center (NSWC), Dahlgren,
Virginia. Details concerning the application of ablative materials under
the two previously mentioned categories shall be addressed here.

117

7.2 Shipboard Fire-Retardant Ablative Applications

Fire at sea is one of the most feared hazards and one of the great-
est dangers confronting shipboard personnel, both in wartime as well as
during peacetime operations. Fire is often the cause of impaired mission
capability, and a major hindrance to continued operation and combat effi-
ciency in battle.[24] This statement attempts to underline the signifi-
cance of continuous improvement in shipboard fire protection and fire-
retardant systems as naval platforms themselves become more sophisticated
and complex. In recent years, during peacetime operations alone, the U.S.
Navy has experienced several devastating shipboard fires which severely
crippled the combat capability of each platform:

(1)   In July, 1967, the aircraft carrier, U.S.S. Forrestal,
        suffered an estimated $200 million of damage and the loss
        of 134 lives when an accidental onboard firing of a rocket
        erupted into a major flight deck fire with subsequent jet
        bomb explosions.[25]

(2)   In January, 1969, a rocket warhead explosion onboard the
        aircraft carrier, U.S.S. Enterprise, resulted in extensive
        damage to the ship and embarked aircraft, and 108 counts of
        serious injury or loss of life.[25]

(3)   More recently, in November 1975, a collision between the
        aircraft carrier, U.S.S. Kennedy, and the guided missile
        cruiser, U.S.S. Belknap, resulted in major fuel fires on-
        board both vessels. The cruiser suffered the loss of six
        lives and millions of dollars in damage, requiring in ex-
        cess of three years to repair. The fire had spread so
        quickly that fire-fighting teams were unable to become or-
        ganized, and eventually, the heat from the fire caused vari-
        ous munitions to detonate, resulting in further damage.

        In contrast, the Kennedy suffered the loss of only one
        life, and only minor damage, and was thus able to continue

118

its assigned mission. This light damage report was due, in part, to the fact that passive, fire-retardant intumescent paint coatings had been applied to various parts of the ship as a result of lessons learned from the previous two carrier fires. The intumecent coatings bought fire-fighting teams enough time to effectively control the spread of the flames, thereby minimizing damage.

Various attempts to minimize the spread of damage during aircraft carrier fires have resulted in the use of intumescent coatings on selected bulkheads in areas where aviation fuel fires are likely to occur, pipes and valves of the aviation fuel handling system, and even on various munitions which would be exposed to the intense heat of a fuel fire. Tests conducted at the Naval Weapons Center showed that unprotected munitions, when exposed to a simulated aircraft carrier deck fire, exploded within three minutes of exposure to the flames. Intumescent ablative coatings, when applied to the warhead of a rocket, increased the average time for self-detonation of the munitions to at least 8.5 minutes.[25] This additional time increment greatly aids a shipboard fire-fighting team, which generally requires approximately five minutes to control and extinguish a fire.

Further tests conducted at the Center for Fire Research resulted in the establishment of a parameter concerning spontaneous ignition, termed "flashover". Flashover is defined as the condition when thermal radiation levels become high enough to spontaneously ignite combustible materials within the lower half of a compartment.[26] The condition of flashover equates to a bulkhead temperature of approximately 1200°F, and a radiant heat flux on the order of 6 Btu/ft^2-s. Tests conducted show that in compartments with the hot bulkhead coated with an intumescent paint, the flashover condition did not occur within 10 minutes. Thus, the intumescent coating sets an effective passive fire barrier which allows the fire-fighting team the needed time to control or extinguish a fire.

The experiments conducted further showed that intumescent coatings greatly reduced the overall generation of carbon monoxide, hydrogen cyanide, hydrogen chloride, and smoke generally found in compartment fires.[27] The intumescent paints, then, are especially suited for use on submarines which, when submerged, carry a very limited and contained atmosphere. Polyvinyl chloride nitrite rubber foam, which is used extensively on the interior of submarine hulls for thermal as well as acoustic insulation, poses a serious fire hazard due to flame spreading. Testing demonstrated that the intumescent coating reduced the fire-spreading danger of the foam insulation, as well as reducing possibly toxic byproducts. The reduction in heat, smoke, and potentially hazardous combustion products would allow the normal cooling and filtering systems of the submarine to maintain a safe atmosphere.[31]

In addition to aircraft carriers and submarines, a third ship type, the mine countermeasure ship, appears to be a good candidate for the use of ablative coatings. To prevent the accidental detonation of magnetic mines, this vessel is constructed with a wooden hull, which obviously is very susceptible to fire damage. Intumescent coatings applied to this design would not only delay the spread of flames, but possibly prevent the sinkage of the vessel.

Although certain ship types have benefited by the use of ablative protection systems, there appears to be a need for further use of these passive fire-retardant coatings on other ships of the fleet in vital areas such as munition magazines, fuel handling stations, cable ways, and areas accommodating personnel life support equipment. Without the added time margin to set fire boundaries and organize fire-fighting efforts, the effectiveness of a fire-fighting team is severely restricted.

7.3 Weapon Delivery System Ablative Applications

Since the early 1960's, the U.S. Navy has used ablative materials to achieve thermal blast protection in the vicinity of its various missile

120

launchers. Previously used materials included charring ablators with asbestos fillers, since removed because of their hazardous nature. In addition to their unsuitability for health reasons, it was also determined during testing at sea that multiple firings at one launcher position placed too great a heat load on the charring ablator, causing thermal-induced stresses throughout the launching assembly.

Ablative testing efforts at the Naval Surface Weapons Center lead to the replacement of these charring ablators with an intumescent ablator for conventional missile launching systems. During thermal testing, each candidate material was subjected to a rocket motor exhaust with an associated time integrated heat flux of less than 1000 Btu/ft^2-s, which is in the operating range for an intumescent ablative material.[28] As discussed briefly in Chapter 3, as the heat flux is reduced, the ablative performance advantage of the intumescent material is increased over that of the charring ablator. Therefore, for the standard above-deck missile launcher, the intumescent ablative coatings are suitable.

However, with the advent of the new rapid fire Vertical Launching System (VLS), the thermal environment in the blast zone is substantially different, the heat load being more severe by at least an order of magnitude. As pointed out previously, the high heat load necessitates selection of a charring ablative material for thermal protection. The result of thermal testing was the design of replaceable charring ablator tiles, which could be inserted or removed by launcher personnel as necessary. These rubber modified, glass phenolic tiles would be located in the launcher plenum, where the most severe thermal environment would be experienced.[31]

During phone conversations with the Naval Surface Weapons Center, designers estimated that the VLS could fire up to seven missile magazines, or allow a complete restrained firing in the launcher before tile replacement becomes necessary. It is quite apparent that the advent of the charring ablator tiles allowed ease of integration of the Vertical Launch System into naval surface ship design.

121

CHAPTER 8

CONCLUSIONS AND RECOMMENDATIONS

The performance of an ablator is strongly dependent on the environment including thermal, chemical, and mechanical effects. Because of this performance dependence on environmental factors, it is imperative that ablation material testing be conducted under conditions as closely approximating the intended service application environment as possible. In the case of this series of experiments, a radiant, low heat flux environment of 10 Btu/ft^2-s was approximated in the laboratory, with inherent experimental errors introduced as described in Chapter 6.

It is felt that the primary goal of achieving good reproducibility of test results was indeed attained. Examination of the specimen temperature histories shows a great deal of consistency of data for each individual material tested. At times, entire portions of the temperature traces overlapped previously recorded data.

Although various performance indices were used to relatively rank candidate materials, it is felt that further study could be conducted to identify a distinct performance index to aid in the ranking of a field of ablators for the environment under consideration. Both the literature and test results compiled here indicate a good starting point would be some adaptation of thermal diffusivity.

It was observed that many of the charring ablators tested under the short burn duration experienced very little charring, thereby not utilizing their full potential of insulative effectiveness. Under a more

122

severe thermal environment, these materials would indeed char, with an increased insulation effect due to surface char reradiation.

The intumescent materials tested also experienced varying degrees of ablation, Firex and 1600B having shown the greatest amounts of intumescence. It appears the intumescent ablators have been readily accepted into several specialized areas of the U.S. Navy, for use as fire-retardant paints and weapon-system protective coatings. On the other hand, there are many more areas of application in new ship design and construction, and ship repair which would benefit greatly through the use of intumescents. Therefore, it is important that senior ship designers be made aware of the potential uses and benefits of these intumescent materials, so that they may be incorporated into the ship repair/ship design process.

Finally, the primary purpose of this thesis was to select, among a group of candidate ablative materials, that material which provided the highest degree of thermal protection in the transient, low heat flux environment previously defined. As detailed in Chapter 6, the overall best performing ablator evaluated of the ten candidates under examination, was Firex RX-2373, which is recommended for use in this specific environment under consideration.

APPENDIX A

RESULTS OF PANEL TEST SPECIMEN
EXPOSED TO QUARTZ-LAMP-GENERATED
HEAT FLUX

Table A-1. Firex.

Specimen Number	7	8	9	11	27
Test Date	9 Feb 83	9 Feb 83	9 Feb 83	11 Feb 83	8 Feb 83
m_0 (g)	23.6093	22.9693	22.9569	22.0985	24.6310
ℓ_0 (in.)	0.250	0.250	0.250	0.250	0.250
T_{BF_0} (°F)	70.0	75.0	75.0	73.8	75.2
T_{amb} (°F)	71.0	77.4°F	77.2	75.0	75.0
$\dot{q}$(Btu/ft^2-s)	10.2	10.09	10.06	10.04	10.2
t_b (s)	45	45	45	45	45
$T_{BF_{MAX}}$ (°F)	143.8	149.4	148.4	153.8	152.6
$t_{T_{MAX}}$ (s)	177	195	195	190	260
m_f (g)	22.9788	22.2486	22.2424	21.5723	23.4905
ℓ_f (in.)	0.330	0.320	0.323	0.287	0.338

125

Table A-1. Firex. (Continued)

Specimen Number	7	8	9	11	27
Δm (g)	0.6305	0.7207	0.7145	0.5262	1.1405
% Δm	3.03	3.57	3.54	2.72	5.23
$\Delta \ell$ (in.)	0.08	0.07	0.073	0.037	0.088
% $\Delta \ell$	32.0	28.0	29.2	14.8	35.4
$\dot{m} \left(\dfrac{lbm}{ft^2-s} \right)$	1.11×10^{-3}	1.27×10^{-3}	1.26×10^{-3}	9.28×10^{-4}	2.01×10^{-3}
$Q^*_{cw} \left(\dfrac{Btu}{lbm} \right)$	9.17×10^3	7.94×10^3	7.98×10^3	1.08×10^4	5.07×10^3
$\left(\dfrac{dT}{dt} \right) t=45 \left(\dfrac{°F}{s} \right)$	1.11	0.88	0.83	0.71	1.03
$\left(\dfrac{dT}{dt} \right) t=100 \left(\dfrac{°F}{s} \right)$	0.67	0.47	0.49	0.10	0.13

Table A-1. Firex. (Continued)

Specimen Number	29	39	40	201	202	205
Test Date	8 Feb 83	2 Feb 83	2 Feb 83	19 Feb 83	17 Feb 83	26 Feb 83
m_0 (g)	26.2151	26.4322	26.1463	22.0273	22.5123	22.7436
ℓ_0 (in.)	0.250	0.253	0.254	0.250	0.250	0.250
T_{BF_0} (°F)	75.6	73.6	75.2	75.6	70.2	71.2
T_{amb} (°F)	75.2	75.0	75.0	75.0	75.0	70.0
$\dot{q}$ (Btu/ft^2-s)	10.2	9.58	9.58	9.95	9.85	10.0
t_b (s)	45	45	45	45	45	45
$T_{BF_{MAX}}$ (°F)	143.4	148.0	149.0	158.6	150.0	150.0
$t_{T_{MAX}}$ (s)	280	240	300	186	195	128
m_f (g)	25.4000	25.7404	25.5898	20.6029	21.1838	21.8199
ℓ_f (in.)	0.349	0.323	0.320	0.284	0.284	0.289

127

Table A-1. Firex. (Continued)

Specimen Number	29	39	40	201	202	205
Δm (g)	0.8151	0.6918	0.5565	1.4244	1.3285	0.9237
% Δm	3.85	2.93	2.39	7.44	6.77	4.65
$\Delta \ell$ (in.)	0.099	0.07	0.066	0.034	0.034	0.039
% $\Delta \ell$	39.6	27.8	25.9	13.6	13.6	15.6
$\dot{m}\left(\dfrac{lbm}{ft^2-s}\right)$	1.44×10^{-3}	1.22×10^{-3}	9.82×10^{-4}	2.51×10^{-3}	2.34×10^{-3}	1.63×10^{-3}
$Q^{\star}_{cw}\left(\dfrac{Btu}{lbm}\right)$	7.10×10^{3}	7.86×10^{3}	9.76×10^{3}	3.96×10^{3}	4.20×10^{3}	6.14×10^{3}
$\left(\dfrac{dT}{dt}\right)_{t=45}\left(\dfrac{°F}{s}\right)$	0.89	1.03	1.10	0.83	1.04	0.79
$\left(\dfrac{dT}{dt}\right)_{t=100}\left(\dfrac{°F}{s}\right)$	0.45	0.39	0.54	0.31	0.36	0.21

Table A-2. Firex with vinyloid coating.

Specimen Number	32	33	36
Test Date	16 Mar 83	16 Mar 83	11 Feb 83
m_0 (g)	23.6003	25.6876	24.8818
ℓ_0 (in.)	0.250	0.250	0.250
T_{BF_0} (°F)	77.8	76.0	81.6
T_{amb} (°F)	75.0	75.0	75.0
$\dot{q}$(Btu/ft^2-s)	9.9	10.0	9.95
t_b (s)	45	45	45
$T_{BF_{MAX}}$ (°F)	145.0	143.0	145.2
$t_{T_{MAX}}$ (s)	195	210	145
m_f (g)	22.0366	24.0577	23.4170
ℓ_f (in.)	0.344	0.359	0.362
Δm (g)	1.5637	1.6299	1.4648
% Δm	7.55	7.15	6.64
$\Delta \ell$ (in.)	0.094	0.109	0.112
% $\Delta \ell$	37.6	43.6	44.8
$\dot{m}(\frac{lbm}{ft^2-s})$	2.76×10^{-3}	2.87×10^{-3}	2.58×10^{-3}
$Q^*_{cw}(\frac{Btu}{lbm})$	3.59×10^3	3.48×10^3	3.85×10^3
$(\frac{dT}{dt})_{t=45}(\frac{°F}{s})$	0.78	0.78	0.93
$(\frac{dT}{dt})_{t=100}(\frac{°F}{s})$	0.49	0.43	0.20

Table A-3. Firex (no aluminum backplate).

Specimen Number	306	307	308
Test Date	11 Mar 83	11 Mar 83	16 Mar 83
m_0 (g)	21.1367	21.1726	24.7692
ℓ_0 (in.)	0.250	0.250	0.250
T_{BF_0} (°F)	76.0	77.5	76.0
T_{amb} (°F)	75.0	75.0	75.0
$\dot{q}$(Btu/ft^2-s)	10.06	10.06	10.0
t_b (s)	45	45	45
$T_{BF_{MAX}}$ (°F)	140.0	140.8	139.5
$t_{T_{MAX}}$ (s)	280	300	290
m_f (g)	20.1447	20.4178	23.9738
ℓ_f (in.)	0.328	0.324	0.310
Δm (g)	0.9920	0.7548	0.7954
% Δm	4.69	3.57	3.21
$\Delta\ell$ (in.)	0.078	0.074	0.06
% $\Delta\ell$	31.2	29.6	24.0
$\dot{m}(\frac{lbm}{ft^2-s})$	1.75×10^{-3}	1.33×10^{-3}	1.40×10^{-3}
$Q^*_{cw}(\frac{Btu}{lbm})$	5.75×10^3	7.56×10^3	7.13×10^3
$(\frac{dT}{dt})_{t=45}(\frac{°F}{s})$	0.74	0.79	0.74
$(\frac{dT}{dt})_{t=100}(\frac{°F}{s})$	0.43	0.45	0.47

Table A-4. Chartek.

Specimen Number	210	211	148
Test Date	14 Feb 83	16 Feb 83	16 Mar 83
m_0 (g)	22.8113	22.1824	21.9827
ℓ_0 (in.)	0.250	0.250	0.250
T_{BF_0} (°F)	78.6	76.2	71.0
T_{amb} (°F)	75.0	75.0	70.0
$\dot{q}(Btu/ft^2\text{-}s)$	10.19	9.99	10.0
t_b (s)	45	45	45
$T_{BF_{MAX}}$ (°F)	193.6	197.0	193.0
$t_{T_{MAX}}$ (s)	150	165	155
m_f (g)	22.2583	21.6866	21.6179
ℓ_f (in.)	0.279	0.281	0.292
Δm (g)	0.5530	0.4958	0.3648
% Δm	2.77	2.57	1.90
$\Delta\ell$ (in.)	0.029	0.031	0.042
% $\Delta\ell$	11.6	12.4	16.8
$\dot{m}(\frac{lbm}{ft^2\text{-}s})$	9.75×10^{-4}	8.74×10^{-4}	6.43×10^{-4}
$Q^*_{cw}(\frac{Btu}{lbm})$	1.05×10^5	1.14×10^5	1.55×10^5
$(\frac{dT}{dt})_{t=45}(\frac{°F}{s})$	1.36	1.43	1.33
$(\frac{dT}{dt})_{t=100}(\frac{°F}{s})$	0.51	0.75	0.99

Table A-5. Flexfram.

Specimen Number	4	5	217
Test Date	10 Feb 83	15 Feb 83	16 Feb 83
m_0 (g)	24.5158	24.7802	23.6472
ℓ_0 (in.)	0.250	0.250	0.250
T_{BF_0} (°F)	73.2	75.0	80.0
T_{amb} (°F)	72.5	75.0	75.0
$\dot{q}$ (Btu/ft^2-s)	10.11	9.95	9.97
t_b (s)	45	45	45
$T_{BF_{MAX}}$ (°F)	266.8	272.4	291.4
$t_{T_{MAX}}$ (s)	132	135	125
m_f (g)	22.8248	23.1157	22.0179
ℓ_f (in.)	0.284	0.284	0.276
Δm (g)	1.6910	1.6645	1.6293
% Δm	7.78	7.56	7.85
$\Delta \ell$ (in.)	0.034	0.034	0.026
% $\Delta \ell$	13.6	13.6	10.4
$\dot{m} \left(\dfrac{lbm}{ft^2-s}\right)$	2.98×10^{-3}	2.94×10^{-3}	2.87×10^{-3}
$Q^*_{cw} \left(\dfrac{Btu}{lbm}\right)$	3.39×10^3	3.39×10^3	3.47×10^3
$\left(\dfrac{dT}{dt}\right)_{t=45} \left(\dfrac{°F}{s}\right)$	1.85	2.72	2.78
$\left(\dfrac{dT}{dt}\right)_{t=100} \left(\dfrac{°F}{s}\right)$	0.85	0.86	0.82

Table A-6. Flamarest 1600B.

Specimen Number	112	114	117
Test Date	9 Feb 83	19 Feb 83	8 Mar 83
m_0 (g)	21.3202	18.9762	18.1241
ℓ_0 (in.)	0.250	0.250	0.250
T_{BF_0} (°F)	77.6	73.0	75.0
T_{amb} (°F)	75.0	75.0	75.0
$\dot{q}$(Btu/ft^2-s)	10.04	10.0	10.0
t_b (s)	45	45	45
$T_{BF_{MAX}}$ (°F)	205.0	227.8	231.8
$t_{T_{MAX}}$ (s)	188	125	135
m_f (g)	19.7380	17.9750	16.7192
ℓ_f (in.)	1.813	1.539	1.406
Δm (g)	1.5822	1.0012	1.4049
% Δm	8.59	6.21	9.21
$\Delta \ell$ (in.)	1.563	1.289	1.156
% $\Delta \ell$	625.2	515.6	462.4
$\dot{m}(\frac{lbm}{ft^2-s})$	2.79×10^{-3}	1.77×10^{-3}	2.48×10^{-3}
$Q^*_{cw}(\frac{Btu}{lbm})$	3.59×10^3	5.66×10^3	4.04×10^3
$(\frac{dT}{dt})_{t=45}(\frac{°F}{s})$	1.17	—	1.45
$(\frac{dT}{dt})_{t=100}(\frac{°F}{s})$	0.99	0.47	0.85

Table A-7. Dynatherm DE-350.

Specimen Number	107	224	221
Test Date	10 Feb 83	14 Feb 83	18 Feb 83
m_0 (g)	17.5640	21.1081	19.7778
ℓ_0 (in.)	0.250	0.250	0.250
T_{BF_0} (°F)	75.8	74.0	75.0
T_{amb} (°F)	74.2	72.0	72.0
$\dot{q}$ (Btu/ft^2-s)	10.13	9.97	9.96
t_b (s)	45	45	45
$T_{BF_{MAX}}$ (°F)	244.0	221.6	211.2
$t_{T_{MAX}}$ (s)	115	150	170
m_f (g)	16.9986	20.4797	19.1836
ℓ_f (in.)	0.250	0.268	0.252
Δm (g)	0.5654	0.6284	0.5942
% Δm	3.85	3.45	3.52
$\Delta \ell$ (in.)	0.0	0.18	0.002
% $\Delta \ell$	0.0	7.2	0.8
$\dot{m} \left(\dfrac{lbm}{ft^2\text{-}s}\right)$	9.97×10^{-4}	1.11×10^{-3}	1.05×10^{-3}
$Q_{cw}^{*} \left(\dfrac{Btu}{lbm}\right)$	1.02×10^4	8.99×10^3	9.50×10^3
$\left(\dfrac{dT}{dt}\right)_{t=45} \left(\dfrac{°F}{s}\right)$	1.69	1.37	0.87
$\left(\dfrac{dT}{dt}\right)_{t=100} \left(\dfrac{°F}{s}\right)$	0.22	0.69	0.36

Table A-8. Dynatherm DE-370.

Specimen Number	103	218	220
Test Date	11 Feb 83	15 Feb 83	18 Feb 83
m_0 (g)	13.6350	12.6231	13.0393
ℓ_0 (in.)	0.250	0.250	0.250
T_{BF_0} (°F)	83.2	74.0	81.0
T_{amb} (°F)	75.0	73.0	75.0
$\dot{q}$ (Btu/ft^2-s)	10.13	9.95	10.27
t_b (s)	45	45	45
$T_{BF_{MAX}}$ (°F)	230.8	242.8	247.2
$t_{T_{MAX}}$ (s)	155	135	120
m_f (g)	12.4919	11.5178	11.7611
ℓ_f (in.)	0.279	0.328	0.279
Δm (g)	1.1431	1.1053	1.2782
% Δm	10.65	11.35	12.58
$\Delta\ell$ (in.)	0.029	0.078	0.029
% $\Delta\ell$	11.6	31.2	11.6
$\dot{m}\left(\dfrac{lbm}{ft^2-s}\right)$	2.02×10^{-3}	1.95×10^{-3}	2.25×10^{-3}
$Q^*_{cw}\left(\dfrac{Btu}{lbm}\right)$	5.03×10^3	5.10×10^3	4.56×10^3
$\left(\dfrac{dT}{dt}\right)_{t=45}\left(\dfrac{°F}{s}\right)$	1.98	2.40	2.50
$\left(\dfrac{dT}{dt}\right)_{t=100}\left(\dfrac{°F}{s}\right)$	0.67	0.63	0.67

Table A-9. Flamemaster S-885.

Specimen Number	213	215	135
Test Date	14 Feb 83	15 Feb 83	8 Mar 83
m_0 (g)	13.2236	12.8245	13.0628
ℓ_0 (in.)	0.250	0.250	0.250
T_{BF_0} (°F)	73.8	74.2	88.0
T_{amb} (°F)	72.0	73.0	75.0
$\dot{q}$(Btu/ft^2-s)	10.09	9.95	9.95
t_b (s)	45	45	45
$T_{BF_{MAX}}$ (°F)	214.0	203.6	185.0
$t_{T_{MAX}}$ (s)	135	145	180
m_f (g)	13.2022	12.8053	13.0493
ℓ_f (in.)	0.250	0.250	0.250
Δm (g)	0.0214	0.0192	0.0135
% Δm	0.21	0.19	0.13
$\Delta \ell$ (in.)	0.0	0.0	0.0
% $\Delta \ell$	0.0	0.0	0.0
$\dot{m}(\frac{lbm}{ft^2-s})$	3.77×10^{-5}	3.39×10^{-5}	2.38×10^{-5}
$Q^*_{cw}(\frac{Btu}{lbm})$	2.67×10^5	2.94×10^5	4.18×10^5
$(\frac{dT}{dt})_{t=45}(\frac{°F}{s})$	1.33	1.26	0.87
$(\frac{dT}{dt})_{t=100}(\frac{°F}{s})$	1.09	1.11	0.80

136

Table A-10. Flamemaster S-886.

Specimen Number	152	153
Test Date	11 Mar 83	10 Mar 83
m_0 (g)	13.1745	13.7524
ℓ_0 (in.)	0.250	0.250
T_{BF_0} (°F)	75.0	88.0
T_{amb} (°F)	75.0	80.0
$\dot{q}$ (Btu/ft^2-s)	10.16	10.29
t_b (s)	45	45
$T_{BF_{MAX}}$ (°F)	250.0	251.8
$t_{T_{MAX}}$ (s)	155	173
m_f (g)	11.3602	11.5345
ℓ_f (in.)	0.307	0.279
Δm (g)	1.8143	2.2179
% Δm	17.61	20.39
$\Delta \ell$ (in.)	0.057	0.029
% $\Delta \ell$	22.8	11.6
$\dot{m}$ ($\frac{lbm}{ft^2-s}$)	3.19×10^{-3}	3.91×10^{-3}
Q^*_{cw} ($\frac{Btu}{lbm}$)	3.18×10^3	2.63×10^3
$(\frac{dT}{dt})_{t=45}$ ($\frac{°F}{s}$)	1.45	1.63
$(\frac{dT}{dt})_{t=100}$ ($\frac{°F}{s}$)	1.21	1.54

Table A-11. Fiberfrax.

Specimen Number	14	17
Test Date	14 Feb 83	19 Feb 83
m_0 (g)	14.6609	15.8745
ℓ_0 (in.)	0.250	0.250
T_{BF_0} (°F)	78.8	73.2
T_{amb} (°F)	75.0	75.0
$\dot{q}$ (Btu/ft^2-s)	10.04	9.9
t_b (s)	45	45
$T_{BF_{MAX}}$ (°F)	224.6	219.2
$t_{T_{MAX}}$ (s)	120	110
m_f (g)	14.6086	15.8254
ℓ_f (in.)	0.250	0.250
Δm (g)	0.0523	0.0491
$\%\Delta m$	0.44	0.38
$\Delta \ell$ (in.)	0.0	0.0
$\%\Delta \ell$	0.0	0.0
$\dot{m}\left(\dfrac{lbm}{ft^2\text{-}s}\right)$	9.22×10^{-5}	8.66×10^{-5}
$Q^{*}_{cw}\left(\dfrac{Btu}{lbm}\right)$	1.09×10^{6}	1.14×10^{6}
$\left(\dfrac{dT}{dt}\right)_{t=45}\left(\dfrac{°F}{s}\right)$	2.08	2.17
$\left(\dfrac{dT}{dt}\right)_{t=100}\left(\dfrac{°F}{s}\right)$	0.59	0.33

Table A-12. Cork.

Specimen Number	47	54	62
Test Date	11 Feb 83	8 Mar 83	18 Feb 83
m_0 (g)	6.8624	6.9440	7.0109
ℓ_0 (in.)	0.250	0.250	0.250
T_{BF_0} (°F)	74.6	74.0	79.0
T_{amb} (°F)	72.5	75.0	75.0
$\dot{q}$ (Btu/ft^2-s)	10.19	9.95	9.96
t_b (s)	45	45	45
$T_{BF_{MAX}}$ (°F)	236.4	222.0	228.6
$t_{T_{MAX}}$ (s)	144	145	140
m_f (g)	5.4865	5.6249	5.6070
ℓ_f (in.)	0.281	0.279	0.279
Δm (g)	1.3759	1.3191	1.4039
% Δm	20.05	18.99	20.02
$\Delta \ell$ (in.)	0.031	0.029	0.029
% $\Delta \ell$	12.4	11.6	11.6
$\dot{m}(\frac{lbm}{ft^2-s})$	2.43×10^{-3}	2.33×10^{-3}	2.48×10^{-3}
$Q_{cw}^{*}(\frac{Btu}{lbm})$	4.2×10^3	4.28×10^3	4.02×10^3
$(\frac{dT}{dt})_{t=45}(\frac{°F}{s})$	2.66	1.53	1.95
$(\frac{dT}{dt})_{t=100}(\frac{°F}{s})$	0.45	1.01	0.58

APPENDIX B

RESULTS OF CYLINDER TEST SPECIMENS
EXPOSED TO QUARTZ-LAMP-GENERATED
HEAT FLUX OF 10 Btu/ft^2-s

Table B-1. Firex (one-dimensional).

Specimen Number	D-1	D-2
Test Date	22 Feb 83	23 Feb 83
Specimen Holder	Fiberboard	Firex Slug
ℓ_0 (in.)	2.00	2.00
T_{ss_0} (°F)	71.6	70.0
T_{amb} (°F)	75.0	70.0
$\dot{q}$ (Btu/ft^2-s)	10.01	10.01
t_b (s)	200	200
$T_{MAX\ RIGHT}$ (°F)	126.5	115.0
$t_{T_{MAX\ R}}$ (s)	590	660
$T_{MAX\ CENTER}$ (°F)	131.0	115.0
$t_{T_{MAX\ C}}$ (s)	705	660
$T_{MAX\ LEFT}$ (°F)	128.2	115.0
$t_{T_{MAX\ L}}$ (s)	660	660
% Deviation at Peak Temp	3.45	0.0

NOTE: All thermocouples were located at 1/2-in. depth across specimen diameter

Table B-2. Firex.

Specimen Number	C-1	C-2	C-3	C-3*	C-3**	C-4
Test Date	16 Feb 83	1 Mar 83	2 Mar 83	2 Mar 83	3 Mar 83	3 Mar 83
ℓ_0 (in.)	2.00	2.00	2.00	2.00	2.00	2.00
T_{ss_0} (°F)	71.2	74.0	74.2	74.2	71.0	73.0
T_{amb} (°F)	72.0	74.0	72.5	72.5	71.0	75.0
$\dot{q}$ (Btu/ft^2-s)	9.98	10.0	10.05	9.9	10.05	10.04
t_b (s)	200	200	45	45	200	200s
T_{MAX} @ 1/4 in. (°F)	180.0	158.8	117.8	122.0	168.8	146.0
$t_{T_{MAX}}$ (s)	400	401	304	273	428	347
T_{MAX} @ 1/2 in. (°F)	147.8	129.3	106.8	108.6	144.8	123.0
$t_{T_{MAX}}$ (s)	840	689	538	535	753	767
T_{MAX} @ 1 in. (°F)	124.0	106.1	92.8	93.3	118.3	106.6
$t_{T_{MAX}}$ (s)	1415	1225	1096	1064	1328	1903
T_{MAX} @ 1-1/2 in. (°F)	111.2	93.9	86.2	86.5	104.5	96.5
$t_{T_{MAX}}$ (s)	1793	1667	1631	1432	1640	2114
ℓ_f (in.)	2.330	2.325	2.290	—	—	2.3125
$\Delta\ell$ (in.)	0.330	0.325	0.290	—	—	0.3125
% $\Delta\ell$	16.5	16.25	14.5	—	—	15.63

*45-s reshot of specimen C-3
**200-s reshot of specimen C-3*

142

Table B-3. Chartek.

Specimen Number	C-60	C-61
Test Date	7 Mar 83	7 Mar 83
ℓ_0 (in.)	2.00	2.00
T_{ss_0} (°F)	77.2	74.0
T_{amb} (°F)	72.0	75.0
$\dot{q}$ (Btu/ft^2-s)	9.96	10.05
t_b (s)	200	45
T_{MAX} @ 1/4 in. (°F)	243.4	148.5
$t_{T_{MAX}}$ (s)	315	143
T_{MAX} @ 1/2 in. (°F)	189.8	114.8
$t_{T_{MAX}}$ (s)	552	275
T_{MAX} @ 1 in. (°F)	147.0	92.2
$t_{T_{MAX}}$ (s)	991	830
T_{MAX} @ 1-1/2 in. (°F)	123.0	86.2
$t_{T_{MAX}}$ (s)	1436	1451
ℓ_f (in.)	2.152	2.055
$\Delta\ell$ (in.)	0.152	0.055
% $\Delta\ell$	7.60	2.75

143

Table B-4. Flexfram.

Specimen Number	C-30	C-31
Test Date	4 Mar 83	10 Mar 83
ℓ_0 (in.)	2.00	2.00
T_{ss_0} (°F)	72.8	74.8
T_{amb} (°F)	72.0	74.0
$\dot{q}$ (Btu/ft^2-s)	9.91	10.11
t_b (s)	200	45
T_{MAX} @ 1/4 in. (°F)	280.2	188.0
$t_{T_{MAX}}$ (s)	320	140
T_{MAX} @ 1/2 in. (°F)	204.2	138.0
$t_{T_{MAX}}$ (s)	497	330
T_{MAX} @ 1 in. (°F)	146.8	108.4
$t_{T_{MAX}}$ (s)	1429	823
T_{MAX} @ 1-1/2 in. (°F)	122.2	97.2
$t_{T_{MAX}}$ (s)	1850	1260
ℓ_f (in.)	2.102	2.078
$\Delta\ell$ (in.)	0.102	0.078
%$\Delta\ell$	5.10	3.9

144

Table B-5. Flamarest 1600B.

Specimen Number	C-70	C-71
Test Date	2 Mar 83	10 Mar 83
ℓ_0 (in.)	2.00	2.00
T_{ss_0} (°F)	73.5	74.0
T_{amb} (°F)	72.5	75.0
$\dot{q}$(Btu/ft^2-s)	10.16	10.27
t_b (s)	200	45
T_{MAX} @ 1/4 in. (°F)	258.8	161.0
$t_{T_{MAX}}$ (s)	290	164
T_{MAX} @ 1/2 in. (°F)	189.4	120.0
$t_{T_{MAX}}$ (s)	635	478
T_{MAX} @ 1 in. (°F)	142.6	99.0
$t_{T_{MAX}}$ (s)	1208	1683
T_{MAX} @ 1-1/2 in. (°F)	118.0	89.5
$t_{T_{MAX}}$ (s)	1706	1904
ℓ_f (in.)	3.3125	2.55
$\Delta\ell$ (in.)	1.3125	0.55
% $\Delta\ell$	65.63	27.5

145

Table B-6. Dynatherm DE-350.

Specimen Number	C-10	C-11	C-11*
Test Date	28 Feb 83	4 Mar 83	4 Mar 83
ℓ_0 (in.)	2.00	2.00	2.00
T_{ss_0} (°F)	74.0	74.0	76.8
T_{amb} (°F)	75.0	74.0	75.0
$\dot{q}$ (Btu/ft^2-s)	10.0	9.9	9.9
t_b (s)	200	45	200
T_{MAX} @ 1/4 in. (°F)	199.0	143.1	240.0
$t_{T_{MAX}}$ (s)	313	268	300
T_{MAX} @ 1/2 in. (°F)	150.6	117.1	179.2
$t_{T_{MAX}}$ (s)	580	627	719
T_{MAX} @ 1 in. (°F)	111.2	97.6	137.1
$t_{T_{MAX}}$ (s)	1106	1386	1232
T_{MAX} @ 1-1/2 in. (°F)	95.4	88.5	115.1
$t_{T_{MAX}}$ (s)	1526	1616	1712
ℓ_f (in.)	2.195	2.086	—
$\Delta\ell$ (in.)	0.195	0.086	—
% $\Delta\ell$	9.75	4.30	—

*200-s reburn of specimen C-11

146

Table B-7. Dynatherm DE-370.

Specimen Number	C-50	C-51
Test Date	5 Mar 83	5 Mar 83
ℓ_0 (in.)	2.00	2.00
T_{ss_0} (°F)	72.8	77.0
T_{amb} (°F)	72.5	75.0
$\dot{q}$ (Btu/ft^2-s)	10.0	10.17
t_b (s)	45	200
T_{MAX} @ 1/4 in. (°F)	156.1	340.0
$t_{T_{MAX}}$ (s)	144	265
T_{MAX} @ 1/2 in. (°F)	113.8	211.4
$t_{T_{MAX}}$ (s)	389	476
T_{MAX} @ 1 in. (°F)	94.5	155.1
$t_{T_{MAX}}$ (s)	900	1134
T_{MAX} @ 1-1/2 in. (°F)	87.0	125.8
$t_{T_{MAX}}$ (s)	1688	1167
ℓ_f (in.)	2.025	2.031
$\Delta\ell$ (in.)	0.025	0.031
% $\Delta\ell$	1.25	1.50

Table B-8.　Flamemaster S-885.

Specimen Number	C-20	C-21
Test Date	3 Mar 83	10 Mar 83
ℓ_0 (in.)	2.00	2.00
T_{ss_0} (°F)	74.3	77.0
T_{amb} (°F)	75.0	75.0
$\dot{q}$(Btu/ft^2-s)	10.06	10.24
t_b(s)	200	45
T_{MAX} @ 1/4 in. (°F)	350.4	184.8
$t_{T_{MAX}}$ (s)	300	129
T_{MAX} @ 1/2 in. (°F)	236.2	140.0
$t_{T_{MAX}}$ (s)	470	347
T_{MAX} @ 1 in. (°F)	164.7	109.8
$t_{T_{MAX}}$ (s)	884	767
T_{MAX} @ 1-1/2 in. (°F)	132.3	94.6
$t_{T_{MAX}}$ (s)	1175	1129
ℓ_f(in.)	2.211	2.085
$\Delta\ell$(in.)	0.211	0.085
%$\Delta\ell$	10.55	4.25

Table B-9. Flamemaster S-886.

Specimen Number	C-40	C-41
Test Date	5 Mar 83	10 Mar 83
ℓ_0 (in.)	2.00	2.00
T_{ss_0} (°F)	78.5	78.0
T_{amb} (°F)	75.0	75.0
$\dot{q}$ (Btu/ft^2-s)	10.11	10.18
t_b (s)	200	45
T_{MAX} @ 1/4 in. (°F)	369.0	160.0
$t_{T_{MAX}}$ (s)	280	197
T_{MAX} @ 1/2 in. (°F)	238.8	131.8
$t_{T_{MAX}}$ (s)	470	361
T_{MAX} @ 1 in. (°F)	165.0	106.0
$t_{T_{MAX}}$ (s)	660	784
T_{MAX} @ 1-1/2 in. (°F)	132.5	95.0
$t_{T_{MAX}}$ (s)	1083	1230
ℓ_f (in.)	2.3125	2.110
$\Delta\ell$ (in.)	0.3125	0.110
%$\Delta\ell$	15.63	5.50

APPENDIX C

EXPERIMENTAL TEMPERATURE PROFILES

FOR PANEL TEST SPECIMENS

(Heat Flux: 10 Btu/ft^2-s, Burn Duration: 45 s)
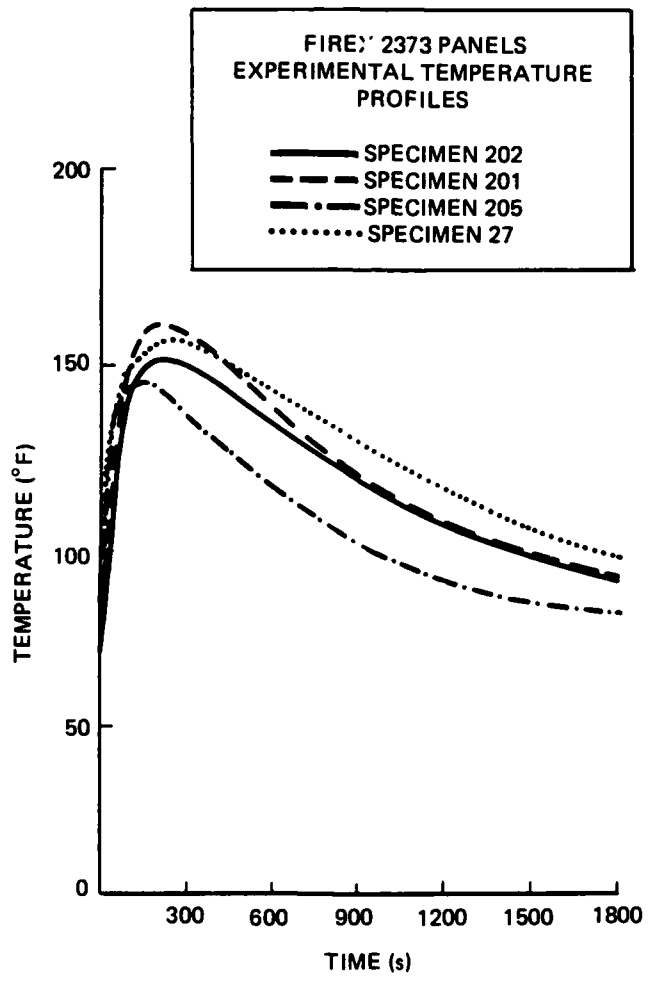
Figure C-1. Firex 2373.

151
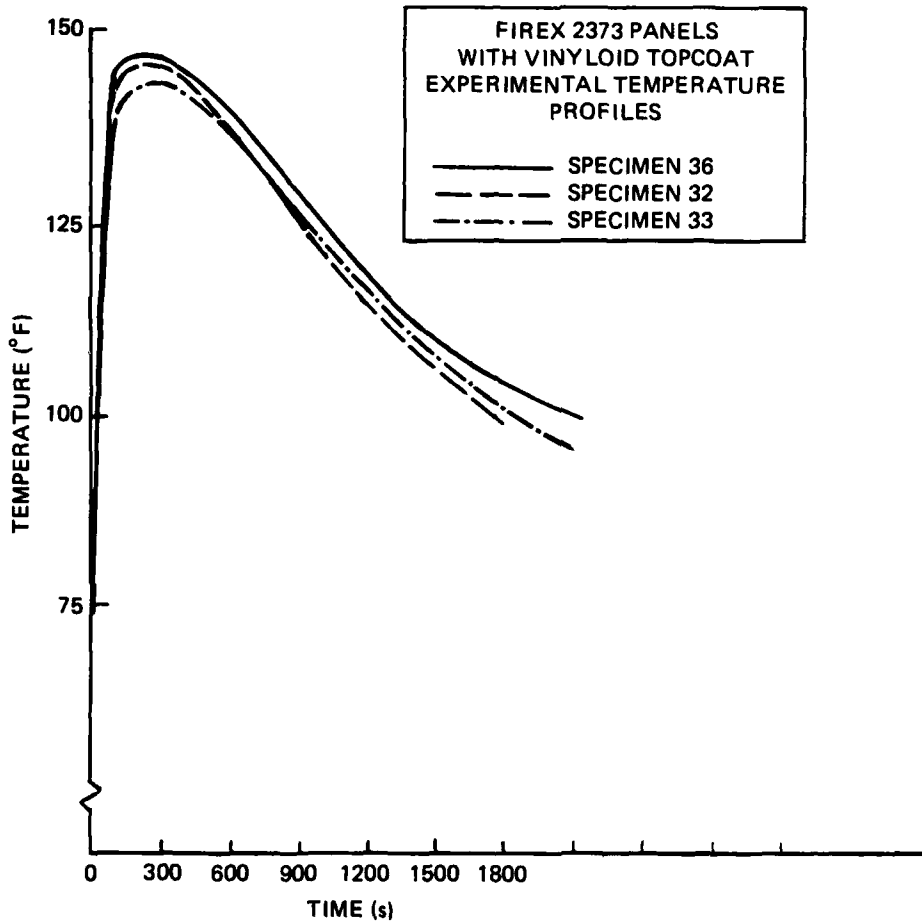
Figure C-2. Firex 2373 (vinyloid topcoat).
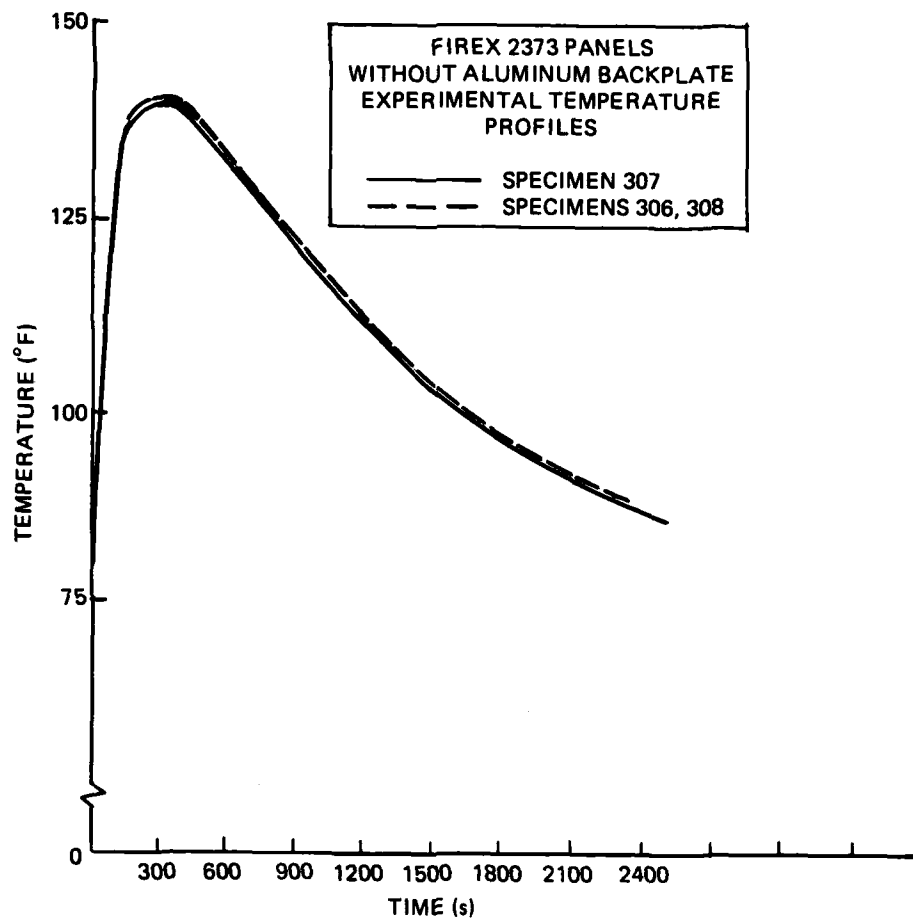
Figure C-3.   Firex 2373 (no aluminum backplate).
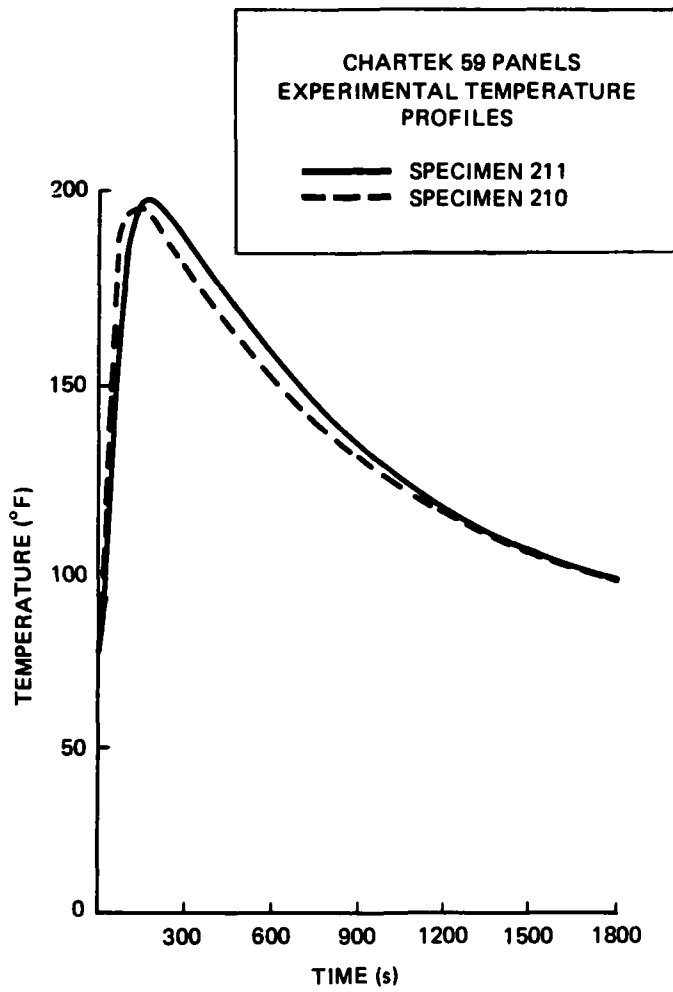
Figure C-4.   Chartek 59.

154
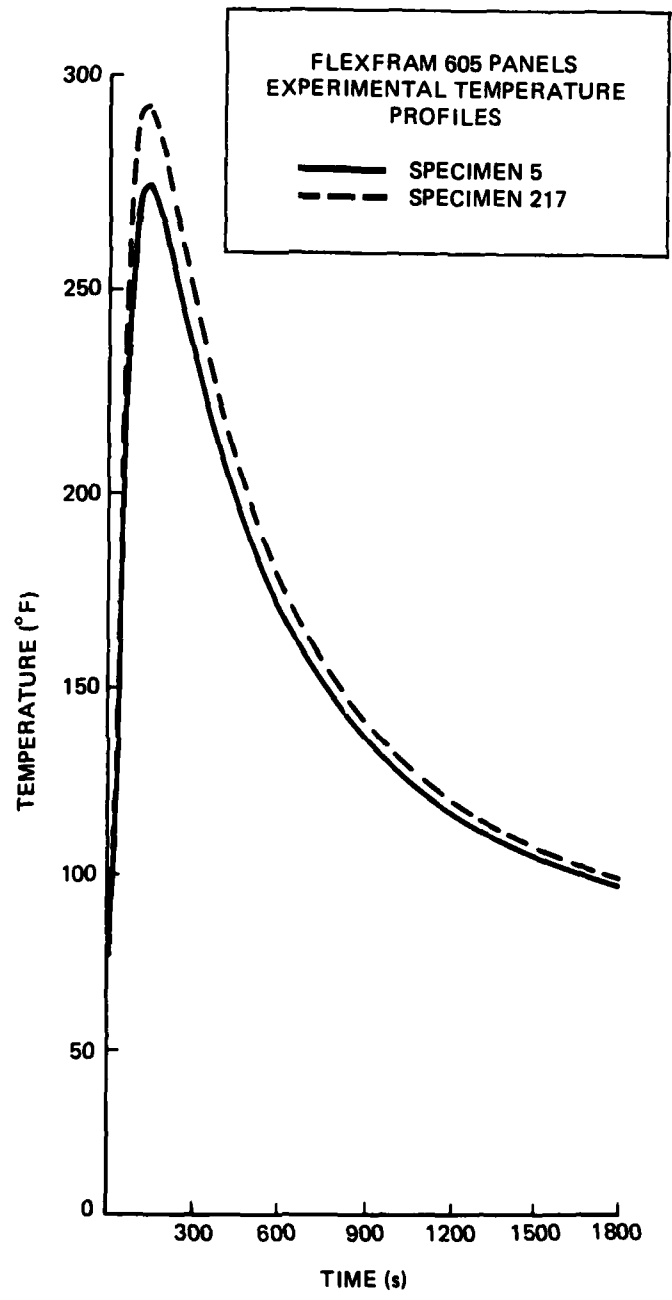
Figure C-5.   Flexfram 605.

155
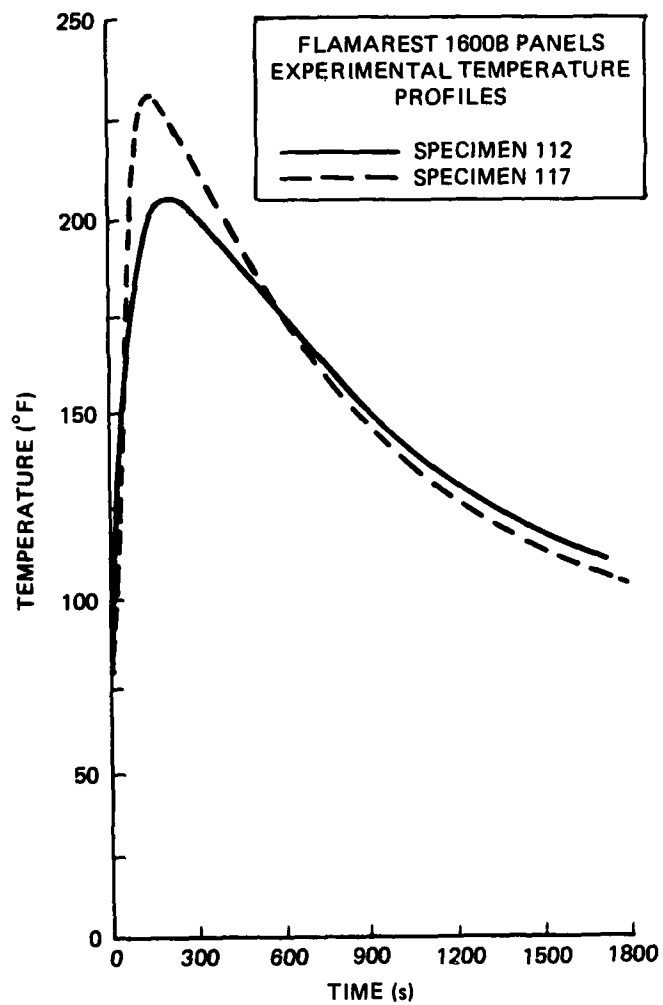
Figure C-6. Flamarest 1600B.

156

DYNATHERM DE-350 PANELS
EXPERIMENTAL TEMPERATURE
PROFILES

	SPECIMEN 224
	SPECIMEN 221
	SPECIMEN 107
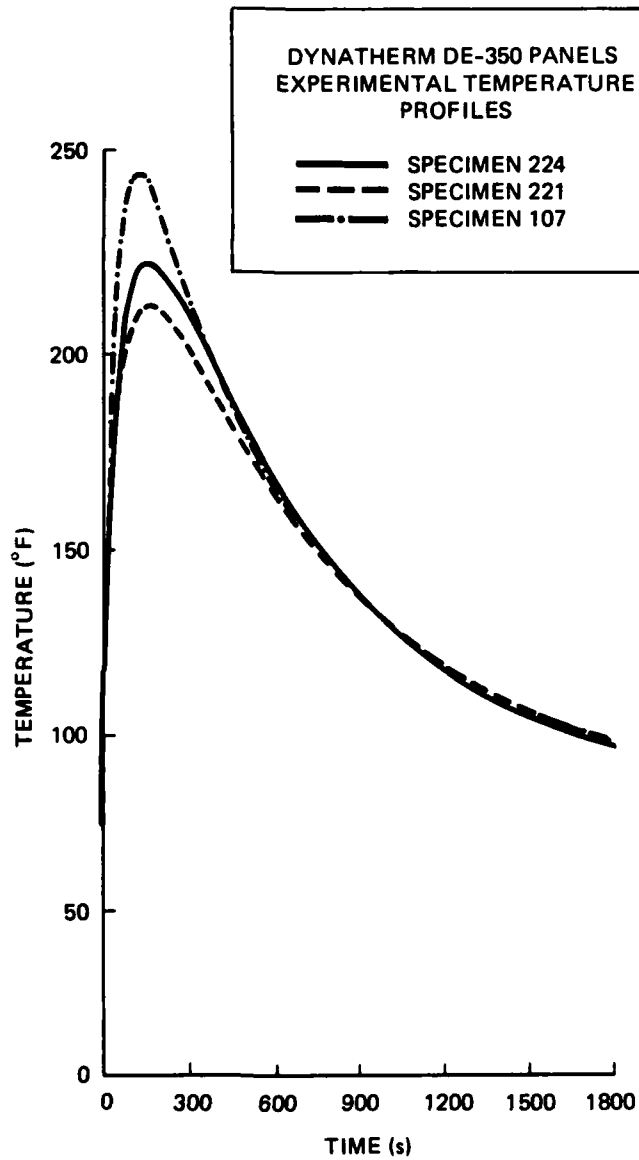
Figure C-7.   Dynatherm DE-350.

157
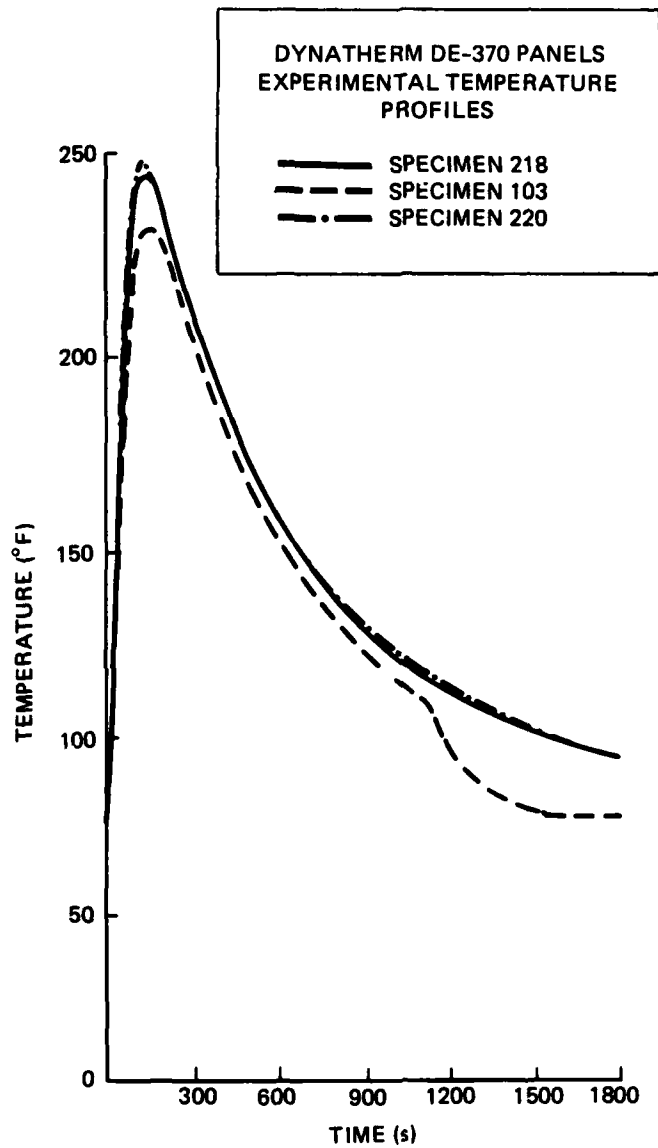
Figure C-8.   Dynatherm DE-370.
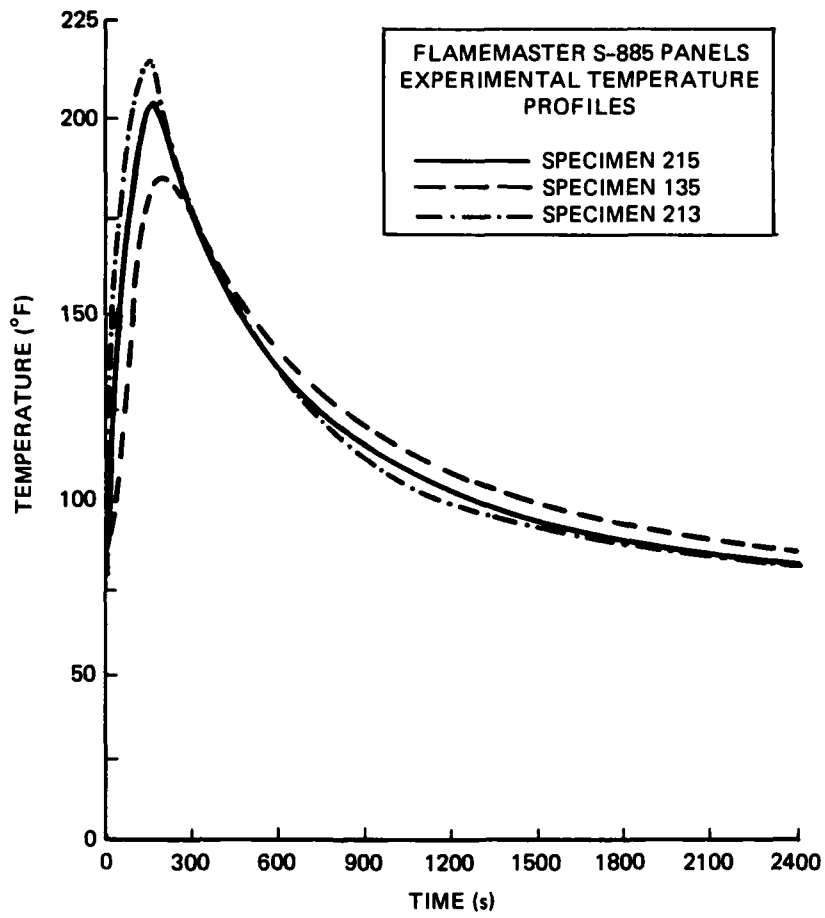
Figure C-9. Flamemaster S-885.
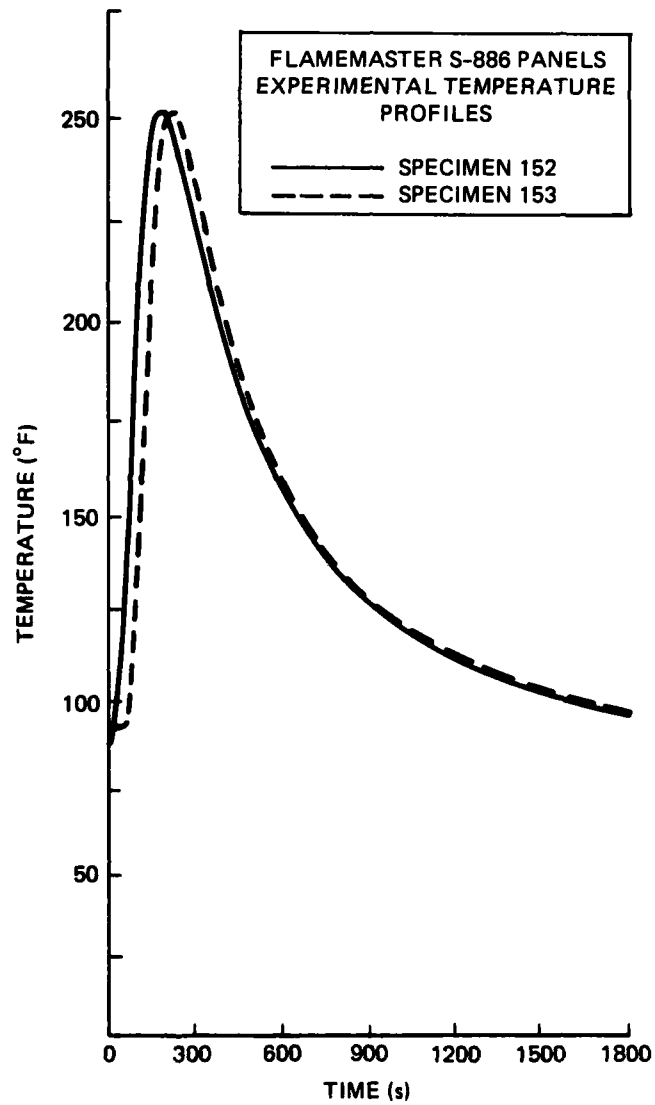
Figure C-10. Flamemaster S-886.

160
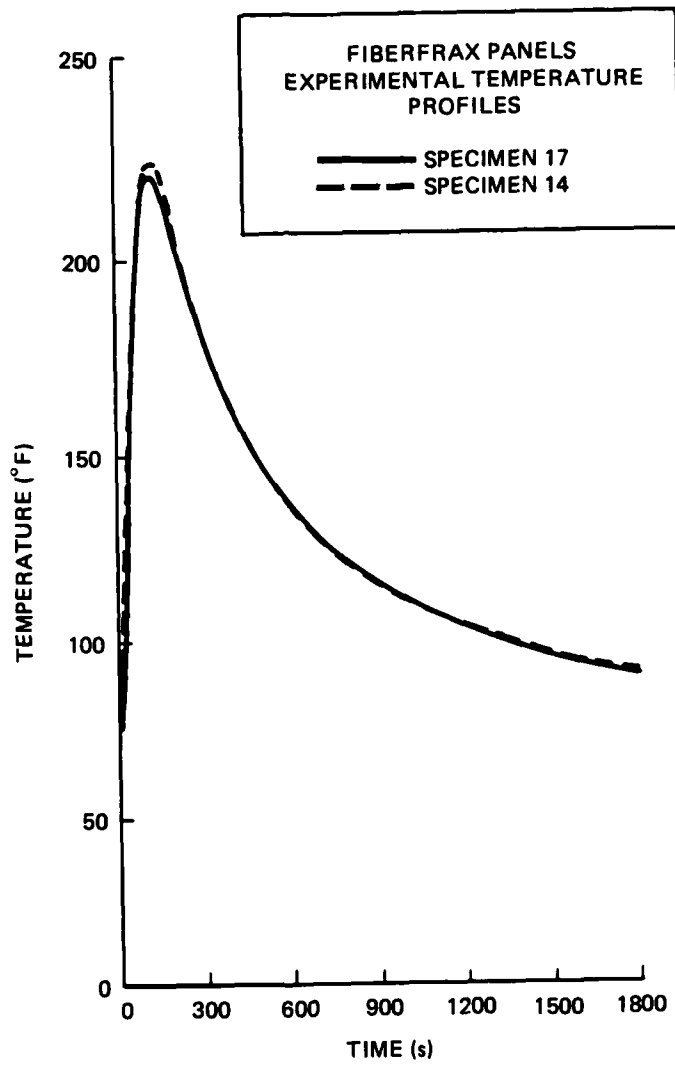
Figure C-11. Fiberfrax.

161
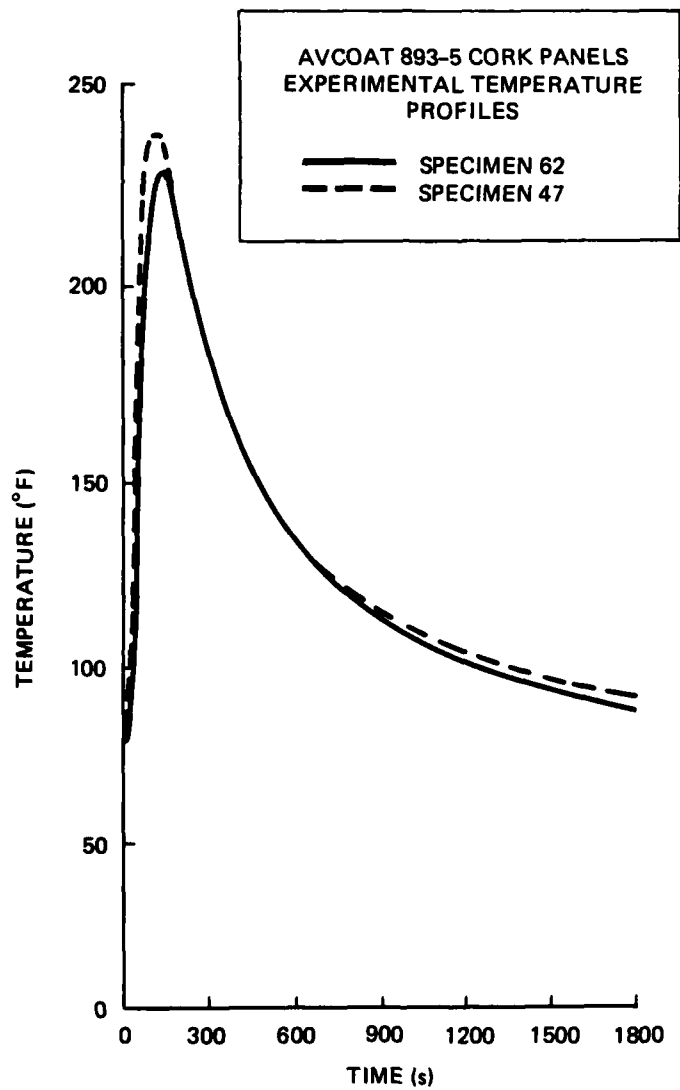
Figure C-12. Avcoat 893-5 cork sheet.

APPENDIX D

EXPERIMENTAL SUBSTRATE TEMPERATURE PROFILES

FOR CYLINDER TEST SPECIMENS

(THERMOCOUPLE DEPTHS INDICATED)

(Heat Flux: 10 Btu/ft^2-s, Burn Duration: 200 s)

163

FIREX 2373
CYLINDER SPECIMEN C-1
EXPERIMENTAL SUBSTRATE
TEMPERATURE PROFILES
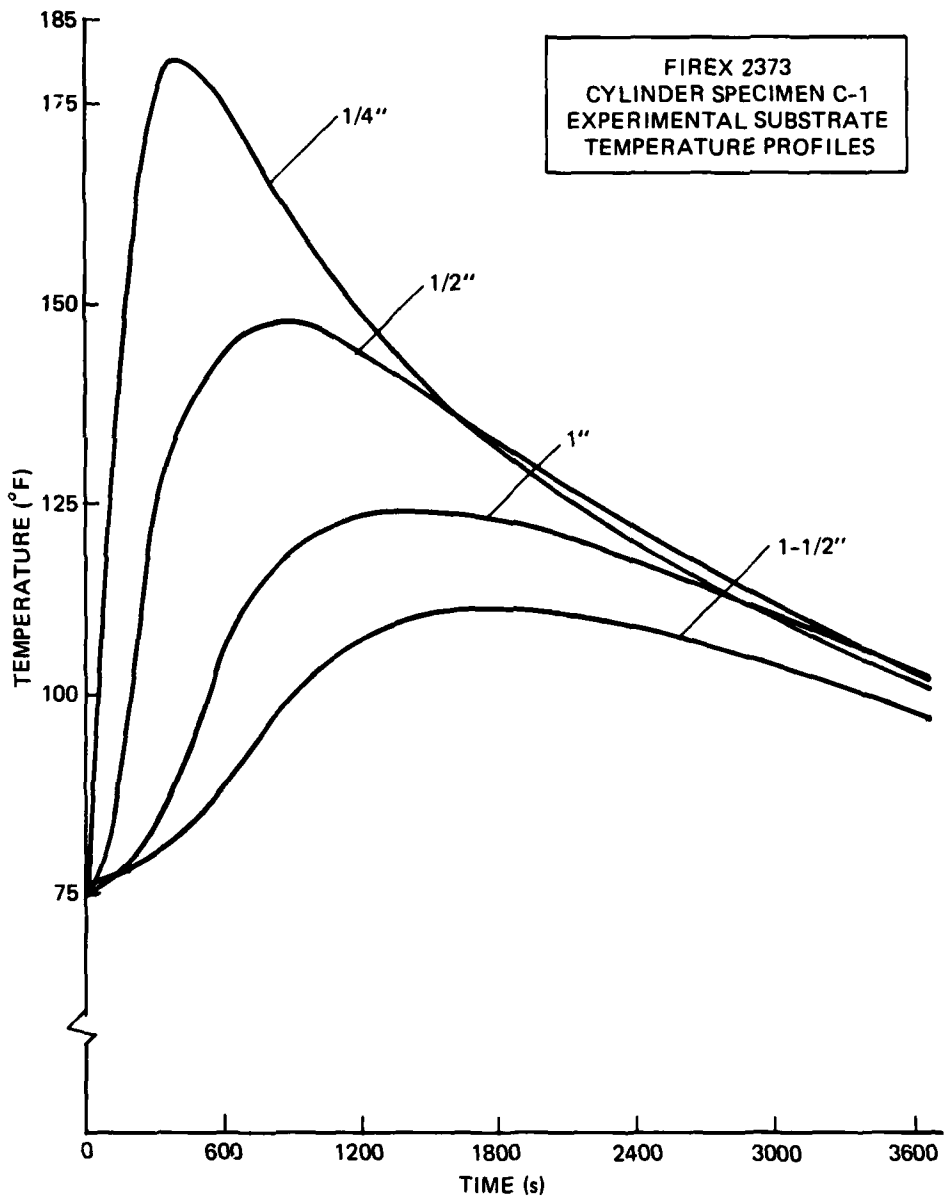
Figure D-1. Firex 2373, specimen C-1.

164
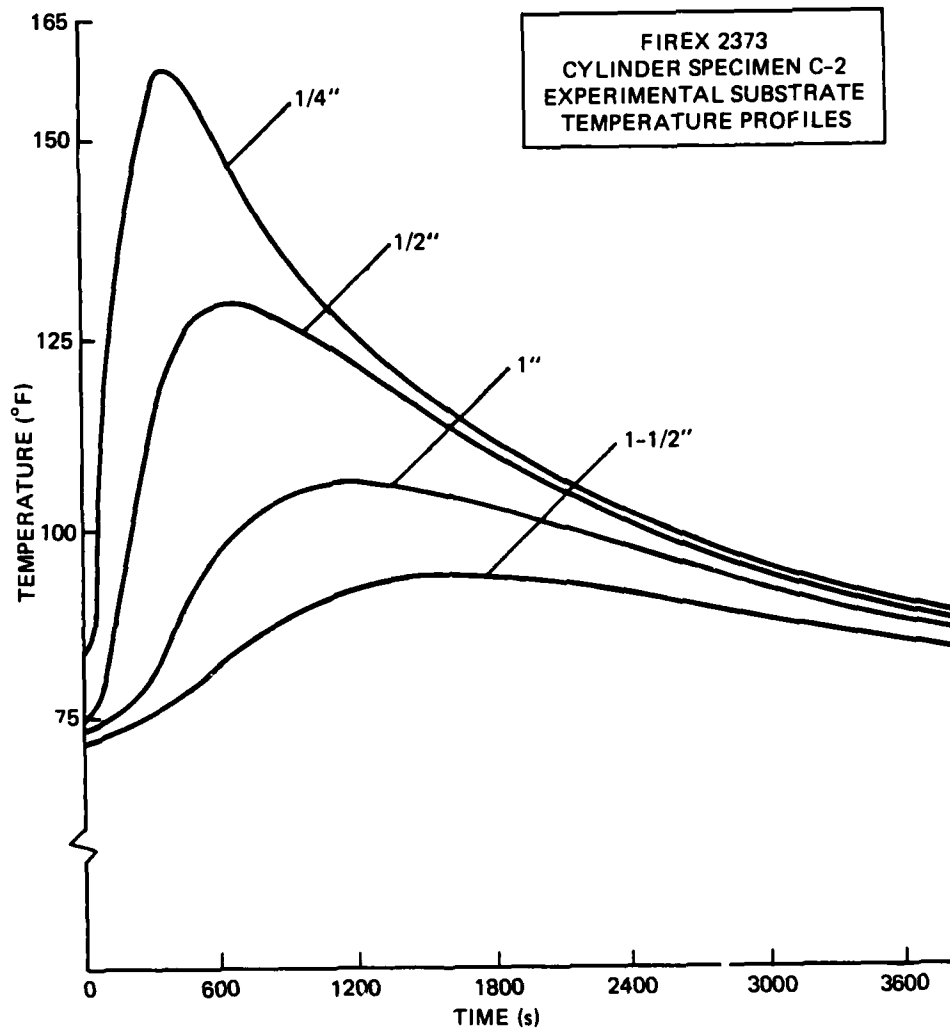
Figure D-2. Firex 2373, specimen C-2.
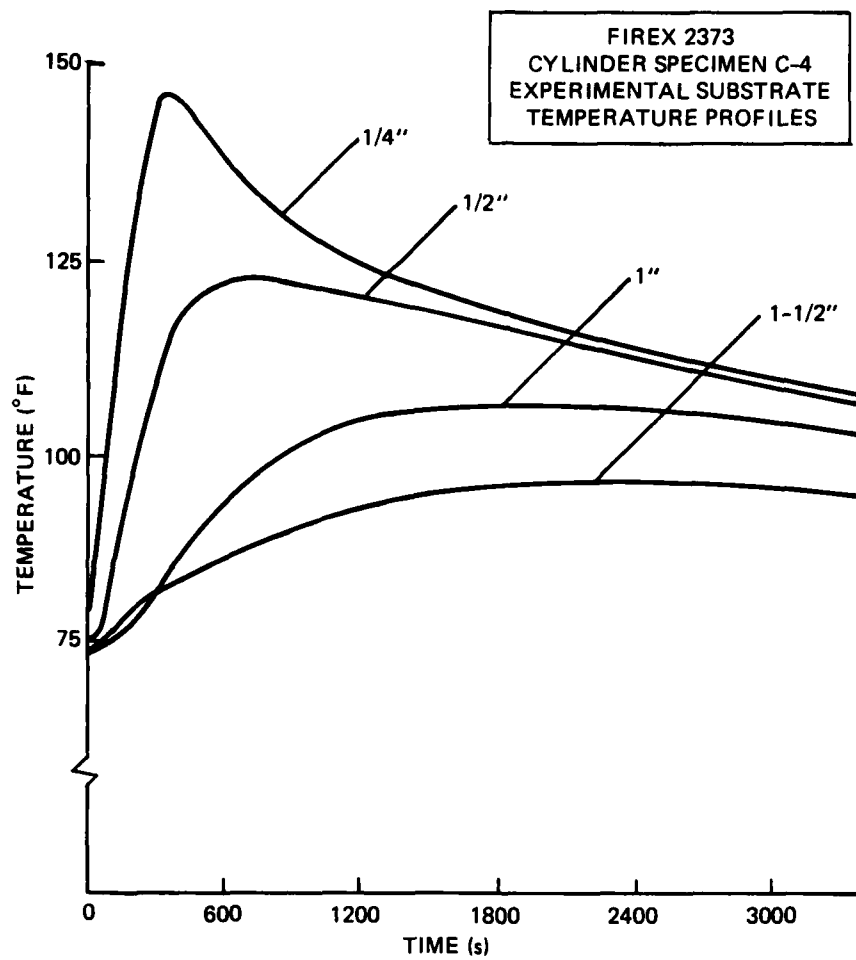
Figure D-3. Firex 2373, specimen C-4.

166
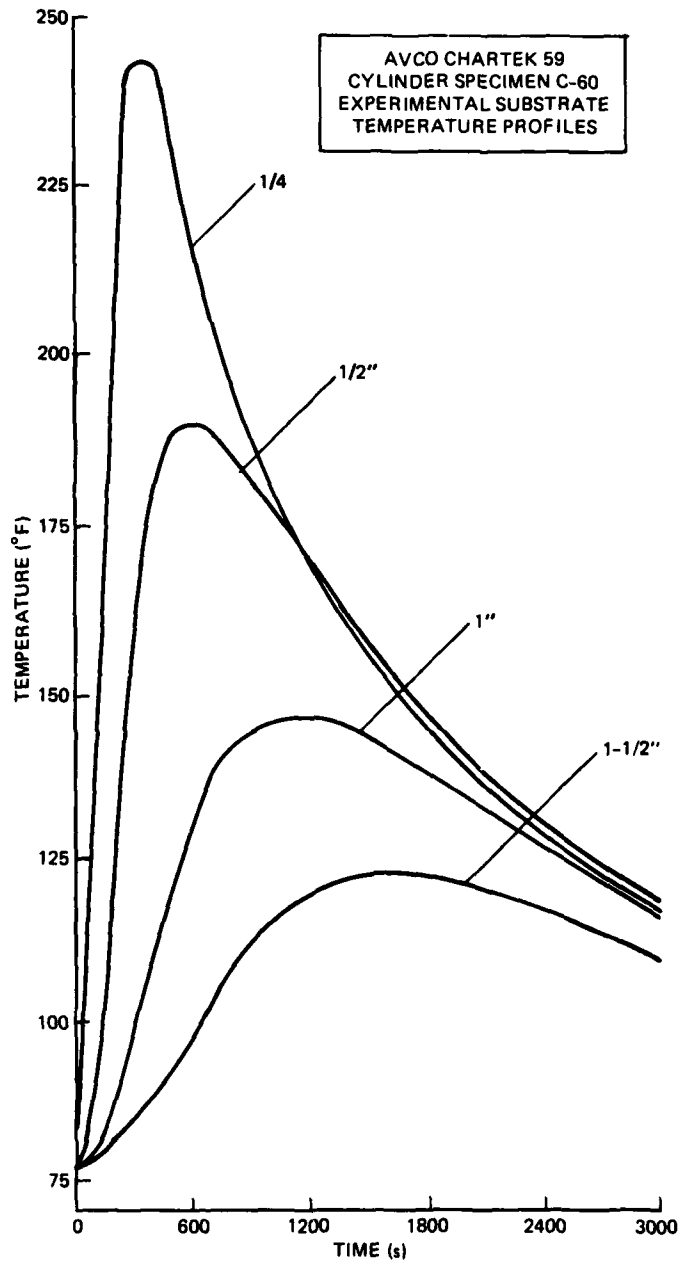
Figure D-4.   Chartek 59, specimen C-60.
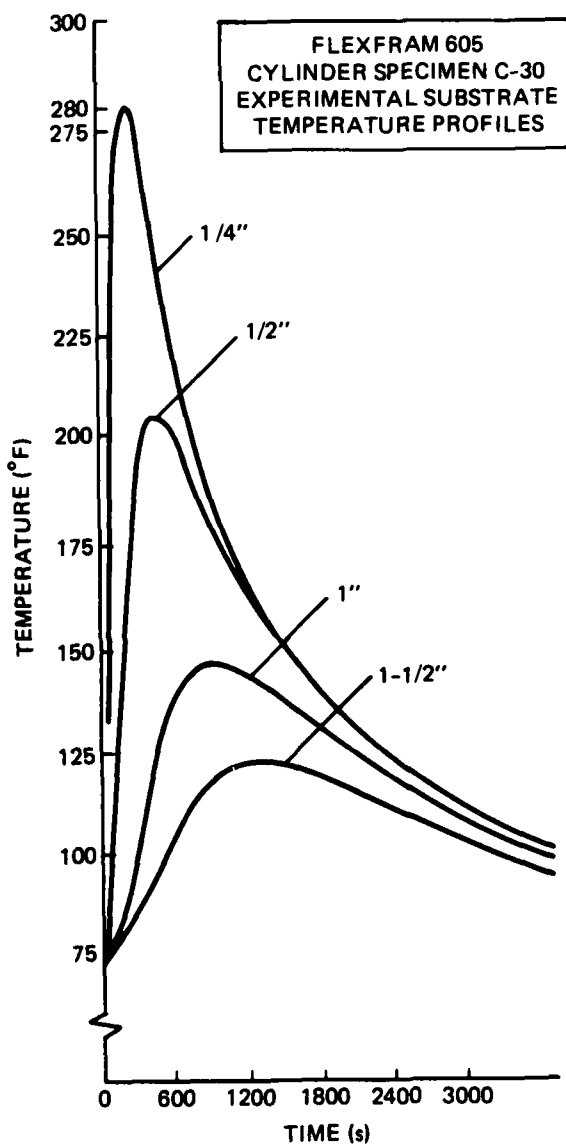
Figure D-5. Flexfram 605, specimen C-30.

168
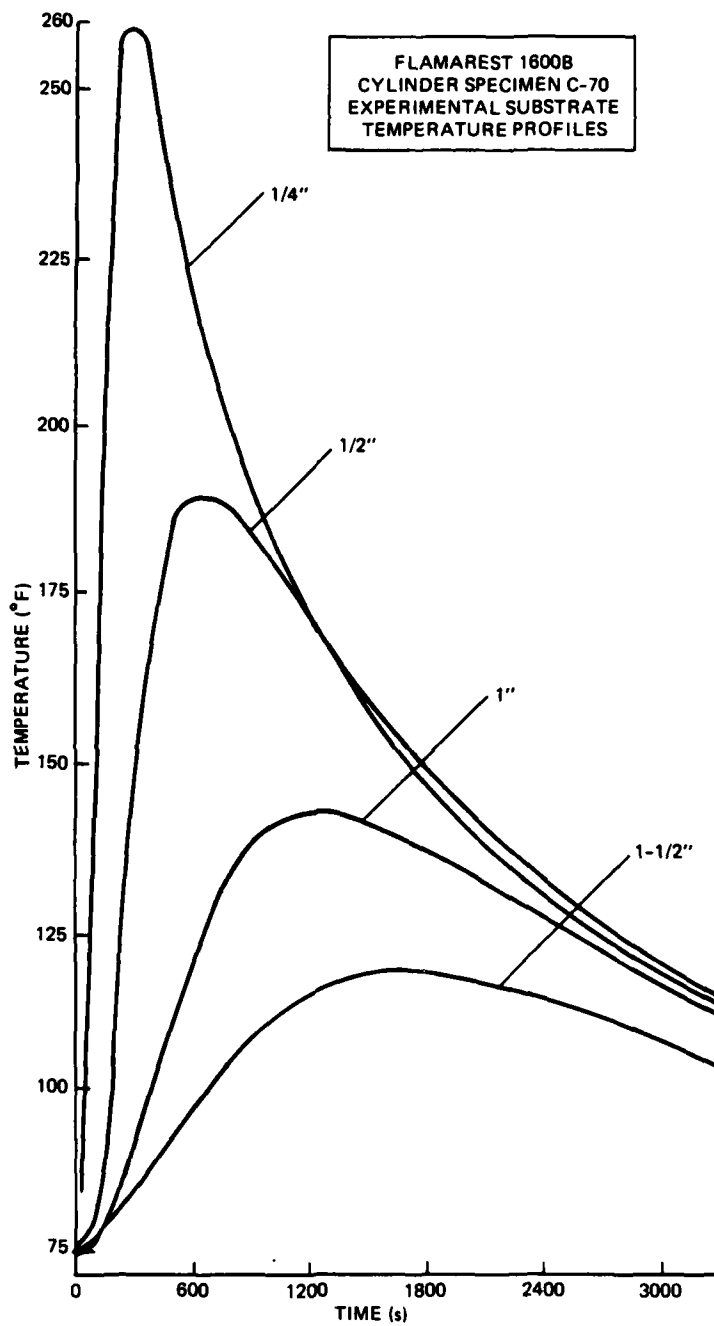
Figure D-6. Flamarest 1600B, specimen C-70.

169
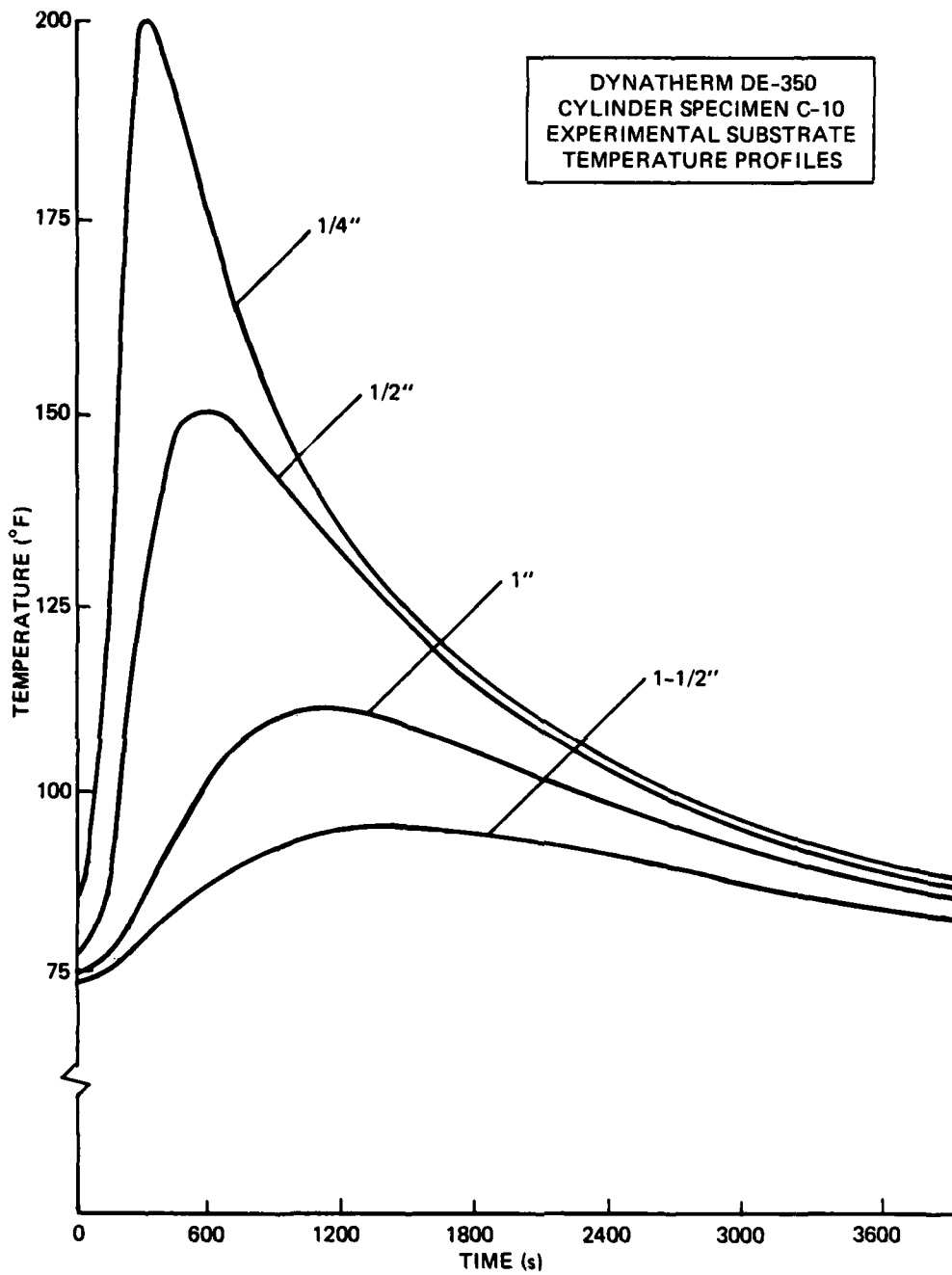
Figure D-7. Dynatherm DE-350, specimen C-10.
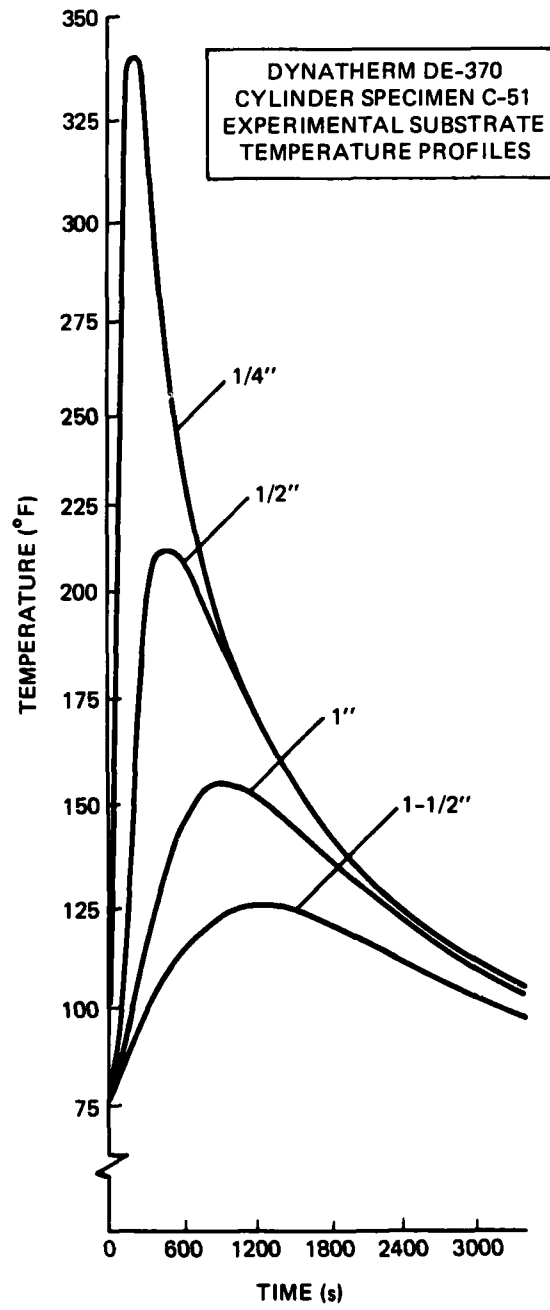
Figure D-8. Dynatherm DE-370, specimen C-51.
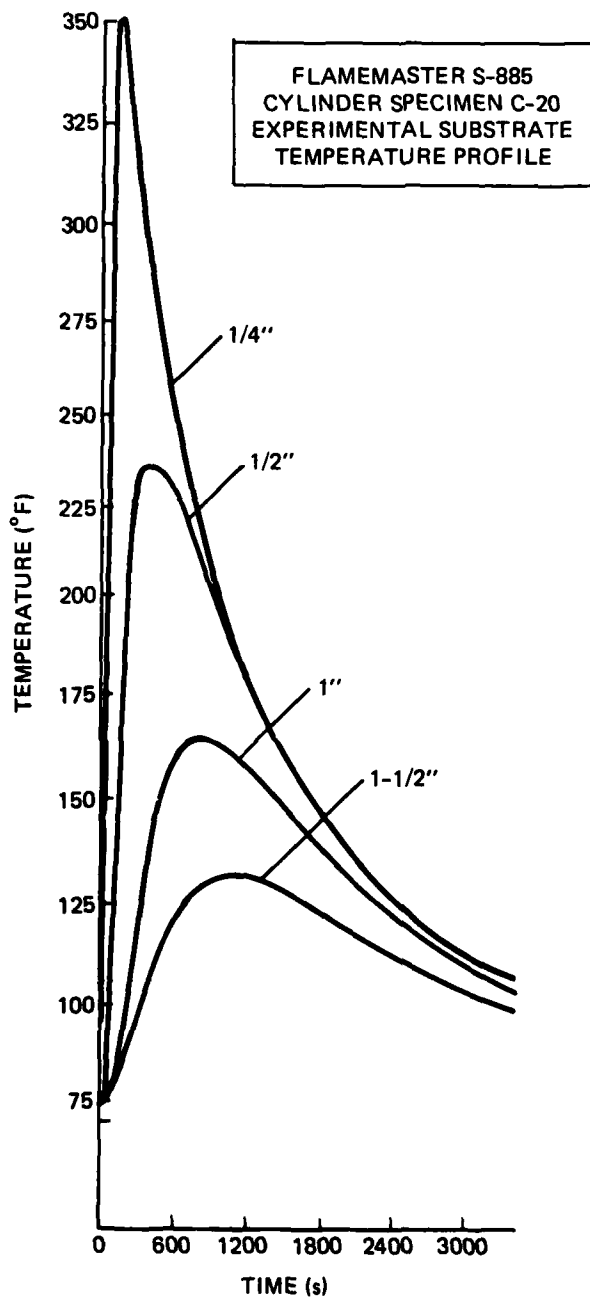
Figure D-9. Flamemaster S-885, specimen C-20.

172

FLAMEMASTER S-886
CYLINDER SPECIMEN C-40
EXPERIMENTAL SUBSTRATE
TEMPERATURE PROFILES
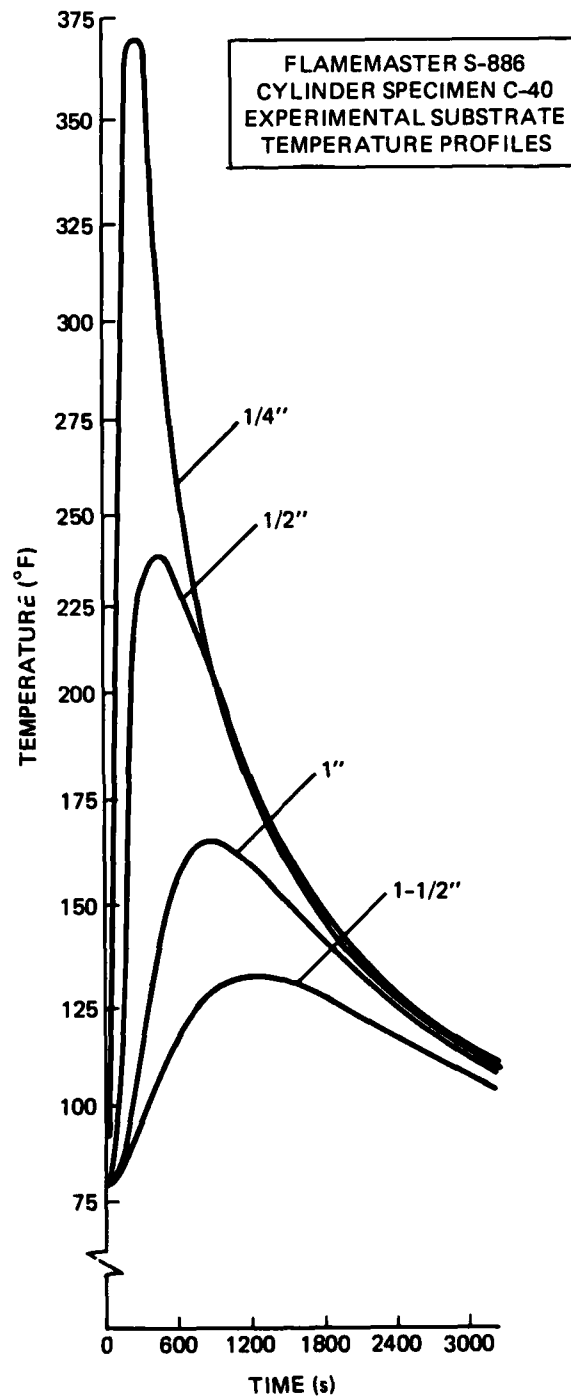
Figure D-10.   Flamemaster S-886, specimen C-40.

173

APPENDIX E

EXPERIMENTAL SUBSTRATE TEMPERATURE PROFILES
FOR CYLINDER TEST SPECIMENS
(THERMOCOUPLE DEPTHS INDICATED)

(Heat Flux: 10 Btu/ft^2-s, Burn Duration: 45s)
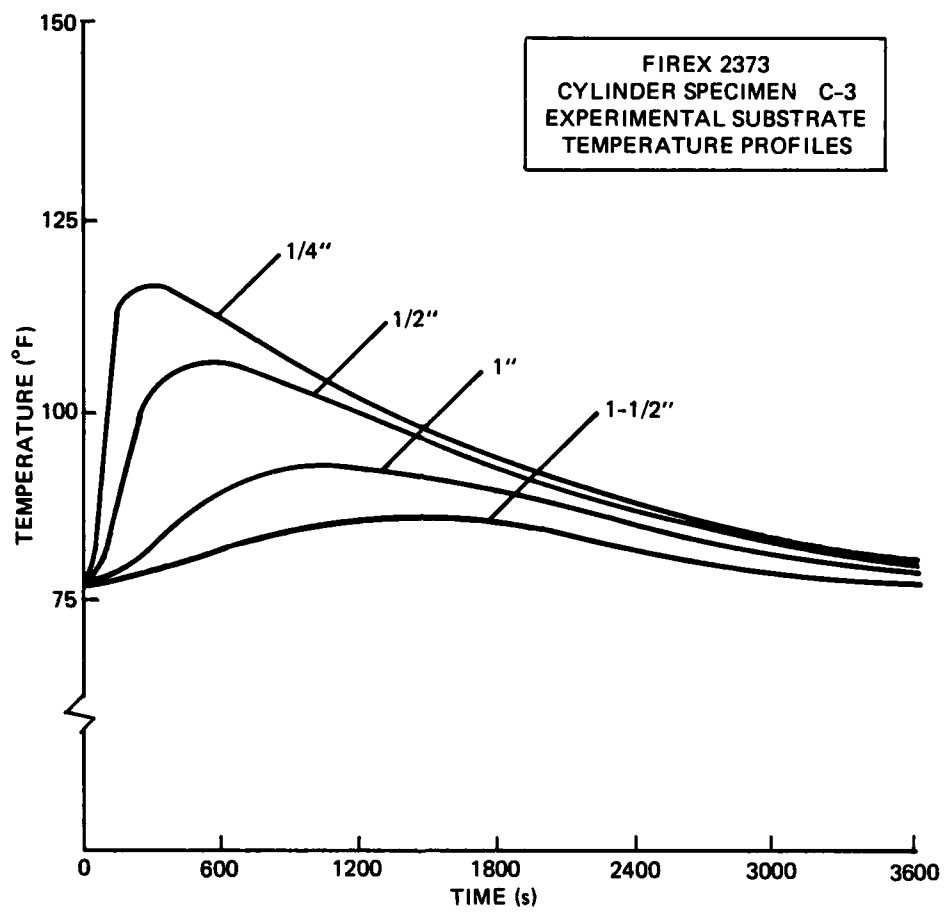
Figure E-1. Firex 2373, specimen C-3.
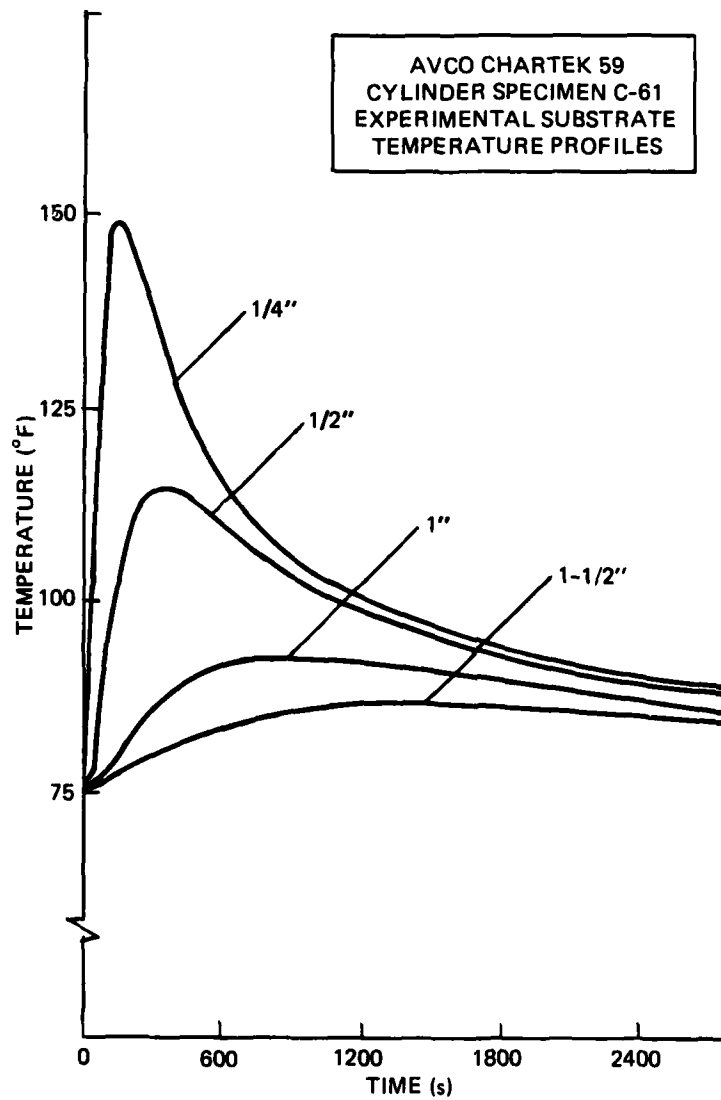
Figure E-2.   Chartek 59, specimen C-61.
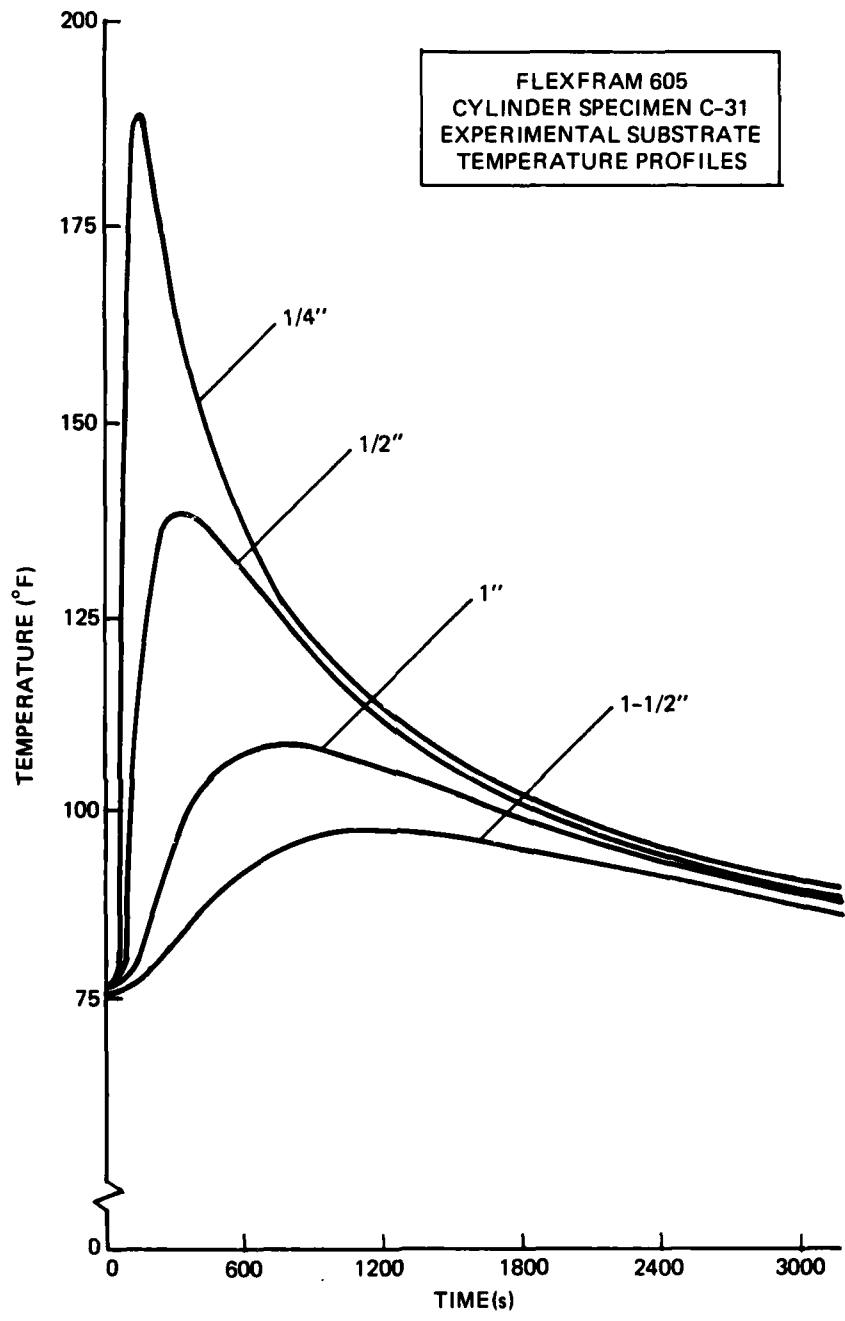
Figure E-3. Flexfram 605, specimen C-31.

177
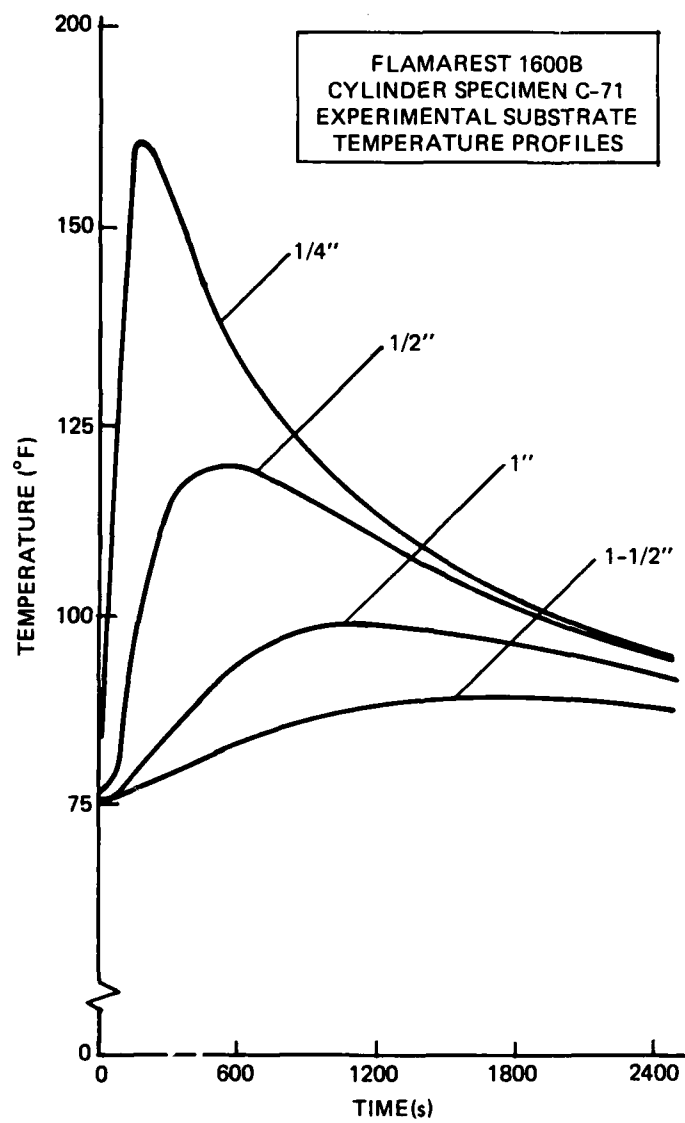
Figure E-4. Flamarest 1600B, specimen C-71.

178
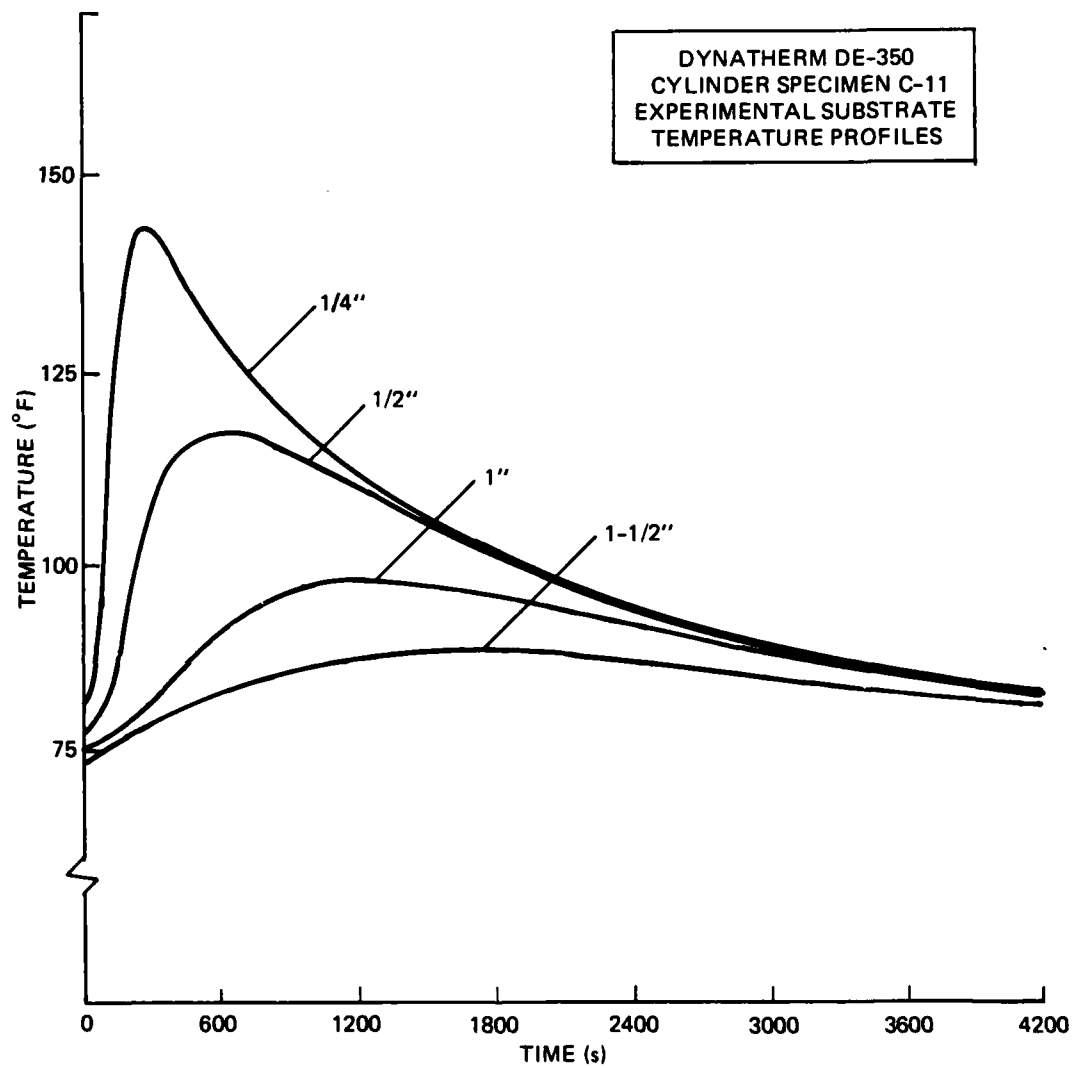
Figure E-5.   Dynatherm DE-350, specimen C-11.

179
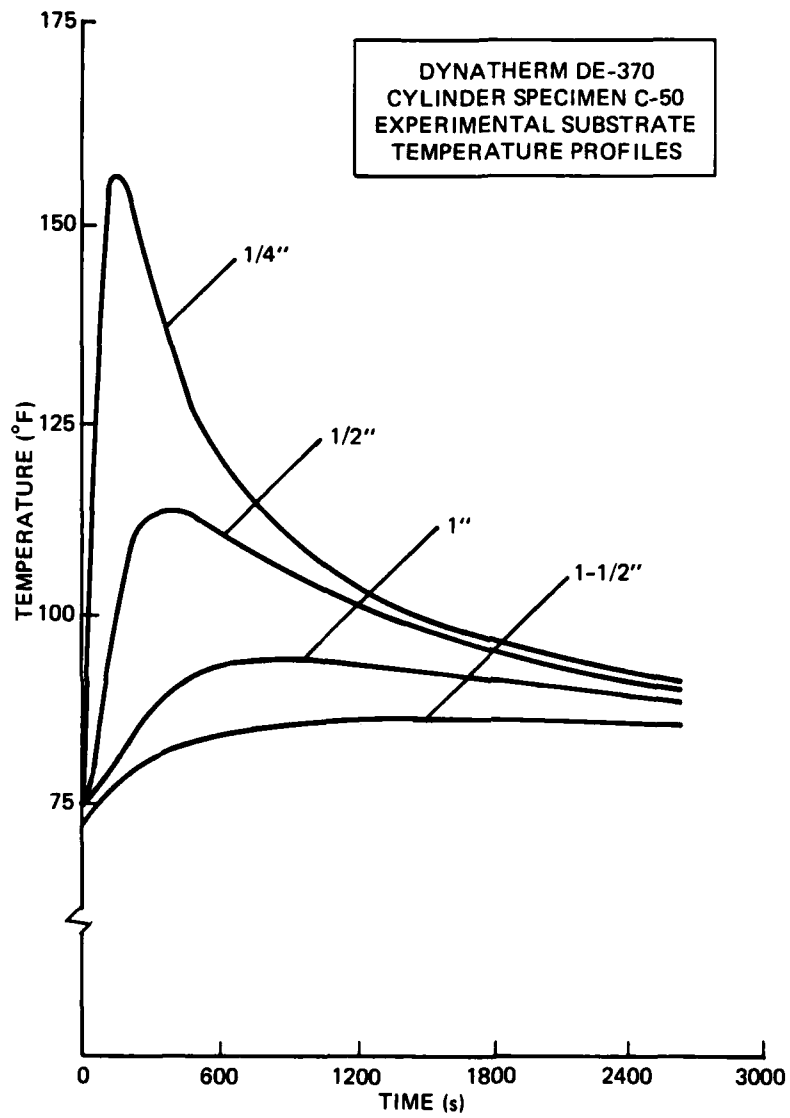
Figure E-6. Dynatherm DE-370, specimen C-50.

180
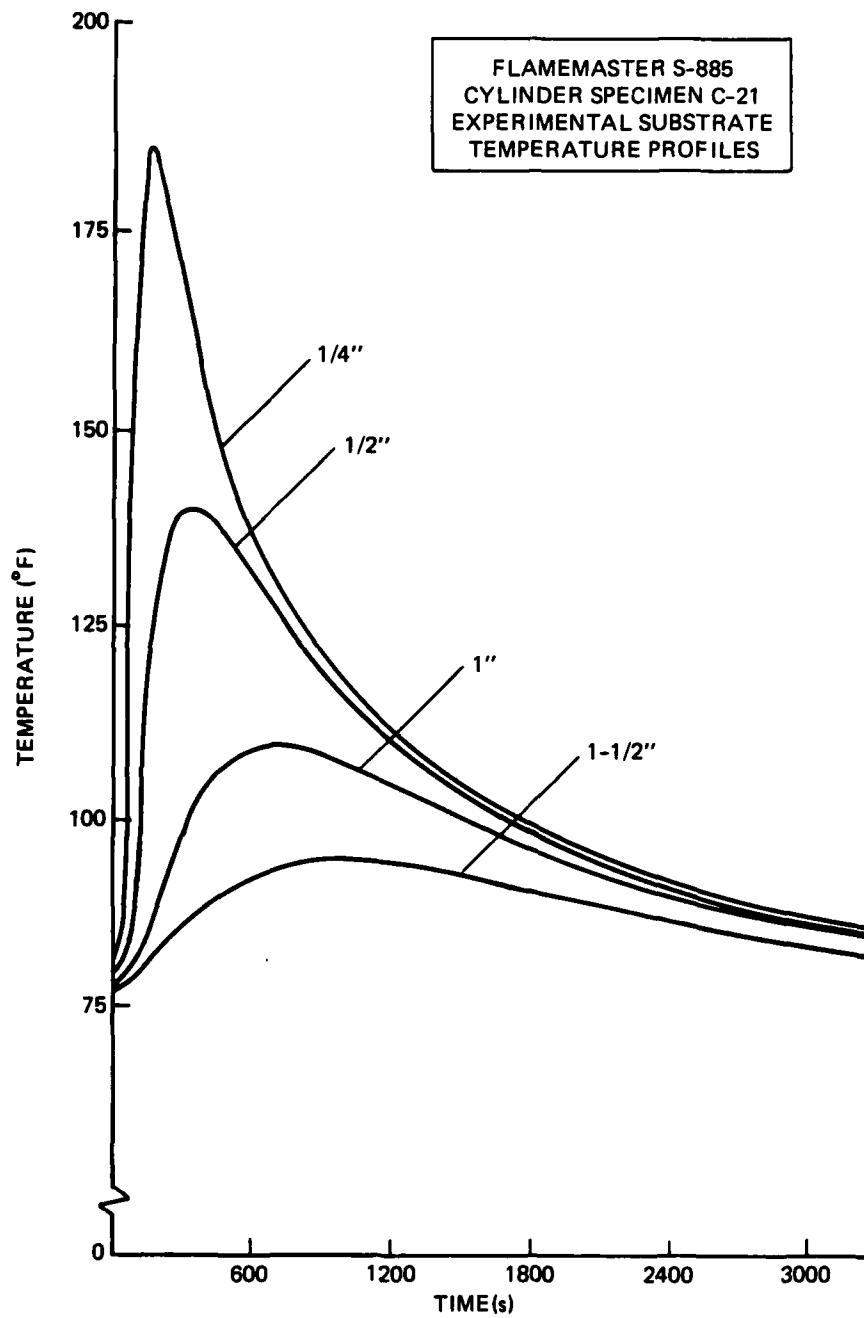
Figure E-7. Flamemaster S-885, specimen C-21.

181
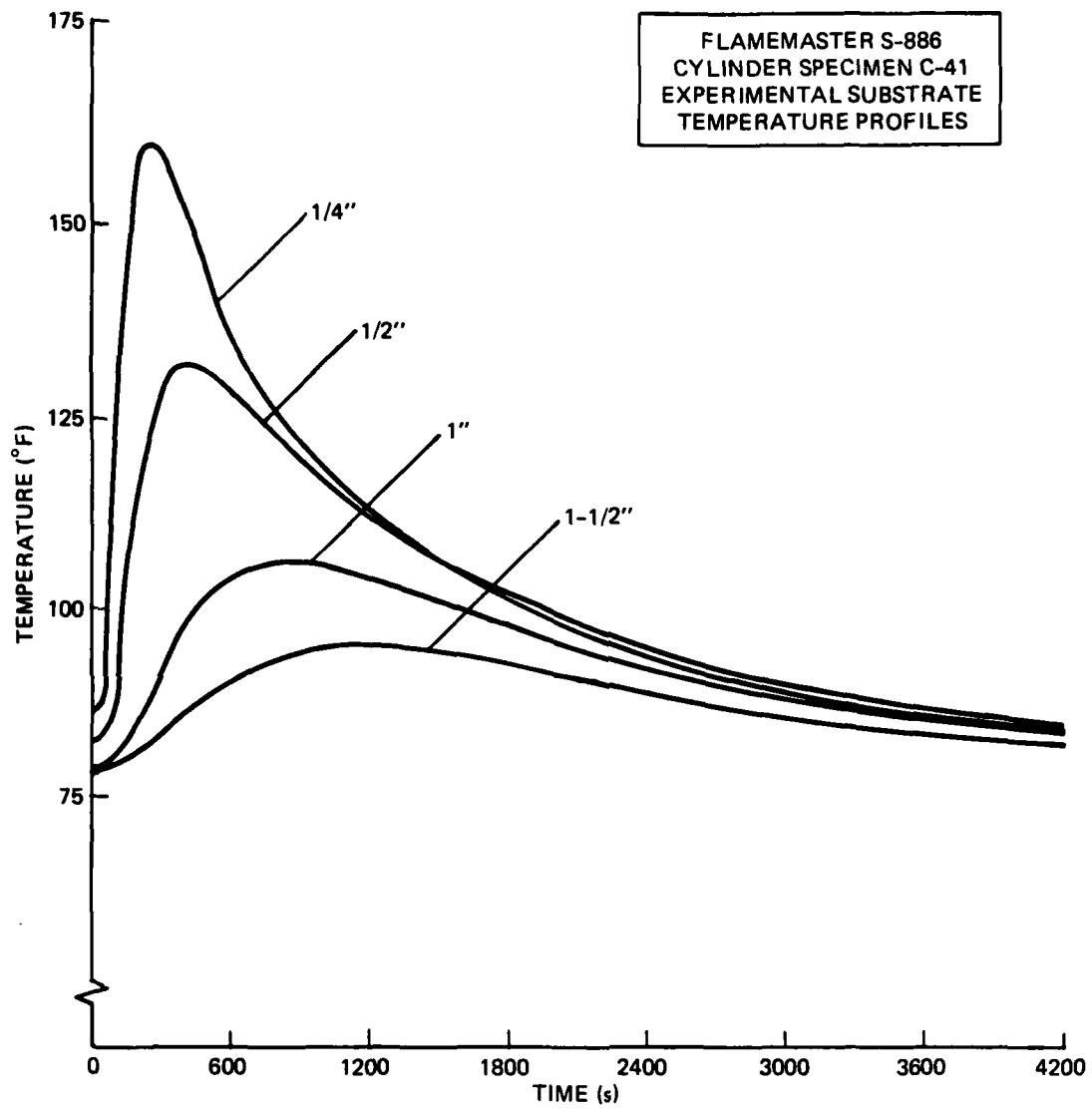
Figure E-8. Flamemaster S-886, specimen C-41.

182

APPENDIX F

PANEL TEST SPECIMENS
BEFORE AND AFTER (a, b) 45-s EXPOSURE
TO 10 Btu/ft^2-s HEAT FLUX
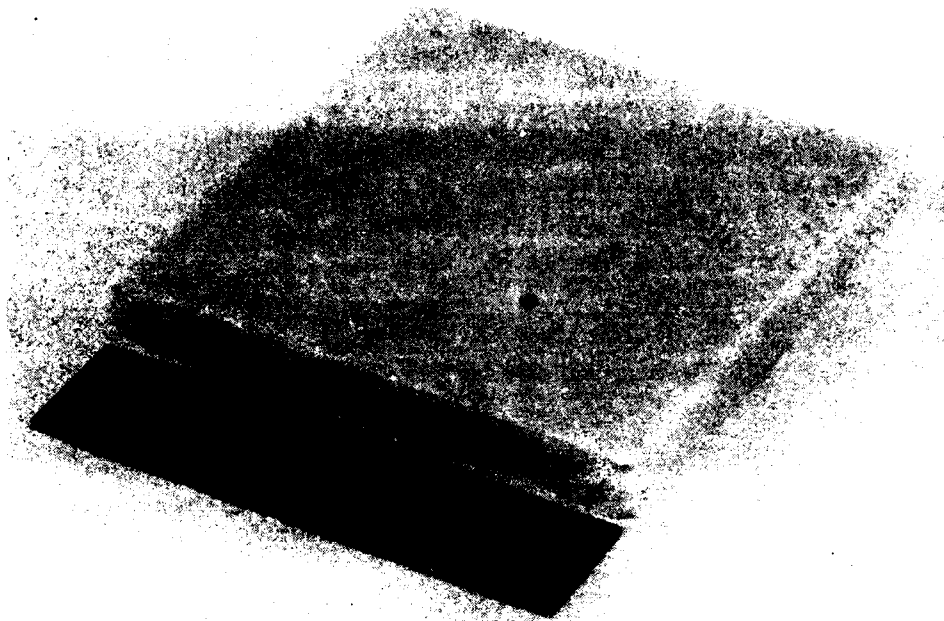
(a)

(b)

Figure F-1. Firex 2373.

184
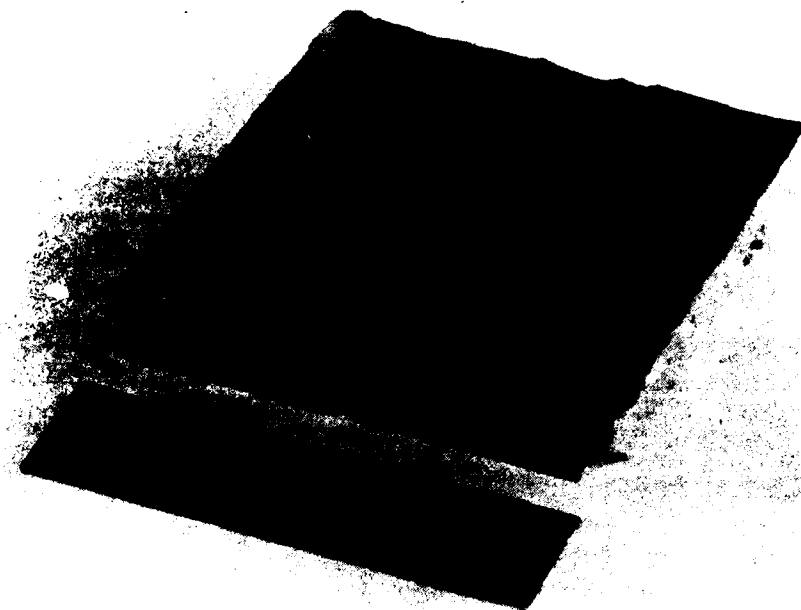
(a)

(b)

Figure F-2. Firex 2373 with vinyloid topcoat.

185
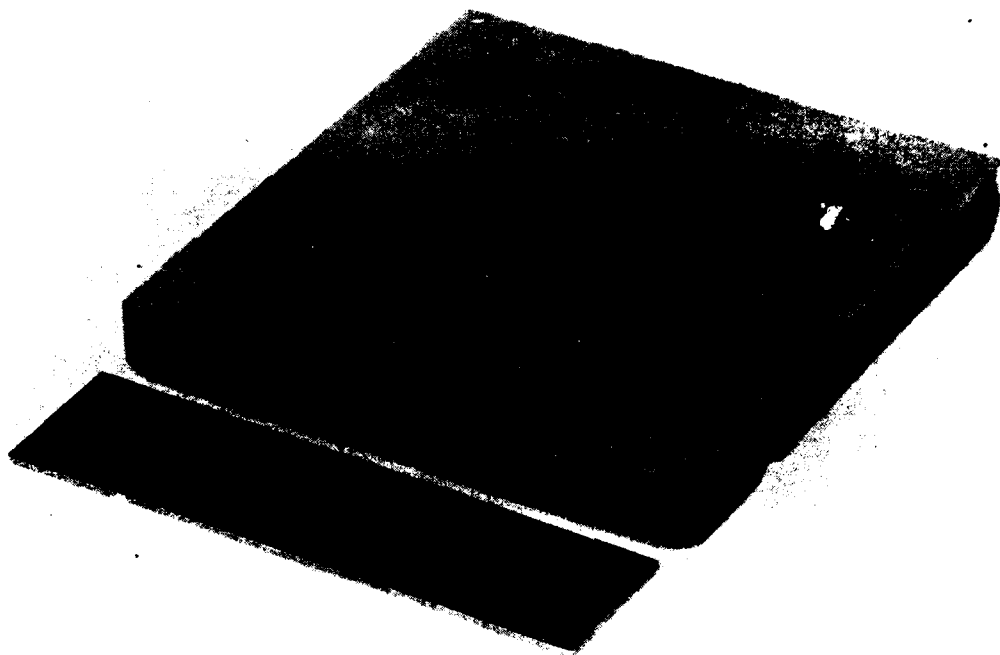
(a)
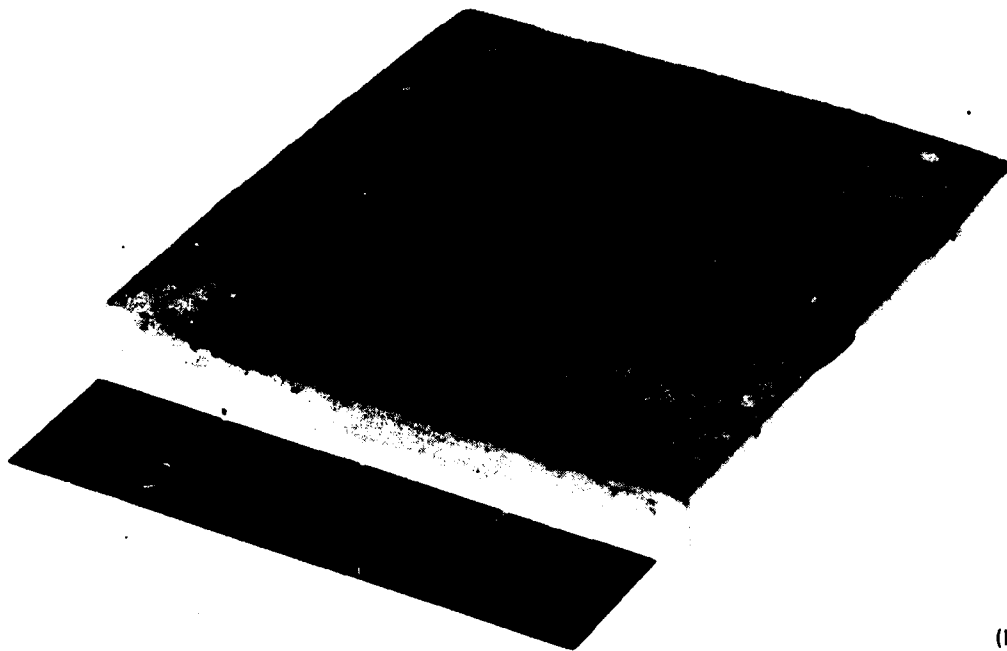
(b)

Figure F-3. Chartek 59.

186
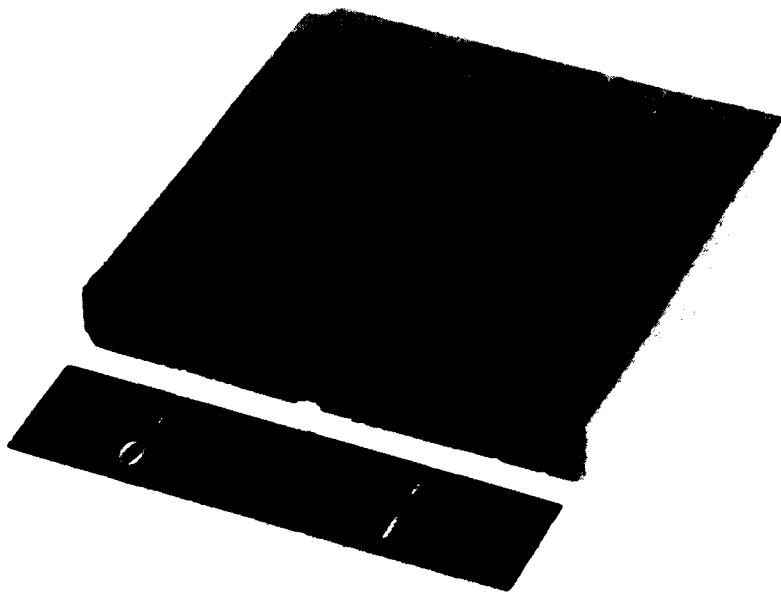
(a)
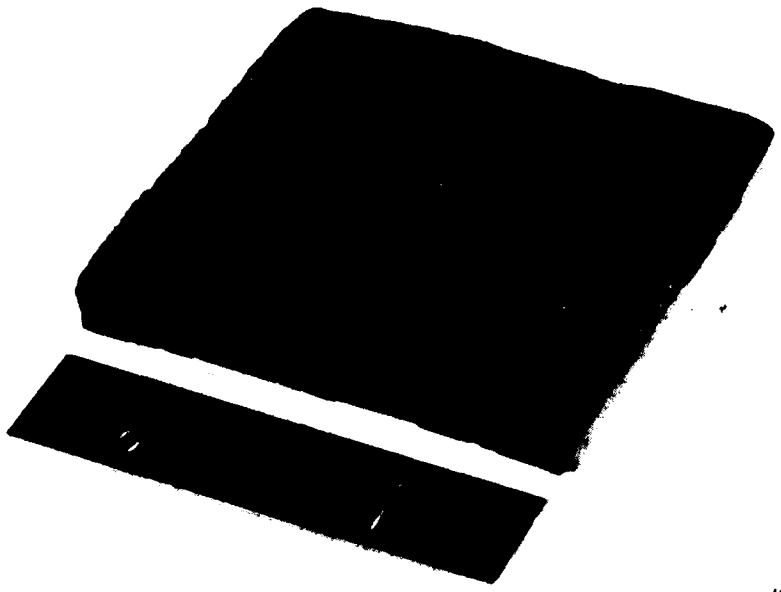
(b)

Figure F-4.   Flexfram 605.

187
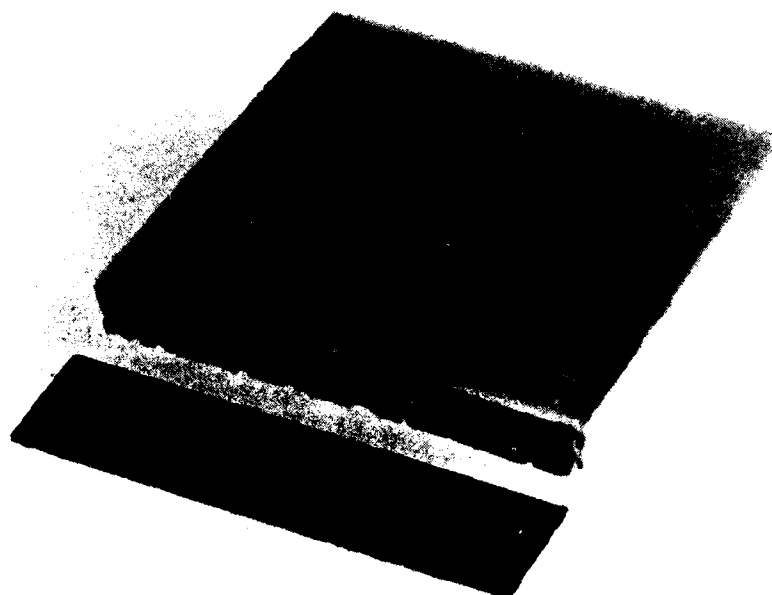
(a)

(b)

Figure F-5.   Flamarest 1600B.
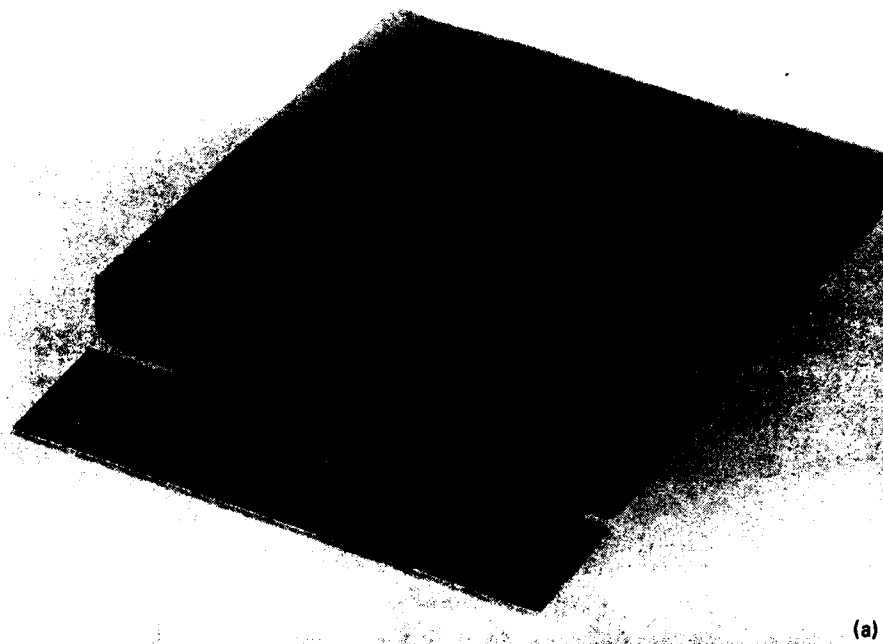
(a)
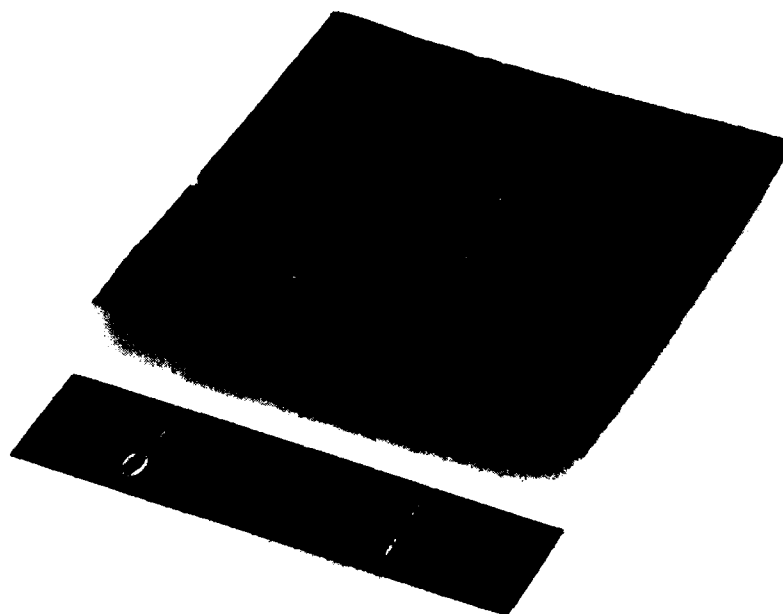
(b)

Figure F-6. Dynatherm DE-350.

189
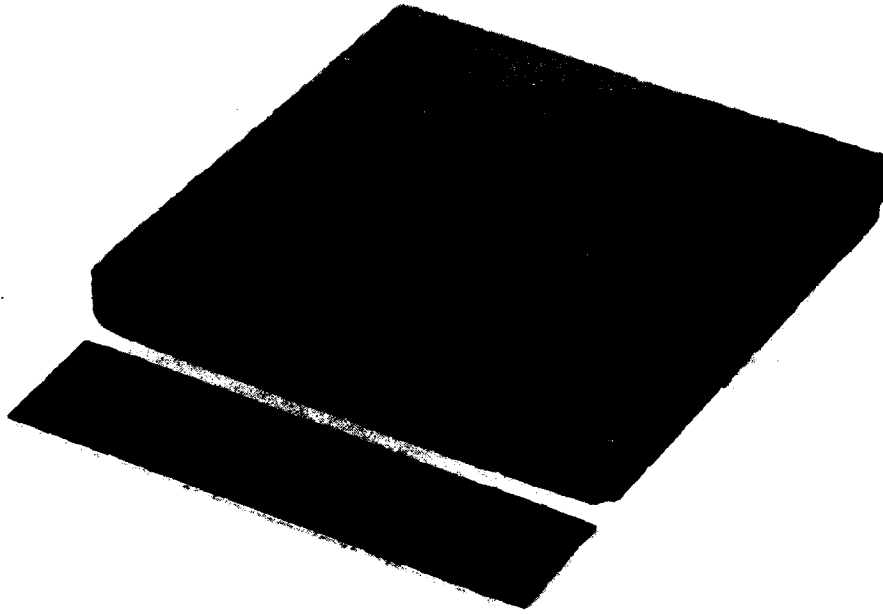
(a)
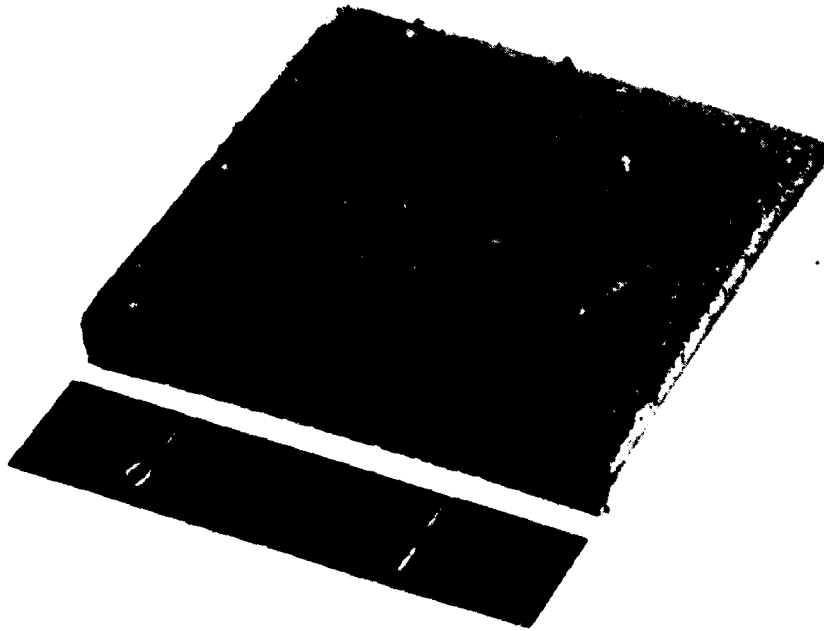
(b)

Figure F-7. Dynatherm DE-370.

190
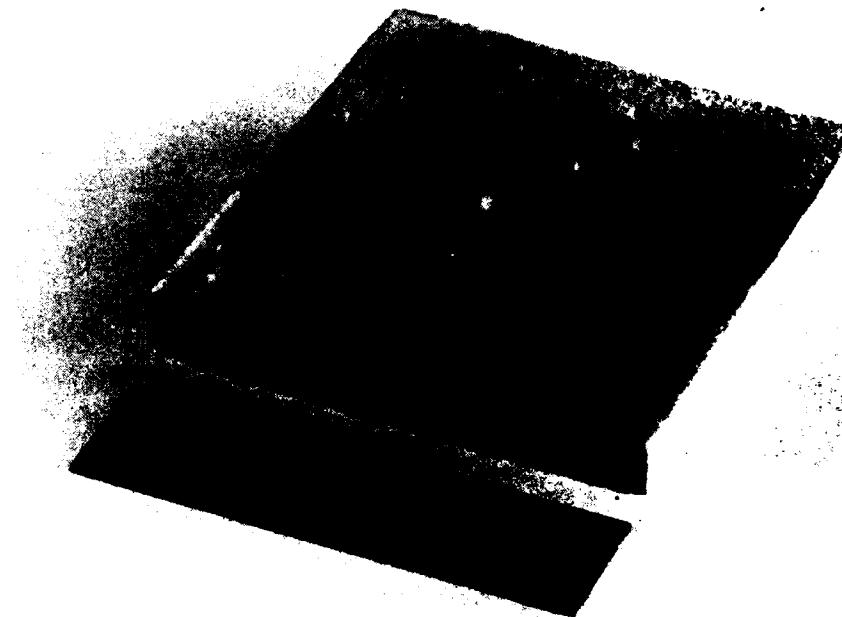
(a)
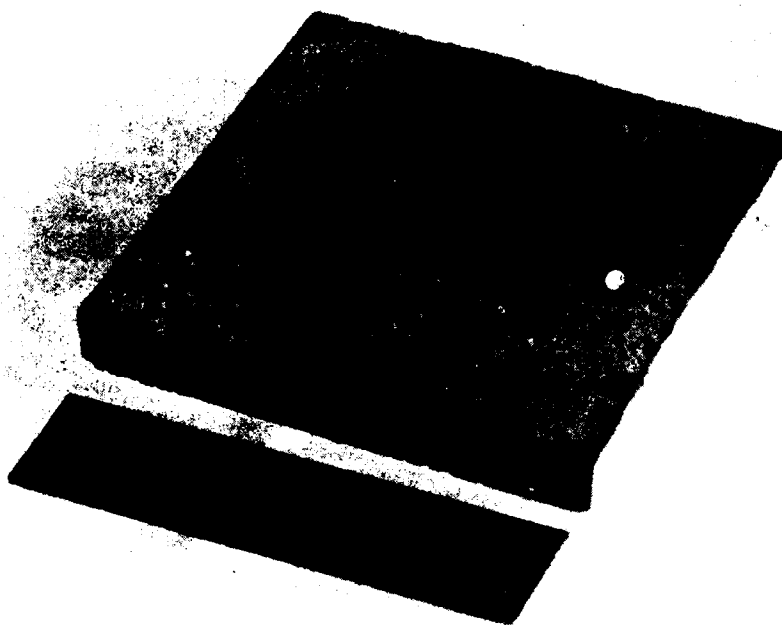
(b)

Figure F-8.   Flamemaster S-885.

191
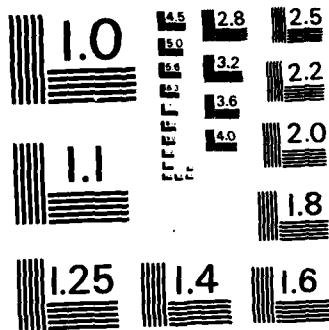
MICROCOPY RESOLUTION TEST CHART

NATIONAL BUREAU OF STANDARDS-1963-A
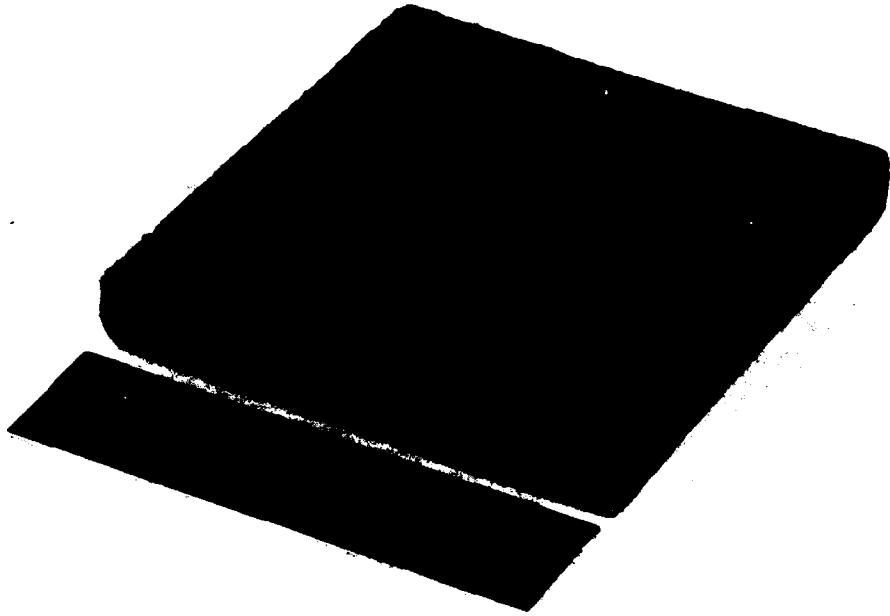
(a)
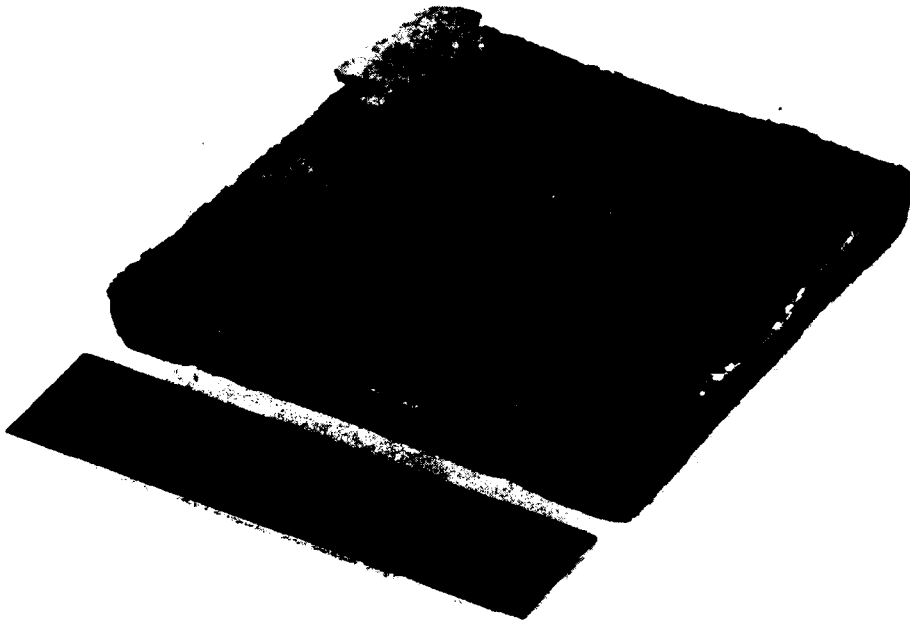
(b)

Figure F-9. Flamemaster S-886.

192
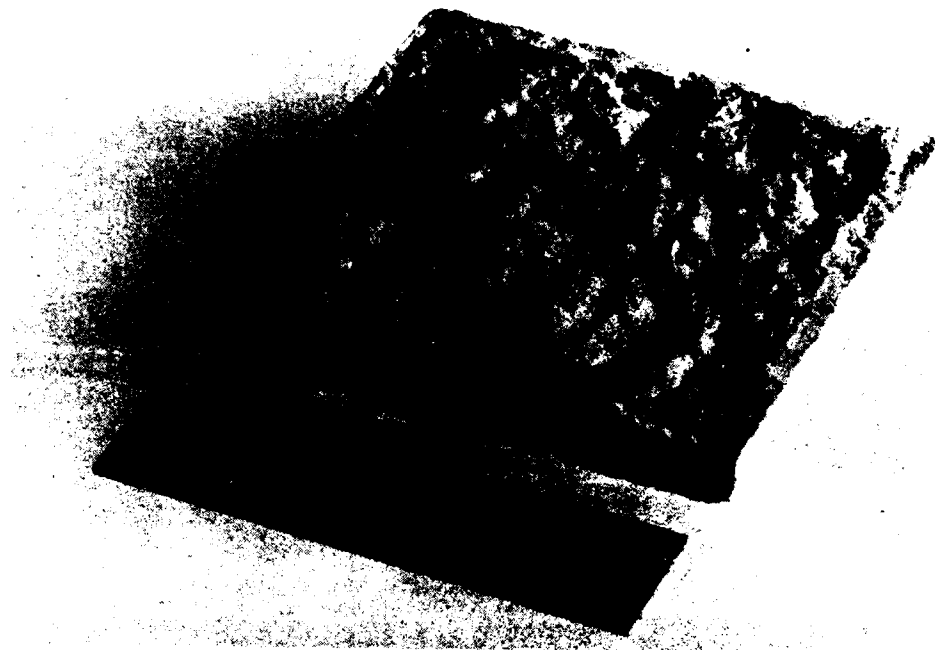
(a)
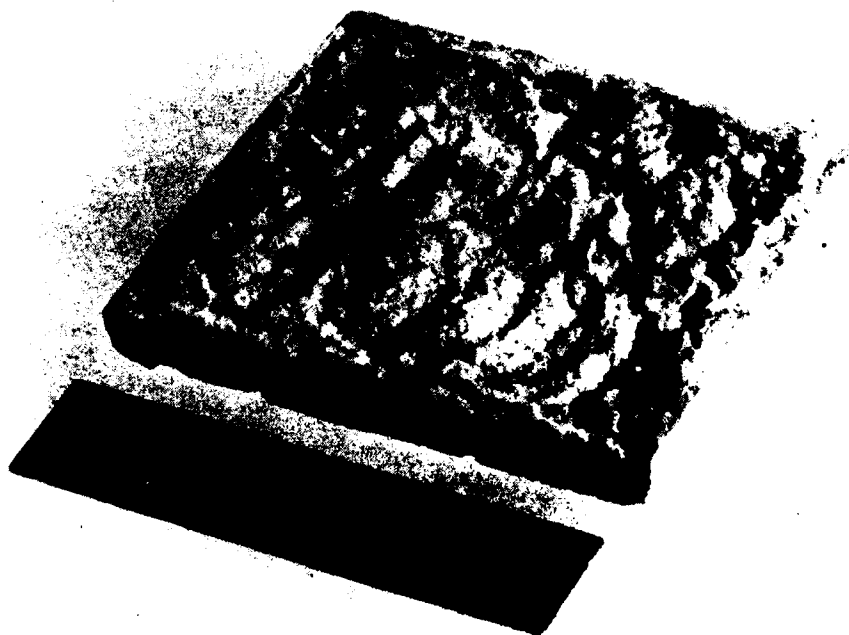
(b)

Figure F-10. Fiberfrax.

193
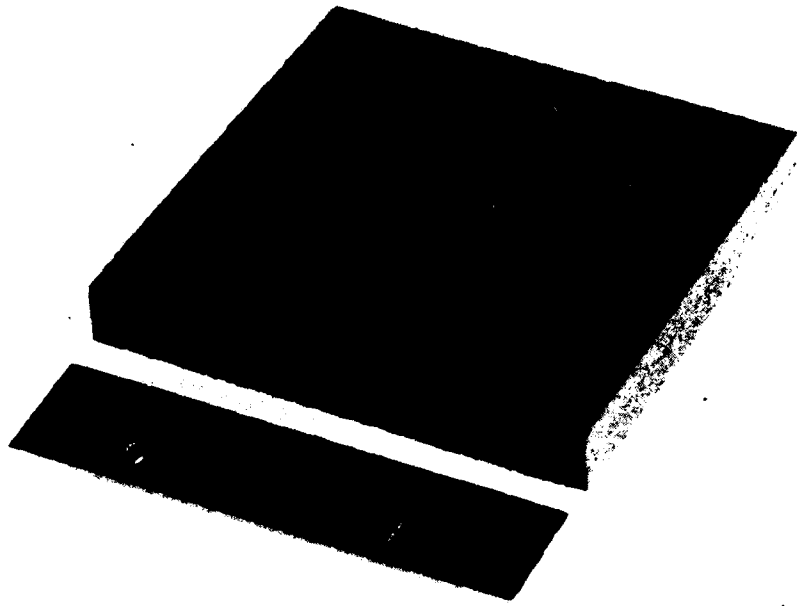
(a)
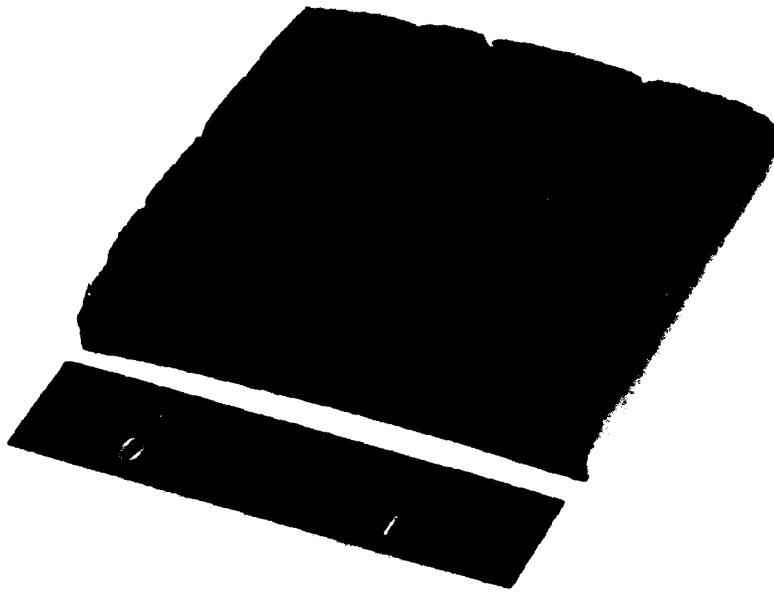
(b)

Figure F-11. Avcoat 893-5 cork.

194

APPENDIX G

CYLINDER TEST SPECIMEN FACE RESULTS
AFTER 200-s HEAT FLUX EXPOSURE
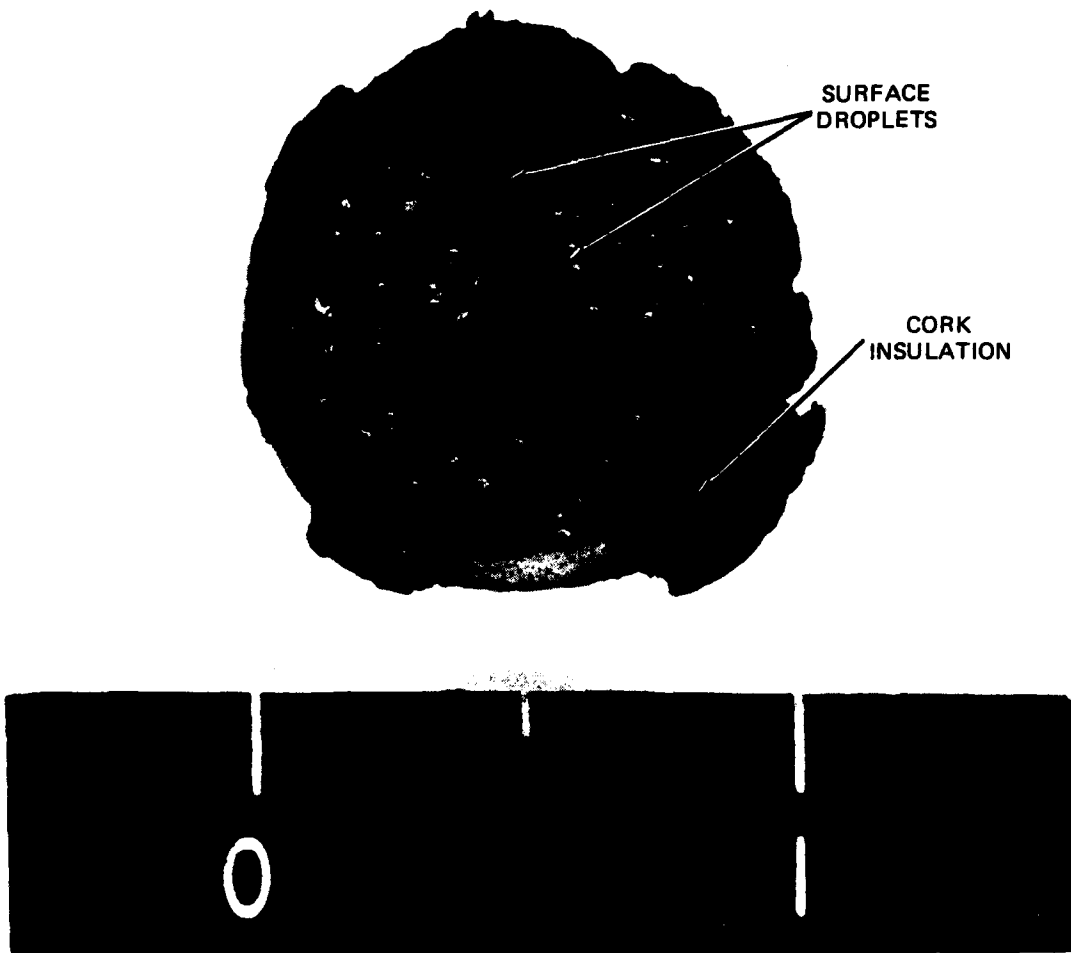
Figure G-1. Firex 2373 (10.04 Btu/ft^2-s heat flux).
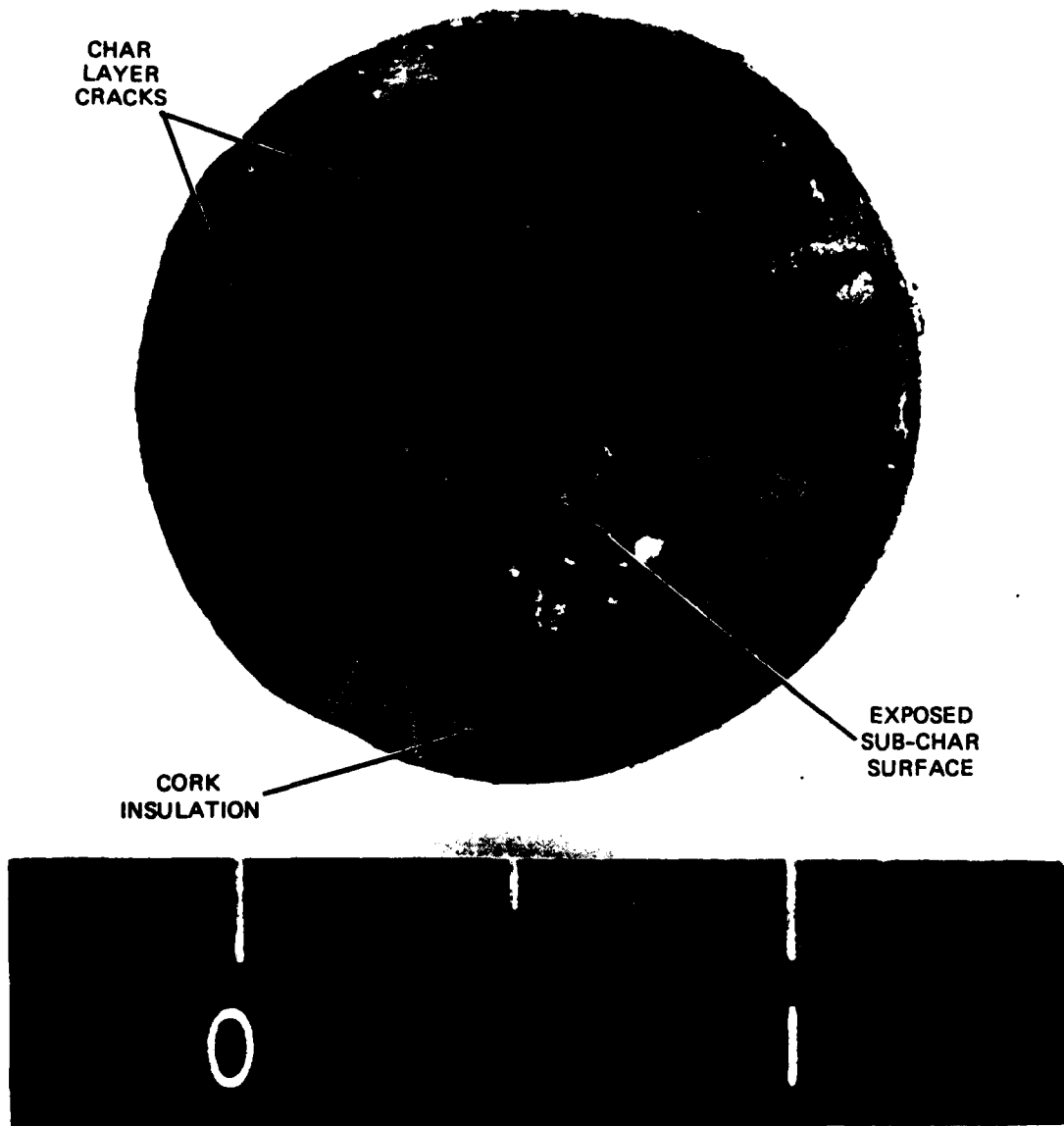
Figure G-2. Chartek 59 (9.96 Btu/ft^2-s heat flux).

CHAR
SURFACE
CRACK

CORK
INSULATION
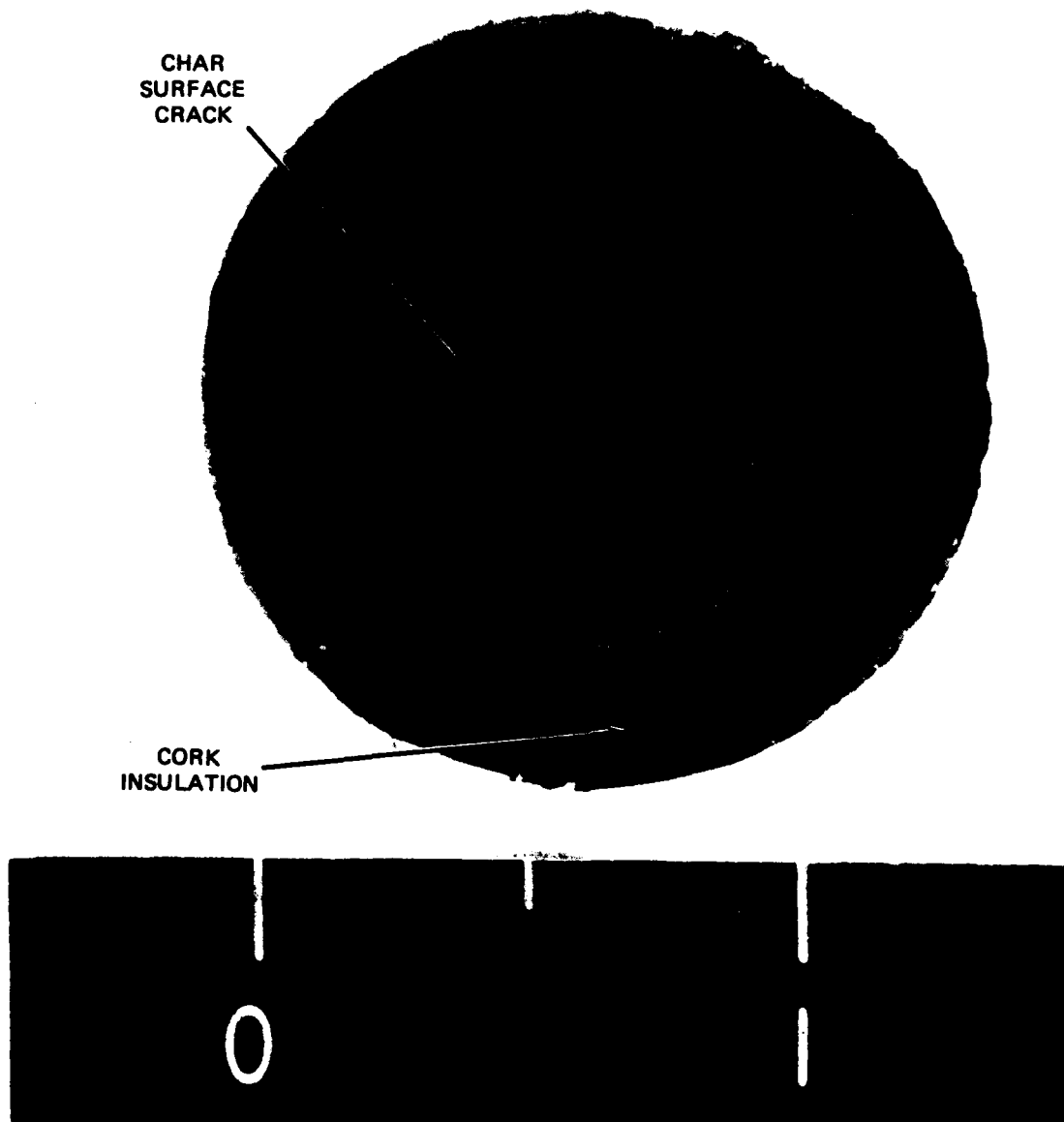
Figure G-3.   Flexfram 605 (9.91 Btu/ft^2-s heat flux).
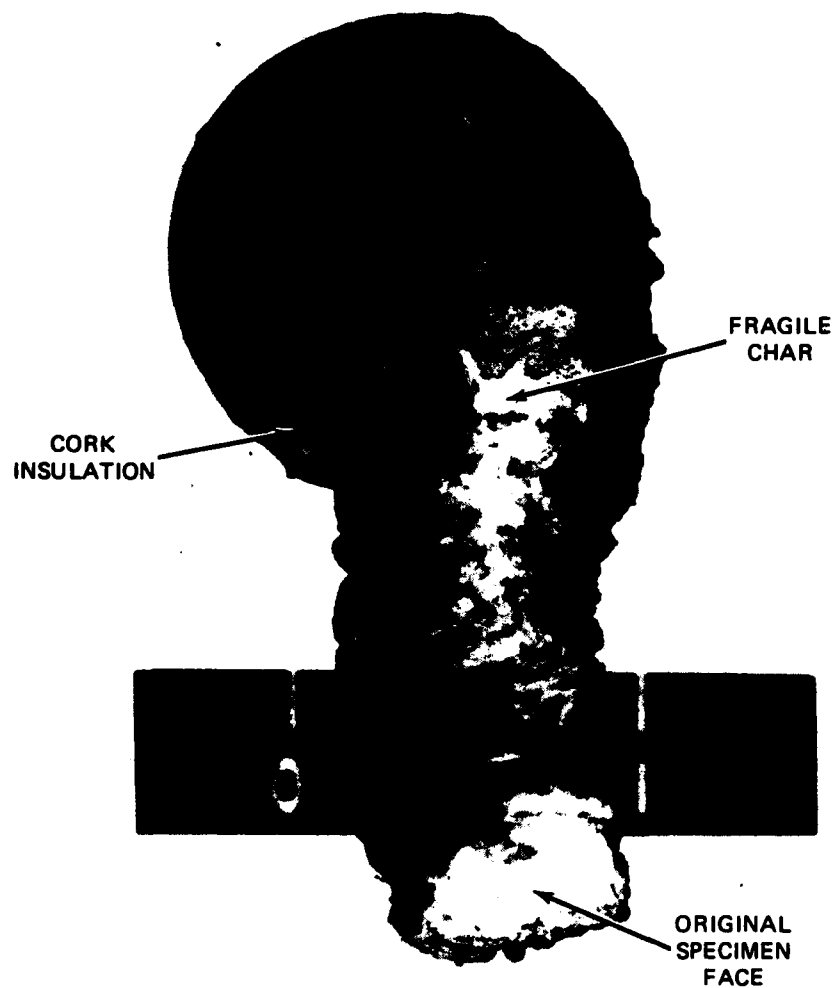
Figure G-4a. Flamarest 1600B—top view
(10.16 Btu/ft^2-s heat flux).

199
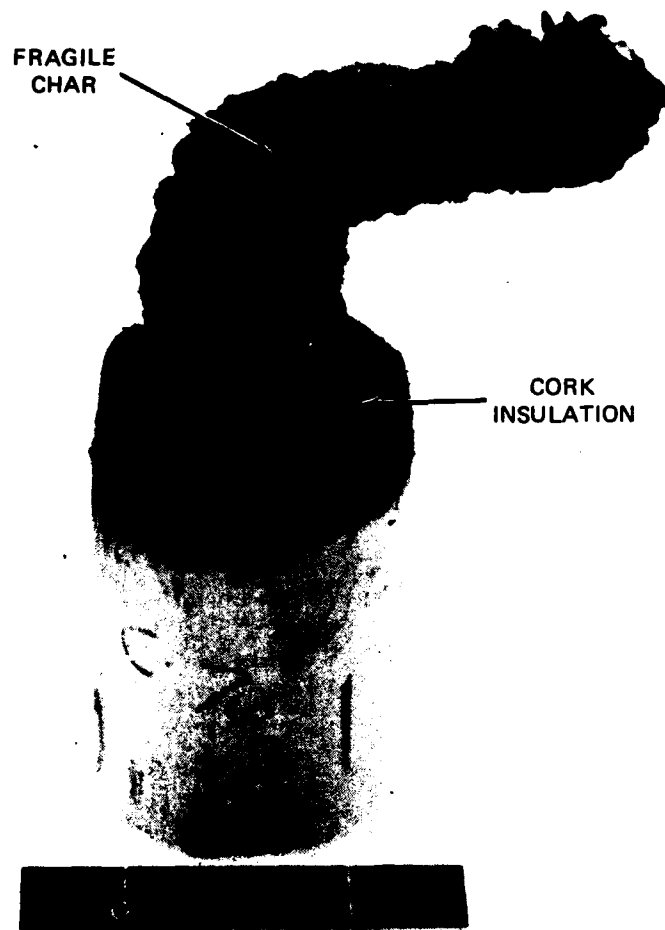
Figure G-4b. Flamarest 1600B—side view
(10.16 Btu/ft^2-s heat flux).
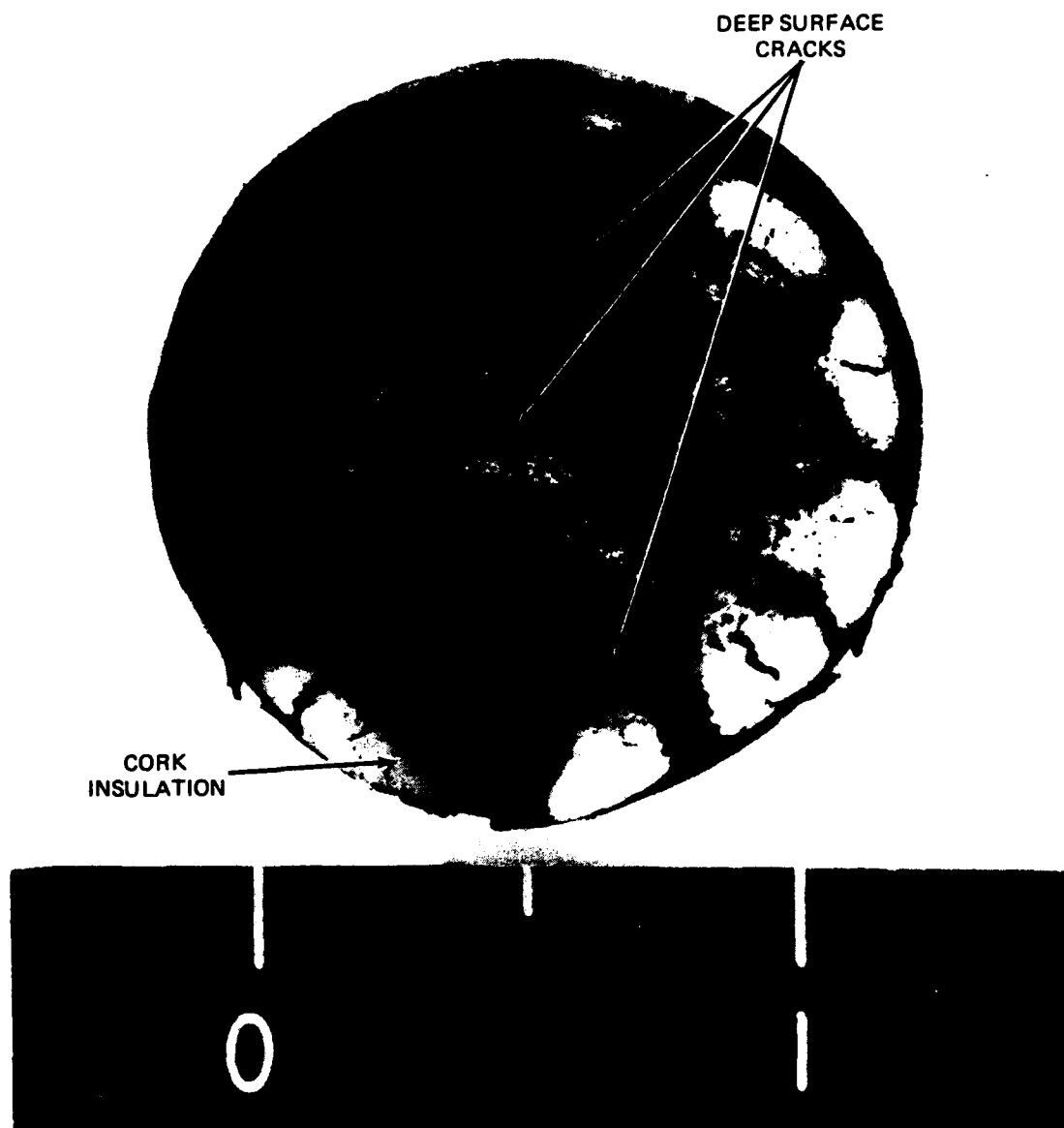
Figure G-5. Dynatherm DE-350 (10.0 Btu/ft^2-s heat flux).
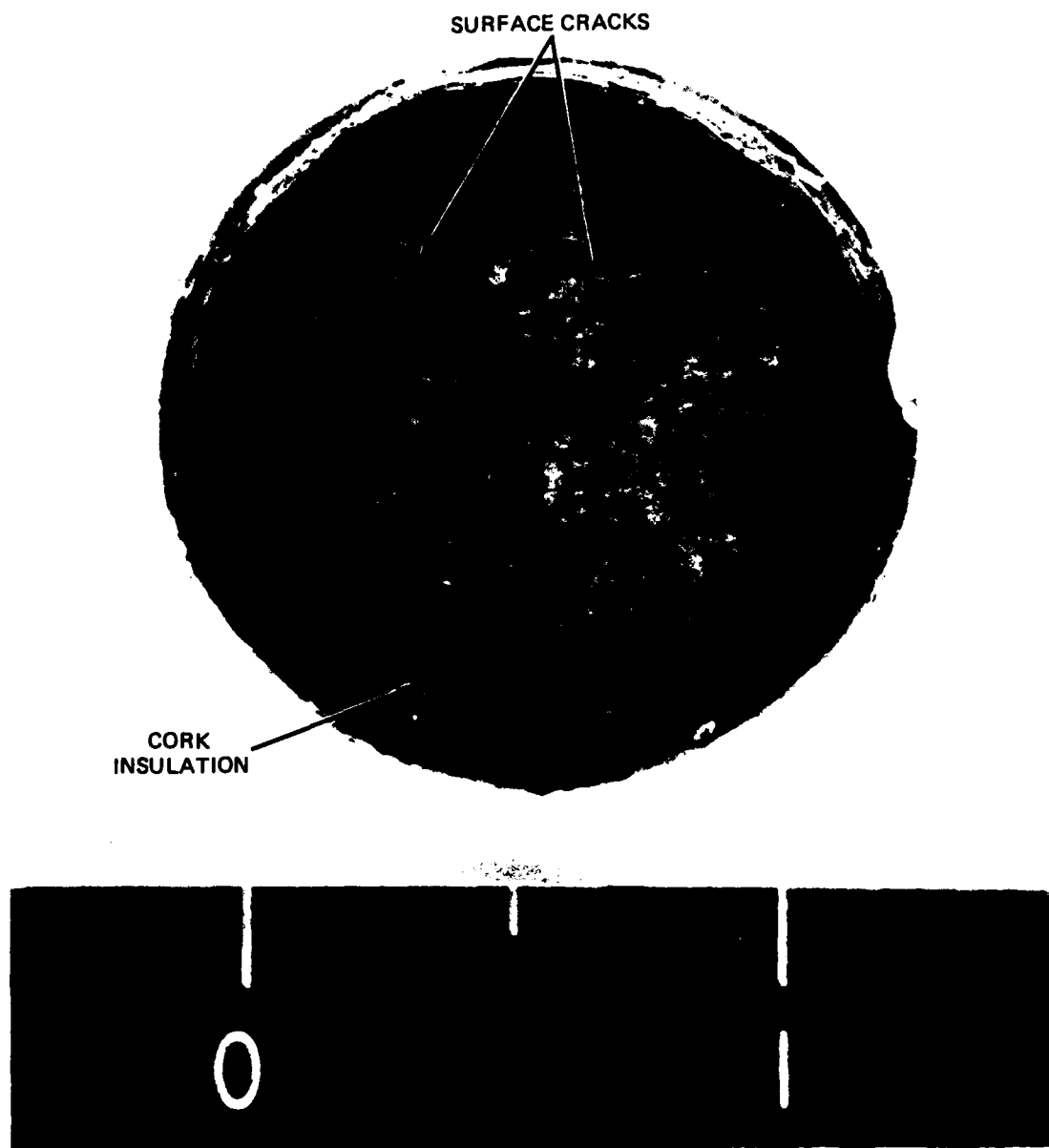
Figure G-6. Dynatherm DE-370 (10.17 Btu/ft^2-s heat flux).
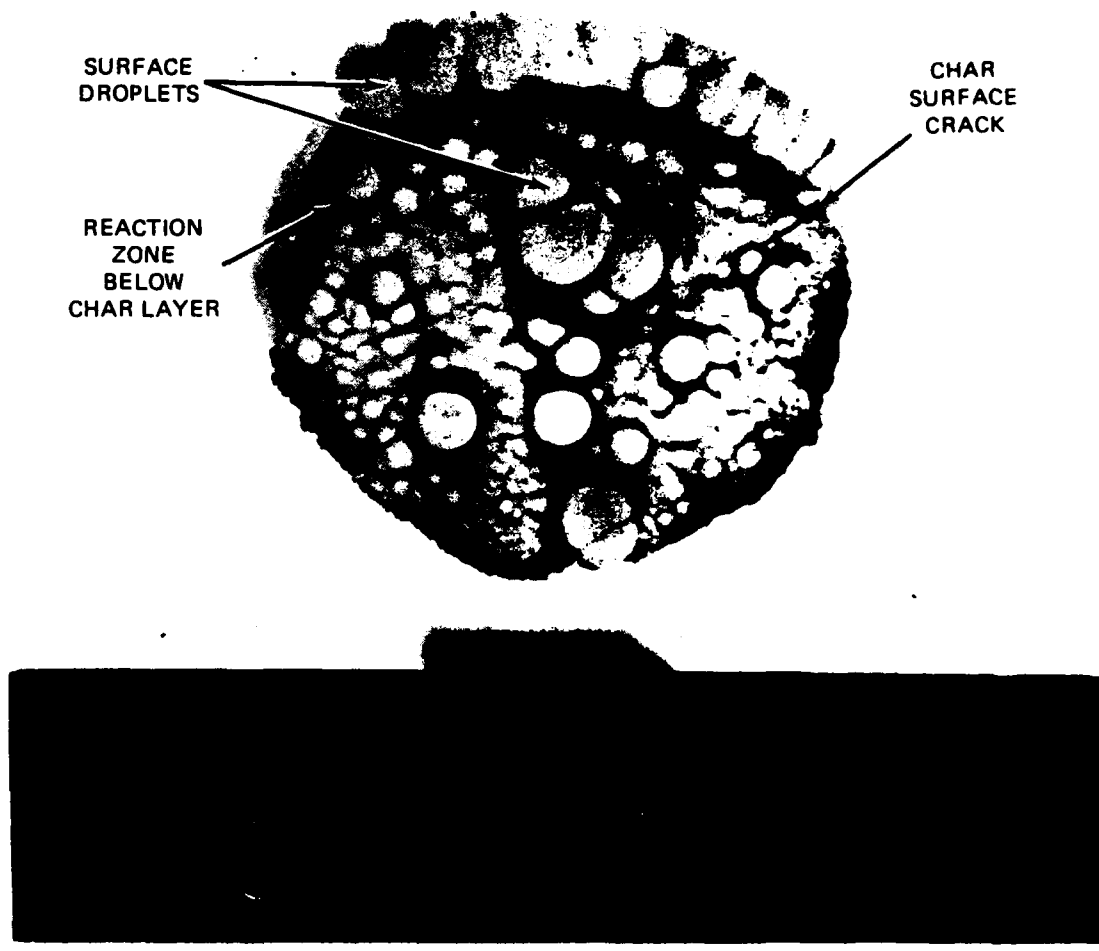
Figure G-7. Flamemaster S-885 (10.06 Btu/ft^2-s heat flux).
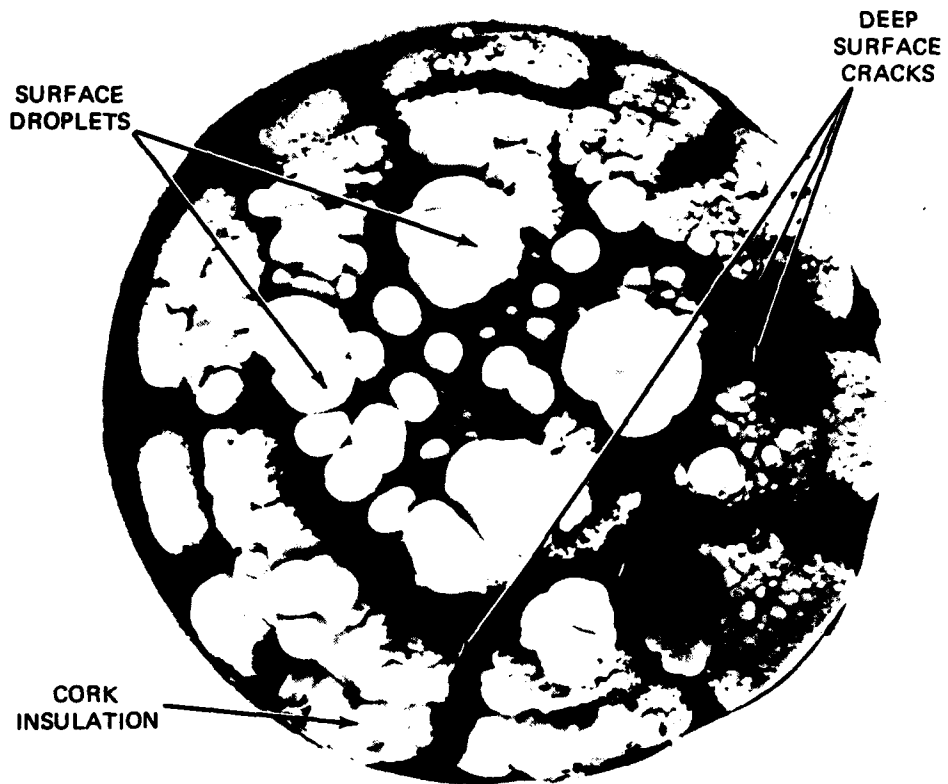
Figure G-8. Flamemaster S-886 (10.11 Btu/ft^2-s heat flux).

APPENDIX H

DETERMINATION OF FIREX THERMAL CONDUCTIVITY[21]

H.1   Experimental Procedure for Determination of Thermal Conductivity

        The comparative method was used to determine thermal conductivity.
Before the test, the sample was accurately measured and weighed and the
density was determined. The sample was then instrumented with thermo-
couples and placed between two reference standards of identical geometry
to the sample, (Figure H-1). Each reference standard (heat meter) was
instrumented with thermocouples at known fixed distances. The composite
stack was fitted between an upper heater and lower heater of appropriate
geometry and the complete system placed on a liquid-cooled heat sink. A
reproducible load was applied to the top of the system to ensure inti-
mate contact between all components. A thermal guard tube which could be
heated or cooled was placed around the system and the interspace and sur-
roundings filled with an insulating powder.

        By setting the top heater to a temperature higher than the lower
heater, a temperature gradient was established in the stack. Radial
heat loss was minimized by establishing a similar gradient in the guard
tube. The system was allowed to reach equilibrium conditions after which
successive readings of temperatures at various points were avaeraged and
evaluated. From this data, heat flux was determined and specimen ther-
mal conductivity calculated as shown in Eq. (H-1).

205
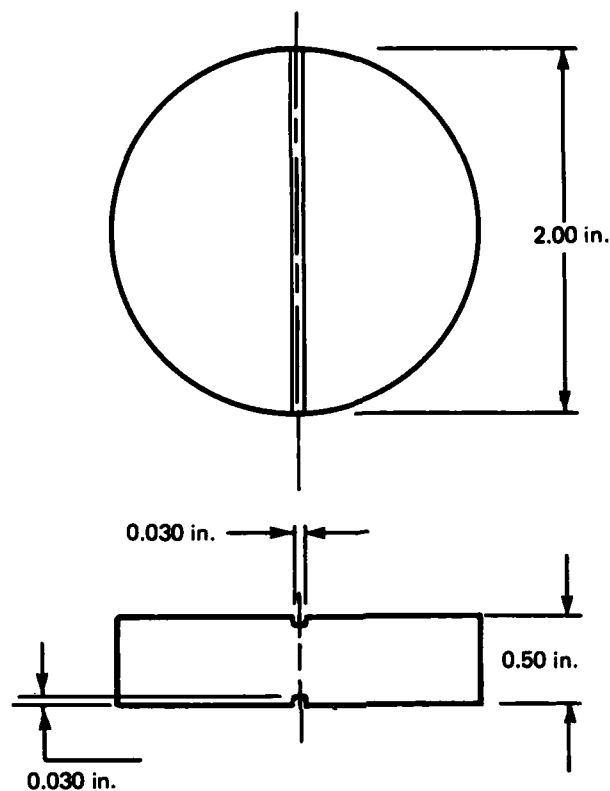
Figure H-1. Comparative method standard sample.

Data Reduction

The thermal conductivity was calculated from

$$\lambda_s = 1/2 \left(\frac{x}{\Delta T}\right)_s \left[\left(\frac{\lambda \Delta T}{x}\right)_R + \left(\frac{\lambda \Delta T}{x}\right)_r\right] \qquad \text{(H-1)}$$

where

λ = thermal conductivity

x = distance between thermocouples

ΔT = temperature drop across material over distance x

206

s = identifies sample parameters

R = identifies top reference material parameters

r = identifies bottom reference material parameters

The results are presented in Table H-1.

Table H-1. Thermal conductivity of a Firex sample.

Sample Density at 24°C = 1350 kg/m^3 [84.2 lb/ft^3]			
Temperature		Conductivity	
°C	°F	W/mK	Btu in/h ft^2 °F
24	75	0.345	2.39
95	203	0.265	1.84

LIST OF REFERENCES

1. "Standard Test Method for Heat of Ablation," American Society for Testing Materials, ASTM E458, September, 1978.

2. "Standard Method for Oxyacetylene Ablation Testing of Thermal Insulation Materials," American Society for Testing Materials, ASTM E285, 1970.

3. Lee, H.M., P.N. Hirasaki, and D.C. Gardner, <u>Standard Ablation Program (STAB II) User's Manual</u>, Manned Space Center, NASA, Houston, TX, Project Technical Report Task E-45B, June, 1969.

4. Schmidt, D.L., <u>Ablation of Plastics</u>, Directorate of Materials and Processes, Aeronautical Systems Division, Wright Patterson Air Force Base, Ohio, TDR No. ASD-TR-61-650, February, 1962.

5. Sawko, P.M., and S.R. Riccitiello, "Intumescent Ablators as Improved Thermal Protection Materials," <u>Journal of Coatings Technology</u>, March 1977.

6. "Firex RX-2373", Technical Data Sheet, Pfizer, Inc., Minerals, Pigments and Metals Division, New York, TR-188-5, 1973.

7. "Evaluation of Flexfram^{TM} 605 as a Firewall Coating for Aluminum," Test Report, Fiber Materials, Inc., Biddeford, Maine, February, 1981.

8. "Chartek 59 Lightweight Intumescent Epoxy Fireproofing," AVCO Specialty Materials Division, Lowell, MA, 7.14/Av.

LIST OF REFERENCES (Continued)

9.   "Fire Protection Materials: Flamarest 1600B Fireproofing Coating,"
      AVCO Specialty Materials Division, Lowell, MA, 0480-2M.

10.   "Dynatherm DE-350," Flamemaster Corp., Sun Valley, CA, Technical
      Bulletin 10377, Application Bulletin, August, 1977.

11.   Omegascope^{TM} Infrared Pyrometer; Operator's Manual for Models
      OS-2000A and OS-3000, Omega Engineering, Inc., M124/052, 1982.

12.   "Dynatherm DE-370," Flamemaster, Corp., Sun Valley, CA, Technical
      Bulletin 10377, Issue 1.

13.   "Low Density Silicone Abaltive Coatings: S-885," Preliminary
      Data Sheet, Flamemaster Corp., Sun Valley, CA, May, 1982.

14.   "Low Density Silicone Ablative Coatings: S-886," Preliminary
      Data Sheet, Flamemaster Corp., Sun Valley, CA, May, 1982.

15.   "Fiberfrax LDS Moldable," Carborundum Resistant Materials Company,
      Form C740-A, December, 1981.

16.   "Avcoat 893-5 Protects Missile Body and Fin Surfaces," Thermal
      Protection Materials Branch, AVCO Systems Division, Lowell, MA,
      TP-110-273-2M.

17.   Bowman, W.H., and R.M. Lawrence, "Ablative Materials for High-
      Temperature Thermal Protection of Space Vehicles," Space Resources
      for Teachers: Chemistry, NASA EP-87, 1971.

18.   Carslaw, H.S., and J.C. Jaegar, Conduction of Heat in Solids,
      Oxford Press, 1959.

19.   Schwarting, R.A., One-Dimensional Model of an Intumescent Ablator,
      Charles Stark Draper Laboratory Report T-812, Massachusetts
      Institute of Technology, SMME/OE Thesis, May, 1983.

LIST OF REFERENCES (Continued)

20. Nelson, J.B., _Determination of Kinetic Parameters of Six Ablation Polymers by Thermogravimetric Analysis_, Langley Research Center, Hampton, Virginia, NASA TN D-3919, April, 1967.

21. _Report on the Thermal Conductivity of a Firex Sample_, Dynatech Research and Development Co., Cambridge, MA, Report No. INS-72, February, 1983.

22. Ofner, R.E., and D.H. Sale, _Development of Flexible Insulation for Solid Propellant Rocket Motor Cases_, Rock Island Arsenal Laboratory, Illinois, Technical Report No. 62-2366, July, 1962.

23. Mihalow, F.A., F.J. Koubek, and H.A. Perry, _Ablation Test Methods for Rocket and Heat Shield Materials_, U.S. Naval Ordnance Laboratory, Maryland, NAVWEPS Report 7314, October, 1961.

24. Darwin, R.L., and R.B. McCann, "Fire Protection Aboard U.S. Navy Ships," _National Safety Congress Transactions_, National Safety Council, Vol. 14, 28 Oct. 1968.

25. Froberg, R.W., "Thermal Coating Slows Fire Progress," _Modern Paint and Coatings_, Nov. 1980.

26. Lee, B.T., and W.J. Parker, _Fire Performance Guidelines for Shipboard Interior Finish_, Center for Fire Research, National Engineering Laboratory, National Bureau of Standards, Report No. NBSIR 79-1700, June 1979.

27. Lee, B.T., and J.N. Breese, _Submarine Compartment Fire Study - Fire Performance Evaluation of Hull Insulation_, Center for Fire Research, National Engineering Laboratory, National Bureau of Standards, Report No. NBSIR 78-1584, May 1979.

LIST OF REFERENCES (Continued)

28.   Shea, J.W., <u>Relative Performance Evaluation of Selected Ablative</u>
       <u>Materials to Replace the Asbestos-Filled Dynatherm E-340N on the</u>
       <u>MK 11 GMLS</u>, Naval Surface Weapon Center, Report No. NSWC TR81-106,
       April 1981.

29.   Mitchel, B.J., and J.V. Recesso, <u>Ablative Plastics Characteriza-</u>
       <u>tion: Part I. Arc Heater Screening</u>, AVCO Research and Advanced
       Development Division, MA, Technical Report AFML-TR-65-156, May,
       1965.

30.   Schmidt, D.L., <u>Behavior of Plastic Materials in Hyperthermal</u>
       <u>Environments</u>, Wright Air Development Center Materials Laboratory,
       Wright-Patterson Air Force Base, Ohio, WADC Technical Report
       59-574, April, 1960.

31.   Leary, J.M., <u>Characteristics of Various Types of Ablative Materials</u>
       <u>with Associated Naval Applications</u>, Charles Stark Draper Report
       T-811, Massachusetts Institute of Technology SMNA/OE Thesis,
       May 1983.

32.   Wurst, J.C., J.A. Cherry, D.A. Gerdeman, and N.L. Hecht, <u>The</u>
       <u>Evaluation of High-Temperature Materials; Second Quarterly Progress</u>
       <u>Report</u>, Dayton University, Ohio, Contract No. AF 33(615)-1312,
       July, 1964.

33.   Hewitt, H.C., Jr., <u>Scope of Experimental Analysis</u>, Tennessee
       Technological University, Prentice-Hall, Inc., 1973.

END

FILMED

4-84

DTIC